NASA CONTRACTOR REPORT

NASA CR-113

NASA CR-113

PRESTRESSED MONOLITHIC AND SEGMENTED BRITTLE STRUCTURES

by R. L. Barnett, Paul Hermann, and James Costello

Prepared under Contract No. NASr-65(04) *by*
IIT RESEARCH INSTITUTE
Chicago, Ill.
for

NATIONAL AERONAUTICS AND SPACE ADMINISTRATION • WASHINGTON, D. C. • OCTOBER 1964

NASA CR-113

PRESTRESSED MONOLITHIC AND SEGMENTED BRITTLE STRUCTURES

By R. L. Barnett, Paul Hermann, and James Costello

Prepared under Contract No. NASr-65(04) by
IIT RESEARCH INSTITUTE
Chicago, Illinois

for

NATIONAL AERONAUTICS AND SPACE ADMINISTRATION

For sale by the Office of Technical Services, Department of Commerce,
Washington, D.C. 20230 -- Price $2.25

ABSTRACT

32431

The premature longitudinal cracking of segmented columns has been identified as one of the most serious problems in the design of prestressed segmented ceramic members. Circumstantial evidence is presented to support the contention that large transverse tensile stresses are developed because of the non-flatness of segment interfaces.

Two first order models are developed for predicting the nonlinear response of prestressed segmented beams. The validity of the models is demonstrated experimentally and many of the characteristics of segmented beams are explored. The strength of prestressed monolithic brittle beams is formulated in terms of reliability and a specific example is treated in which the prestress leads to a twenty-five fold increase in strength when compared to a conventional beam of equal weight and reliability.

Authors

TABLE OF CONTENTS

TABLE OF CONTENTS (Cont'd)

LIST OF ILLUSTRATIONS

LIST OF ILLUSTRATIONS (Cont'd)

PRESTRESSED MONOLITHIC AND SEGMENTED BRITTLE STRUCTURES

I. INTRODUCTION AND PROGRAM SUMMARY

A. Objectives

The principal aim of the aerospace structural designer is to provide structures of minimum weight and volume. To accomplish this objective in an environment of high temperature and severe oxidation, he is being forced more and more to consider the family of brittle materials composed of cermets, ceramics and refractory metals. In addition to the remarkable high temperature properties of such materials, one finds exceptional compressive strengths and abrasion resistance. Furthermore, most of the materials occur abundantly in nature. Notwithstanding these attractive features, many of these materials are produced only in small sizes, their costs are usually very high, some are toxic, often large residual stresses are unavoidable, and all too frequently the mechanical properties exhibit enormous variability. Saving the worst for last, their greatest shortcoming from the structural designers point of view is brittleness.

The overall objective of this program is to study the techniques of prestressing and segmenting as one possible approach to the problems of brittleness and small section size. Specifically, it is the goal of this program to develop an analytical capability for predicting the behavior of prestressed monolithic and segmented brittle structures.

In this first phase of the program, three fundamental problems have been considered. The first of these deals with the development of transverse tensile stress in a segmented column under axial compressive loading. The second, involves the prediction of the non-linear response of a prestressed segmented beam. And the last, concerns itself with the benefits which occur from prestressing a monolithic brittle element.

B. Summary of Current Progress

1. Transverse Cracking Phenomenon

Cracking in a direction transverse to a uniaxial compressive load was first recognized by F. R. Shanley to be a major deterrent to the application of prestressing to segmented members. In 1957, the authors conducted a study of minimum weight deflection design for prestressed segmented beams in which the roughness of the segment interfaces played a predominant role. Based on this background, it was hypothesized that the interface roughness causes transverse cracking. To support this view the following evidence was established.

1. The slope of the compressive stress-strain diagram of a segmented column increases with increasing stress. This is caused by the fact that the contact area increases with axial load and hence the stiffness correspondingly increases.

2. Column strength increases with increasing flatness.

3. Specimens increase in compressive strength with decreasing cross-sectional area.

4. Internal transverse crack lenses can be observed in glass columns (2 in x 4 in x 1/2in).

5. Photoelastic and two-dimensional elasticity results indicate that an uneven load distribution on a segment will cause internal tensile stresses in directions parallel to the interfaces.

6. Triaxial compressive tests indicate a very substantial increase in axial strength when a lateral biaxial prestress is imposed.

2. Load-Deflection Characteristics of Prestressed Segmented Beams

Two quite different mathematical models were developed to describe the nonlinear behavior of a prestressed segmented beam. Identical closed form results were obtained for these models using rectangular beams in which the tendon stiffness was neglected. The complication of tendon stiffness gives rise to a computer analysis which can be extended to beams of complicated cross-section.

The load-deflection curve for a prestressed segmented beam has an initial linear region followed by a non-linear region of continuously decreasing slope. With respect to the non-linear region, it has been possible to demonstrate excellent agreement between the bending theory and carefully performed bending tests.

In the linear range, the prediction of the slope is equivalent to the problem of relating the effective area of a segmented column to the effective moment of inertia of the corresponding beam. The statistical nature of this problem was not recognized in sufficient time to properly deal with it during the first phase of this program.

3. Strength of Prestressed Monolithic Brittle Beams

Applying Weibull's statistical fracture theory, it was possible to theoretically establish for simple beams a relationship among prestress level, reliability, loading, member geometry, and material properties. A specific example is treated in which the prestress results in a twenty-five fold increase in capacity over a conventional beam of equal weight and reliability.

II. STATE OF THE PRESTRESSING ART

Prestressing is a technique whereby permanent stresses are introduced into a structure prior to the application of its service loads. The resulting initial state of stress can be made to have a profound influence upon the strength and stiffness of the structure. A brief systematic treatment of the general characteristics of prestressing may be found in Roark.[1/]

A. Prestressed Concrete

The application of prestressing principles to concrete - that is, of applying artificial compression to negate any tensile stresses developed in the loaded structure- was conceived many years ago and attempts were made to apply them as early as the 1880's. These first attempts were frustrated by the presence of creep in the concrete and in the mild steel tendons used by the early investigators. Their prestressed members eventually developed tension cracks even though they behaved according to theory when the prestress was first applied.

Eugene Freyssinet was apparently the first man to suggest a remedy to this problem and in 1928 he took out a French patent for concrete prestressed with high strength wire. The ultimate strength of this wire is sufficiently high that creep losses which occur subsequent to the prestressing represent only a small per cent of the original prestress level. Consequently, after long periods of time the tension under load can still be eliminated or reduced to a specified small value. It is important to point out that all of the modern design methods deal explicitly with the creep problem.

Over the last 35 years, the development of prestressed concrete has rapidly gained ground. Applications to beams, trusses, plates,and shells are almost commonplace. Indicative of the high level of development enjoyed by prestressed concrete is the design, using this material, of the wings of a special guided missile ordered in 1947 by the French Air Ministry.[2/] It was verified that the stiffness of the resulting wing structure was about 50 per cent higher than ones built of steel or light alloy. The

weight turned out to be 12 per cent of the total weight of the craft (which was considered quite reasonable) and the ultimate strength was even higher than they forecasted. A more recent unusual application of prestressing was used in the Philips Pavilion at Brussels.[3] Here, a torsional prestress was introduced into the main ribs of the pavilion by the technique illustrated in Fig. 1. A similar application was proposed by Shanley[4] in connection with high performance ceramic shell structures.

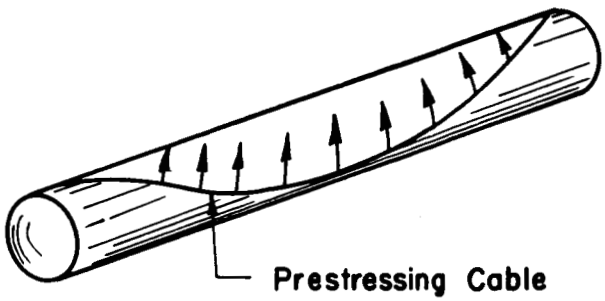

Fig. 1 TORSIONAL PRESTRESSING

B. Prestressed and Segmented Concrete

Prestressed and segmented concrete structures appear frequently in practice; for example, the Gladesville Bridge in Sydney, Australia furnishes a dramatic example of 1000-ft arch span assembled with precast segments. This bridge and a number of other long-span segmented concrete bridges are discussed in a recent paper by Gerwick.[5] In this country, use of concrete blocks in beams and panels has been extensively exploited by the firms of Bryan and Dozier of Nashville, Tennessee, and the Nashville Breeko Block Company. The basic idea of this construction is illustrated in Fig. 2.

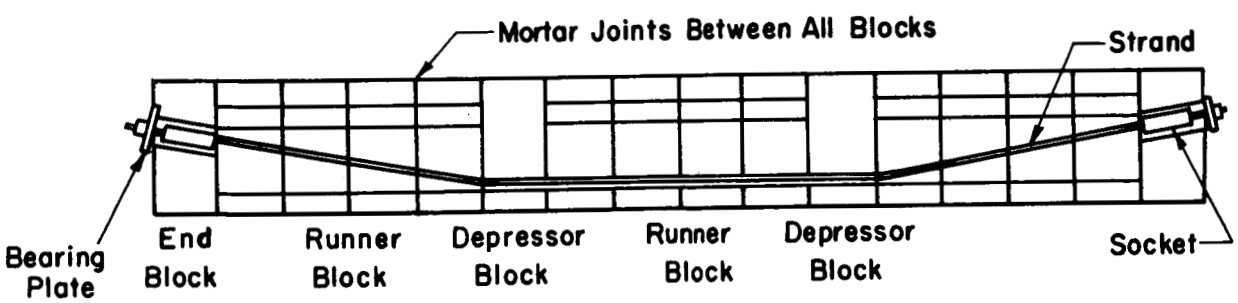

Fig. 2 TYPICAL PRESTRESSED CONCRETE BLOCK CONSTRUCTION

C. Prestressed Metallic Structures

Prestressing of metal structures was proposed in 1947 by the late Gustave Magnel. He presented a method of utilizing high-strength steel in the lower chord of a truss without the accompanying large deformations.[6] In 1949, Dr. Ing. F. Dischinger, Professor at the Technical University of Berlin, proposed a method of prestressing steel girders with concrete slabs solidly attached to their top flanges. In England, a number of old steel bridge trusses have been reinforced by prestressing their lower chords. To achieve greater lateral stiffness in a Canadian skyscraper, prestressed X-bracing was used in various bays. Recently, a practical method was proposed for effecting substantial weight savings in rolled sections by using a prestressed Queen Post arrangement.[7] In 1960, the Iowa State Highway Commission began the development of a method of prestressing steel beams which involves loading or deflecting a mild steel beam and welding on a high strength steel cover plate while the beam is deformed. The load is then removed leaving a beam with an attractive strength to weight ratio.

D. Prestressed and Segmented Ceramics

Applications of prestressing and segmenting methods to ceramic materials appear infrequently. Scattered examples can be found where the techniques are used for nonstructural purposes; the Kennametal Company shrink fits steel jackets over carbide tools, and the Norton Company threads short boron carbide cylinders over a central steel rod for use as reactor control elements. The idea of using prestressed segmented ceramic materials in high performance structures was motivated in part by a report prepared by the Ohio State University Research Foundation[8] which indicated that great possibilities could be derived from an all-ceramic wing design if means could be found to circumvent the poor tensile properties of ceramics. The possibility of using prestressing techniques for this purpose was investigated by Shanley in a report prepared for the Rand Corporation[9] in 1951.

A number of investigations of prestressed ceramics have been conducted by the staff of the University of California under the direction of

Shanley.[4, 10] Several types of civil engineering structures were studied including a 4-ft cantilever beam made from four ceramic building blocks and a number of wall panels and slabs also constructed from ceramic blocks. In all of these investigations, very low stress levels were achieved and the results were primarily of a feasibility nature.

For aircraft application, the four high-alumina porcelain wing structures shown in Fig. 3 were fabricated and tested. In the first three of these wings, failure occurred while the prestressing loads were being applied. The failures were quite interesting in that the initial cracks were formed parallel to the wing axis, suggesting the presence of circumferential tension. Nadai, in discussing compression members of porcelain, mentions that failure often occurs in the form of longitudinal cleavage cracks.[11] This phenomenon is attributed by him to a wedging action of the column caused by frictional restraint of the compression plates against radial expansion of the column. Further explanation is seen in wedging action produced by filler material, most noticeably lead, penetrating the crevices of the material and thus initiating such cracks. In the test of ceramic wing No. IV, an average prestress of 2000 psi was applied. The structure was then uniformly loaded to failure, which occurred at a maximum bending stress of 1590 psi. Tests of the individual wing sections showed a compression strength of 12, 000 psi, and tests of smaller samples developed compression strengths averaging 40, 000 psi. It should be noted that compressive strengths of 400, 000 psi are not uncommon in ceramics.

A series of exploratory experiments on prestressed segmented titanium carbide elements were conducted by Barnett[12] as part of a minimum weight investigation of rocket launcher structures. One of the bending members studied in this program is shown in Fig. 4. The member sustained bending stresses of 8000 psi and prestressing levels as high as 120, 000 psi without signs of distress. No attempt was made to attain the ultimate bending strength since stiffness and not strength was the main concern of this study.

Results of the bending tests are shown in Fig. 5 where we observe that the initial stiffness increases with increasing prestress. Titanium carbide has a straight-line compressive stress-strain curve up to about

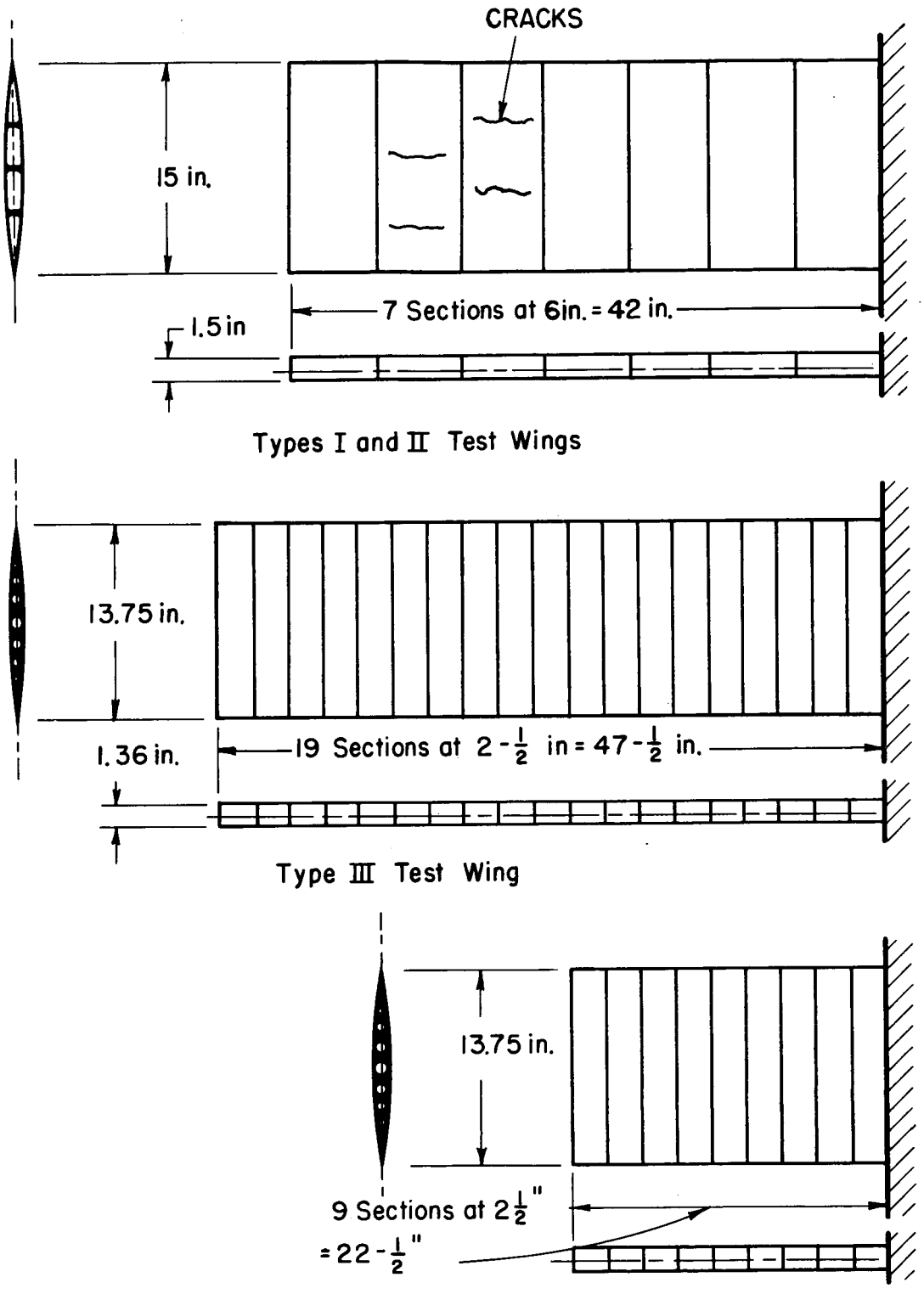

Fig.3 PRESTRESSED SEGMENTED CERAMIC WINGS
(after F. R. SHANLEY)

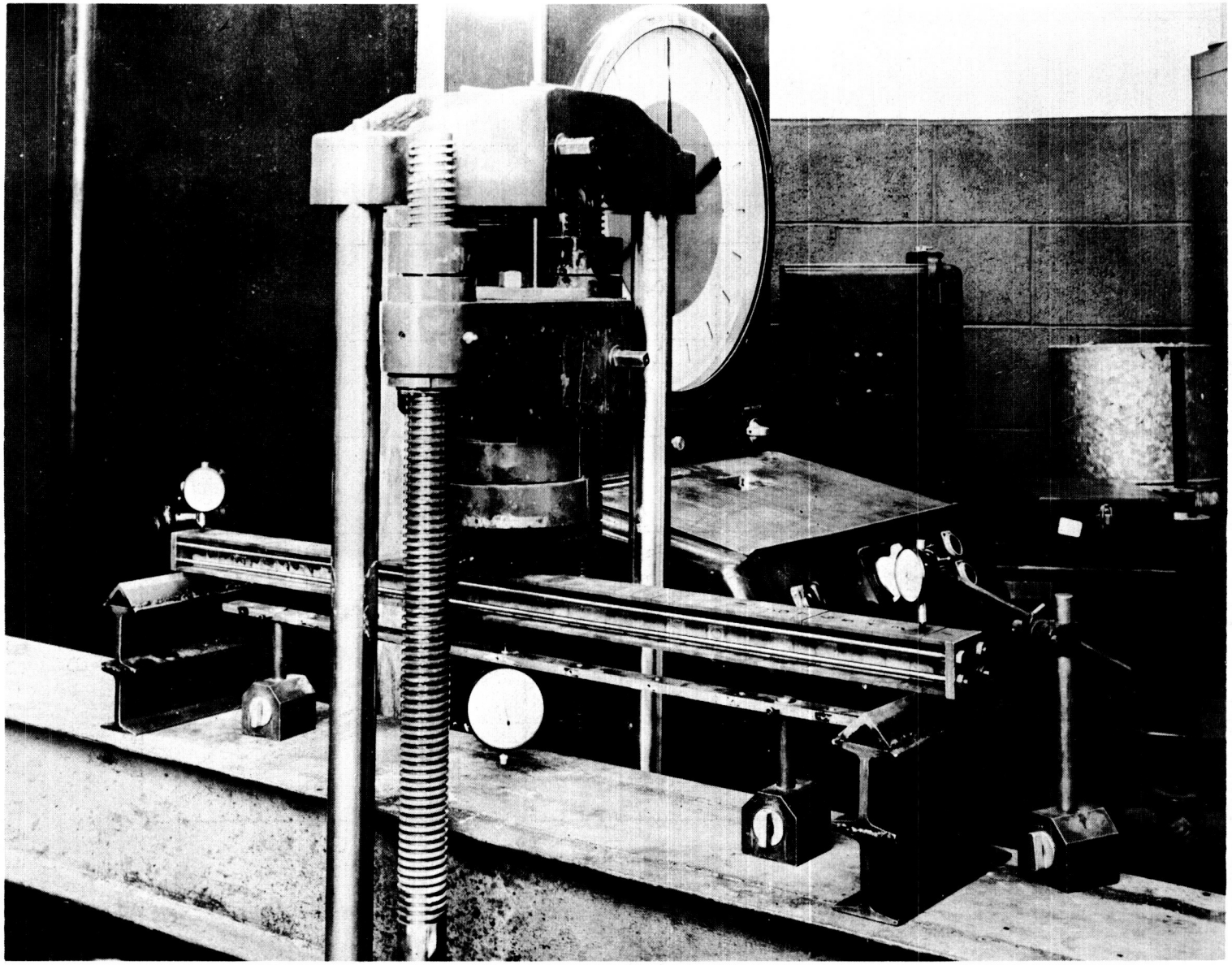

Fig.4 BENDING TEST OF A TITANIUM CARBIDE BEAM

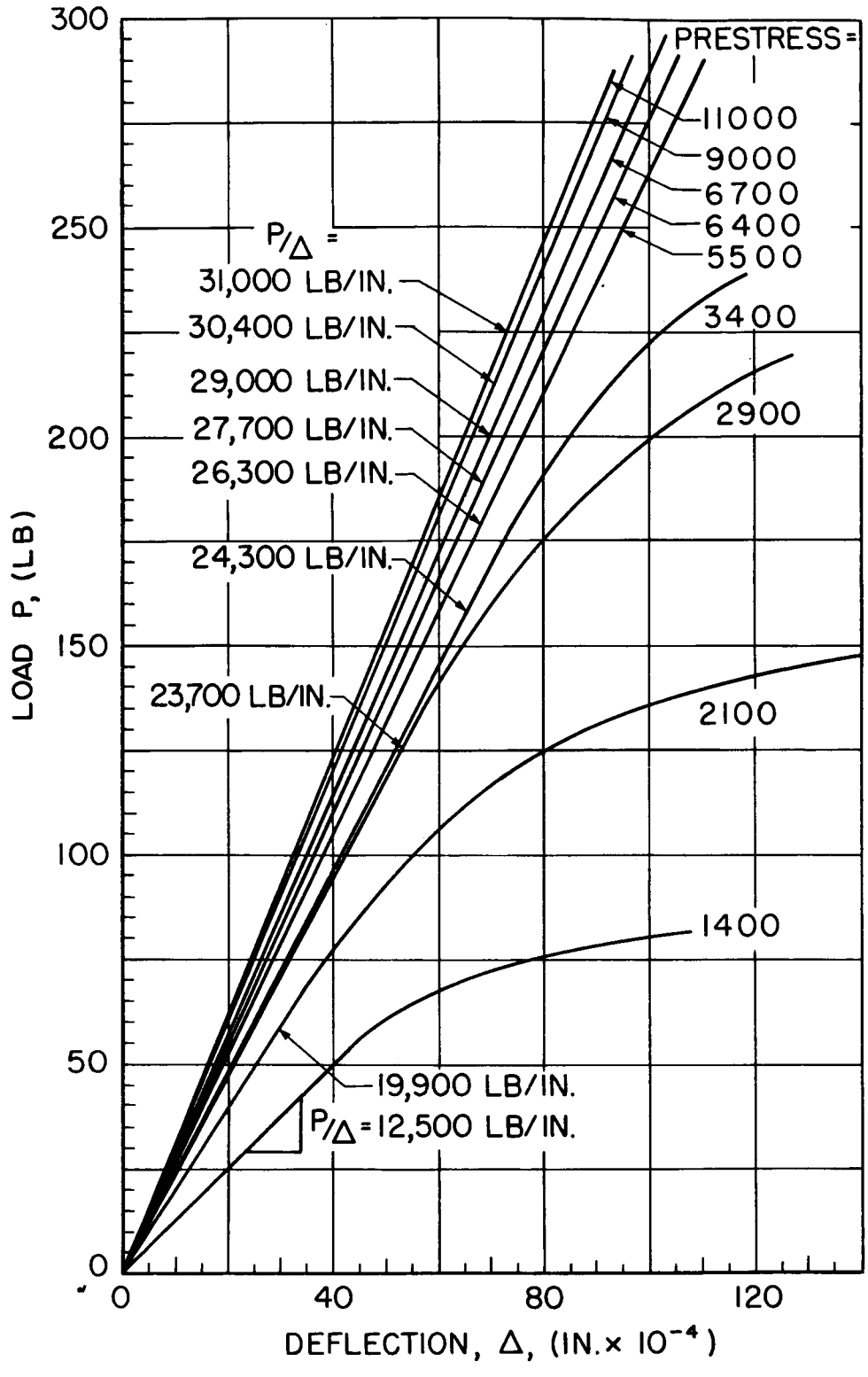

Fig.5 LOAD-DEFLECTION CURVES OF A SEGMENTED TITANIUM CARBIDE BEAM

500,000 psi; consequently, the segmenting has the effect of lowering the stiffness. This effect also appeared in the direct compression test of the beam segments. A typical compressive stress-strain diagram is shown in Fig. 6. The observed curvilinearity is caused by the fact that the segment interfaces are not flat, and consequently, the contact area, and hence stiffness, increases monotonically with increasing axial load. To check this premise and to determine means for dealing with it, an investigation was conducted which involved lapping the interfaces, using shims of various materials between the segments, and buttering the interfaces with hydrocal. The lapping and the hydrocal gave rise to considerable improvement--the shims were not effective. It is of some interest that Shanley reported considerable difficulty with the gasket materials he used between the segments of the first three wings.

A remarkably complete account of the characteristics of prestressed segmented brittle materials can be found in a brief article by A. J. Harris. [13]

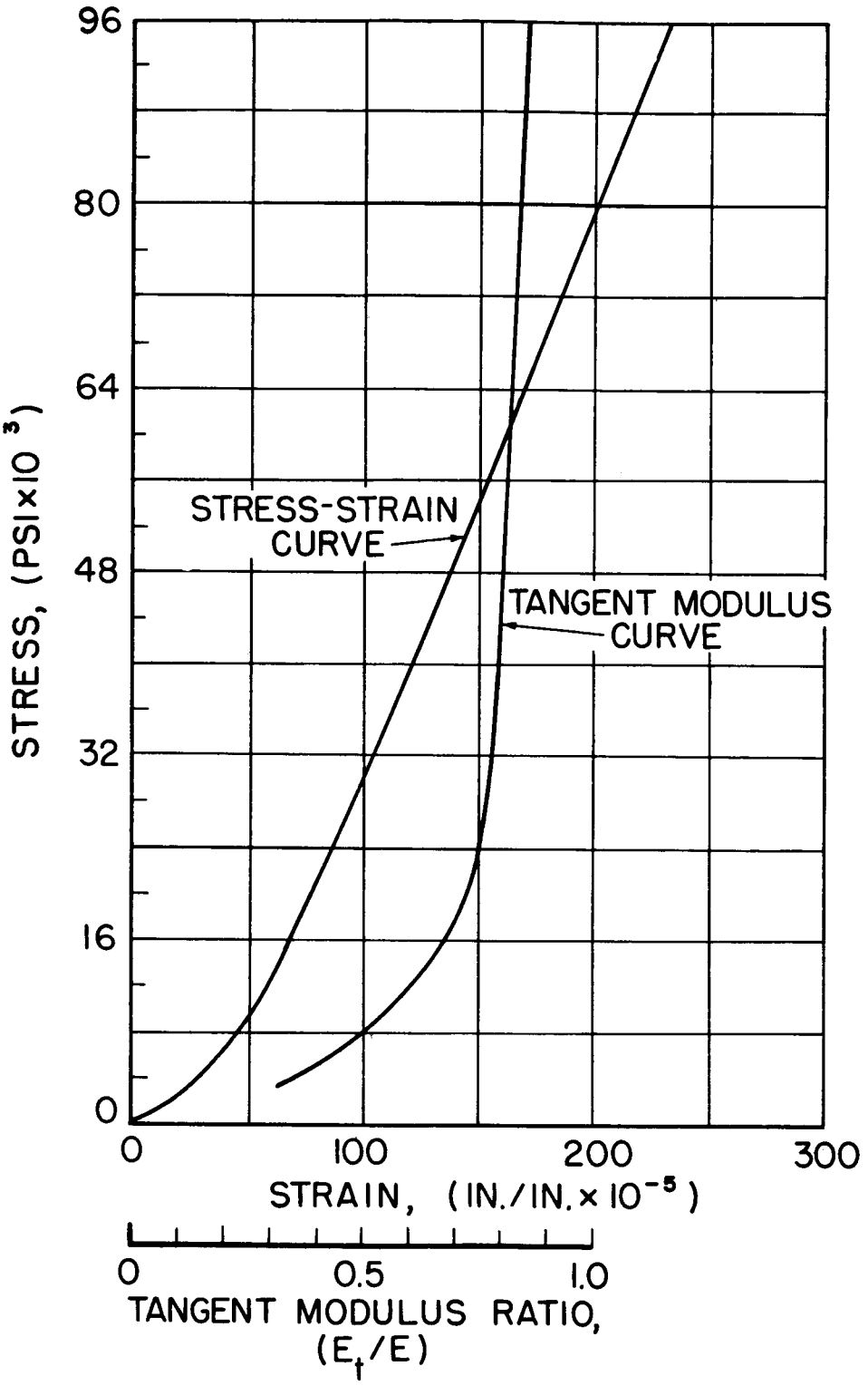

Fig.6 STRESS-STRAIN DIAGRAM OF A TITANIUM CARBIDE COLUMN

III. TRANSVERSE CRACKING OF SEGMENTED COLUMNS

In summarizing his work on ceramic wings, Shanley identifies the premature cracking of the ceramic elements in the spanwise direction as the most serious problem in the design of prestressed ceramics. For this reason, a portion of this program has been directed toward this problem.

A. Interface Roughness Hypothesis

Because the roughness of segment interfaces played such a significant role in the stiffness experiments with titanium carbide, it seemed reasonable to adopt this premise as a first hypothesis for explaining the transverse cracking of segmented elements under axial compressive loads. Indeed, the studies described in this chapter appear to support this position.

B. Support of Hypothesis

For reasons of cost, availability, transparency, and extreme brittleness, plate glass was chosen as the model material for the experimental phases of this program. The glass was received in the form of blocks with nominal dimensions of 2 x 4 x 1/2 inches where the eight square inch surfaces were 5 to 7 lightbands out of flat.

The first test performed was a simple determination of the compressive stress-strain diagram of the 2 x 4 x 1/2 inch glass blocks shown in Fig. 7. The test was terminated at about 10, 000 psi when spalling was observed on the periphery of the glass segments. Examination of the glass segments subsequent to the test revealed that all of the blocks contained lens-like cracks. The normals to these lenses were perpendicular to the axis of loading and their centers were located near the central plane of the segments. The cracks did not penetrate to the surfaces.

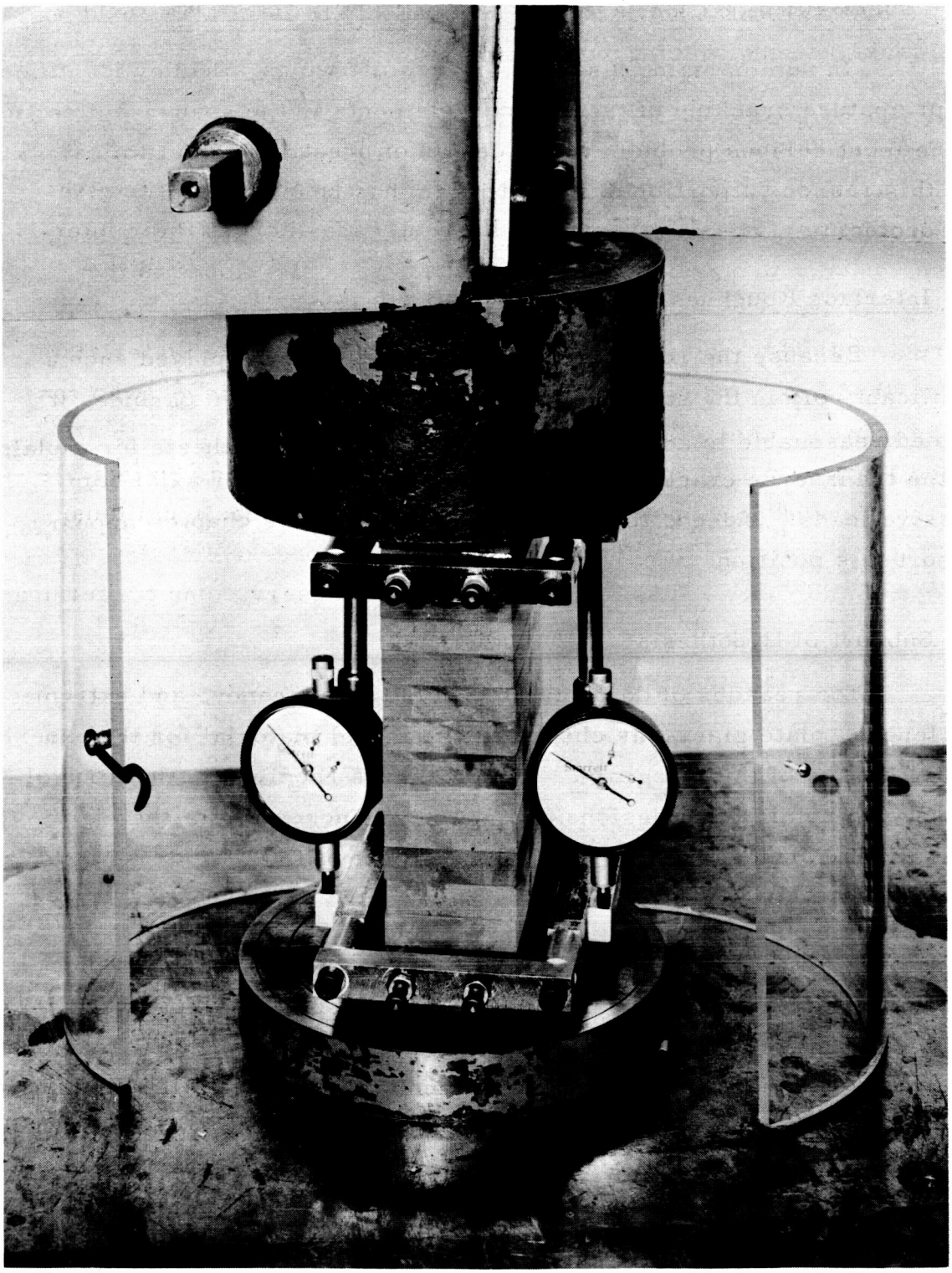

Fig.7 COMPRESSOMETER FOR 2"× 4" SEGMENTED GLASS COLUMN

Figure 8 is an artists rendering of a typical crack lens. We could not obtain photographs which gave a satisfactory prospective.

1. Lateral Tensile Stresses

In a segmented column, the roughness of the segments gives rise to a nonuniform distribution of axial stresses across their interfaces. This in turn causes tensile stresses to be developed in the transverse direction to the loading. This principle has been used as a indirect method of obtaining the tensile strength of brittle materials. The method has been described by Berenbaum and Brodie [14] who conducted a two-dimensional photoelastic analysis of the nonuniformly loaded block shown in Fig. 9a. The results shown in Fig. 9b indicate that the transverse stress under the load assumes a maximum tensile value at the center of the block and becomes compressive at the top and bottom surfaces. This corresponds to our observations concerning the internal crack lenses which did not penetrate to the surfaces.

Additional insight into the nature of the transverse tensile stresses can be gained by studying the stress distribution in the strip shown in Fig. 10. The intensity of the vertical forces acting on the top and bottom surfaces is $A(1 + \sin \frac{m\pi x}{L})$ where the interger m represents the number of waves and L is the strip length. Referring to Timoshenko and Goodier, [15] the stress distribution becomes

$$\sigma_x = 2A \frac{(a \cosh a - \sinh a) \cosh \alpha y - \alpha y \sinh \alpha y \sinh a}{\sinh 2a + 2a} \sin \alpha x \qquad (1)$$

$$\sigma_y = -2A \frac{(a \cosh a + \sinh a) \cosh \alpha y - \alpha y \sinh \alpha y \sinh a}{\sinh 2a + 2a} \sin \alpha x - A \qquad (2)$$

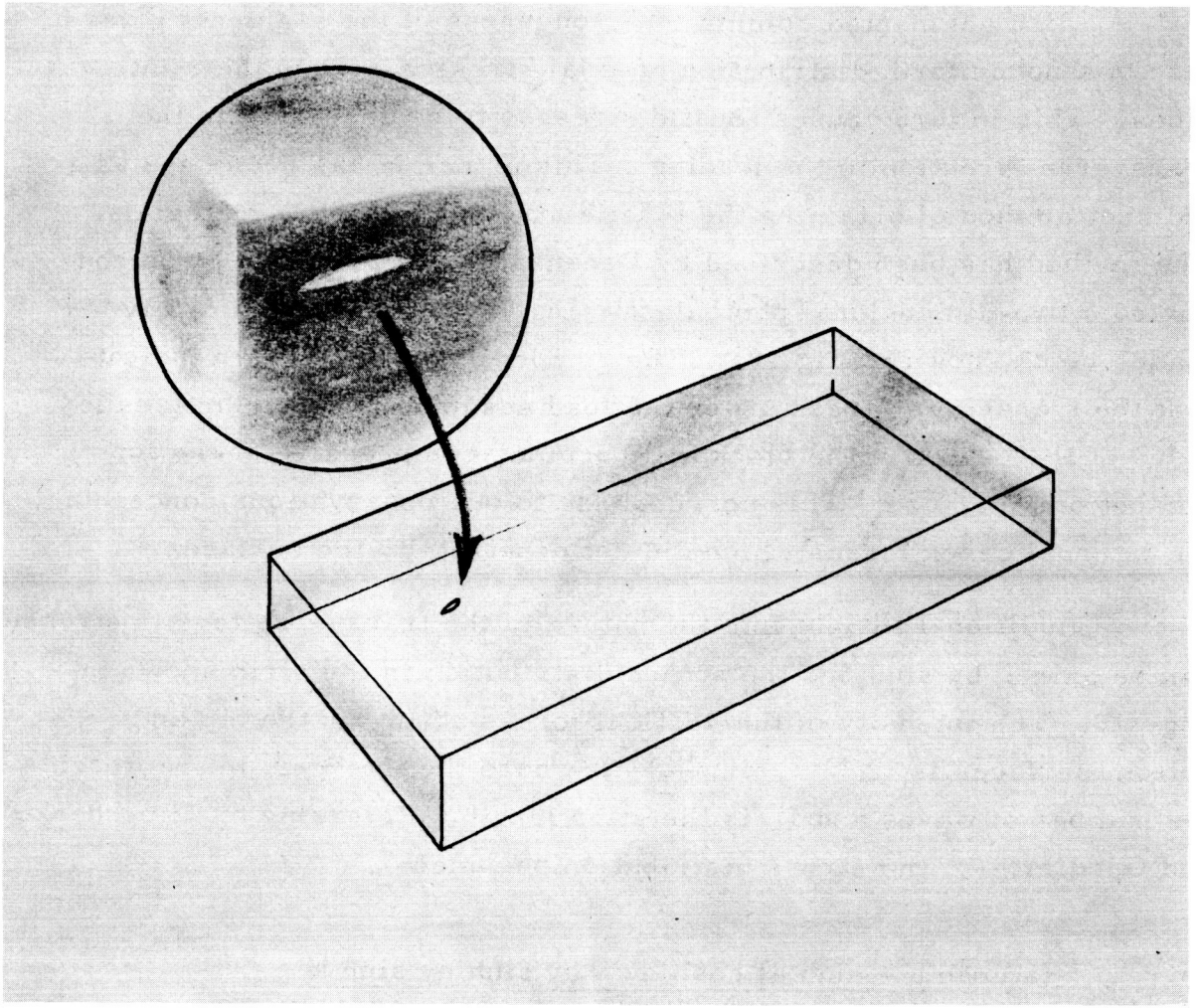

Fig. 8 TRANSVERSE INTERNAL CRACK RESULTING FROM DIRECT COMPRESSION

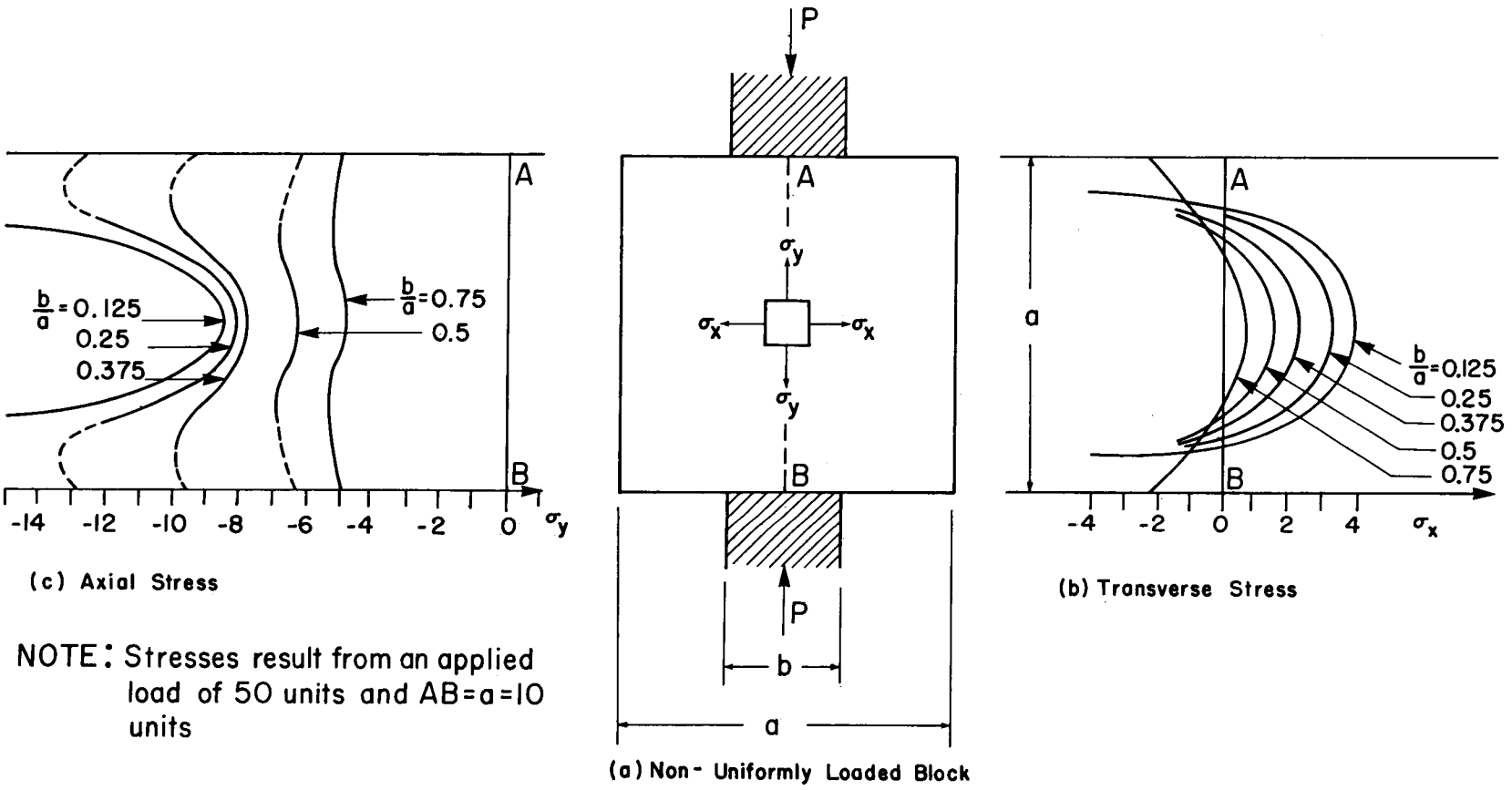

(c) Axial Stress

(b) Transverse Stress

(a) Non- Uniformly Loaded Block

NOTE: Stresses result from an applied load of 50 units and AB=a=10 units

Fig.9 INDIRECT TENSION TEST
AFTER R. BERENBAUM AND I. BRODIE

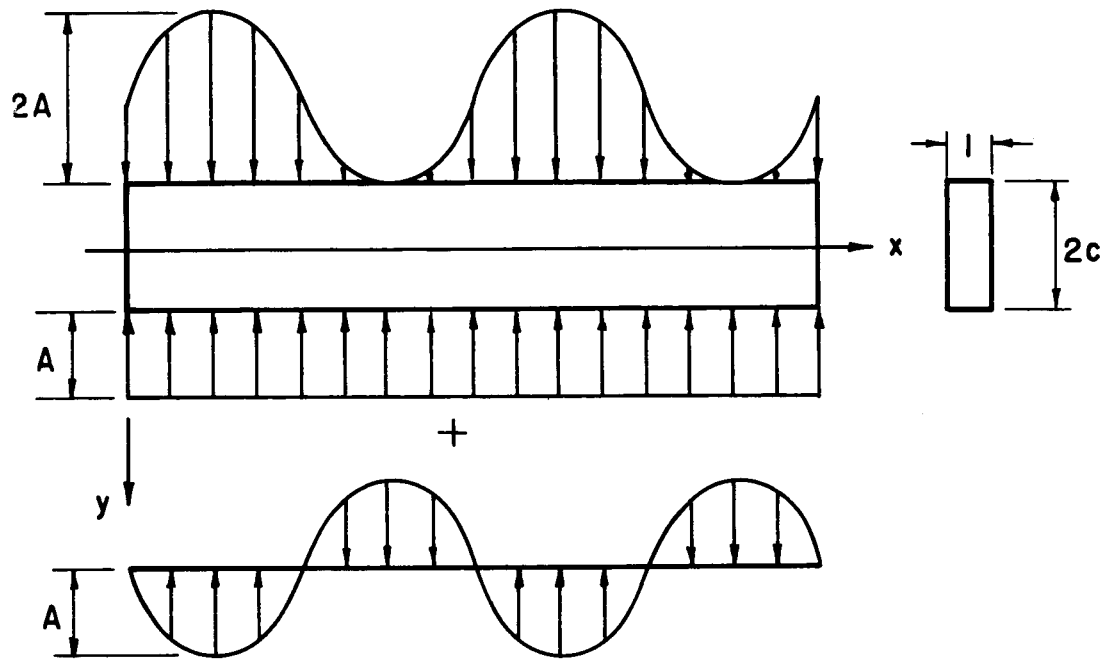

ig.10 STRIP SUBJECTED TO A NON-UNIFORM AXIAL LOAD

$$\tau_{xy} = -2A \frac{a \cosh a \sinh \alpha y - \alpha y \cosh \alpha y \sinh a}{\sinh 2a + 2a} \cos \alpha x \qquad (3)$$

where $a = \frac{m\pi c}{L}$ and $\alpha = \frac{m\pi}{L}$ and c is half the strip depth. Specializing these formulas to give the maximum stresses in the middle plane ($y = 0$, $\sin \alpha x = 1$), the ratio of transverse to axial stress becomes

$$-\frac{\sigma_x}{\sigma_y} = \frac{a \cosh a - \sinh a}{(1 + \cosh a)(a + \sinh a)} \qquad (4)$$

This relationship has been plotted in Fig. 11 where we observe that somewhere between very few waves and very many waves there exists a "worst" condition. We observe further that tensile failures can occur if the tensile strength of the strip material is less than 15.3 per cent of its compressive strength. For most ceramic materials the tensile strength is less than 10 per cent of their compressive strength.

There are two important similarities between the photoelastic and the elasticity solutions considered. Both show the existence of transverse tensile stresses of the same order of magnitude as the axial stresses, and both show the transverse stresses to be maximum in the middle plane and compressive near the top and bottom surfaces. Equation 1 shows that σ_x is negative at $y = \pm c$.

2. Flatter Specimens and Smaller Specimens

Examination of the interfaces of the 2 x 4 x 1/2 inch glass blocks with optical flats seemed to indicate that the surfaces contained a relatively small number of waves. The amplitudes of these waves can be reduced by lapping which, according to our roughness hypothesis, should increase the ultimate compressive strength of a segmented column. Further, if the larger amplitude waves are the more influential in controlling surface

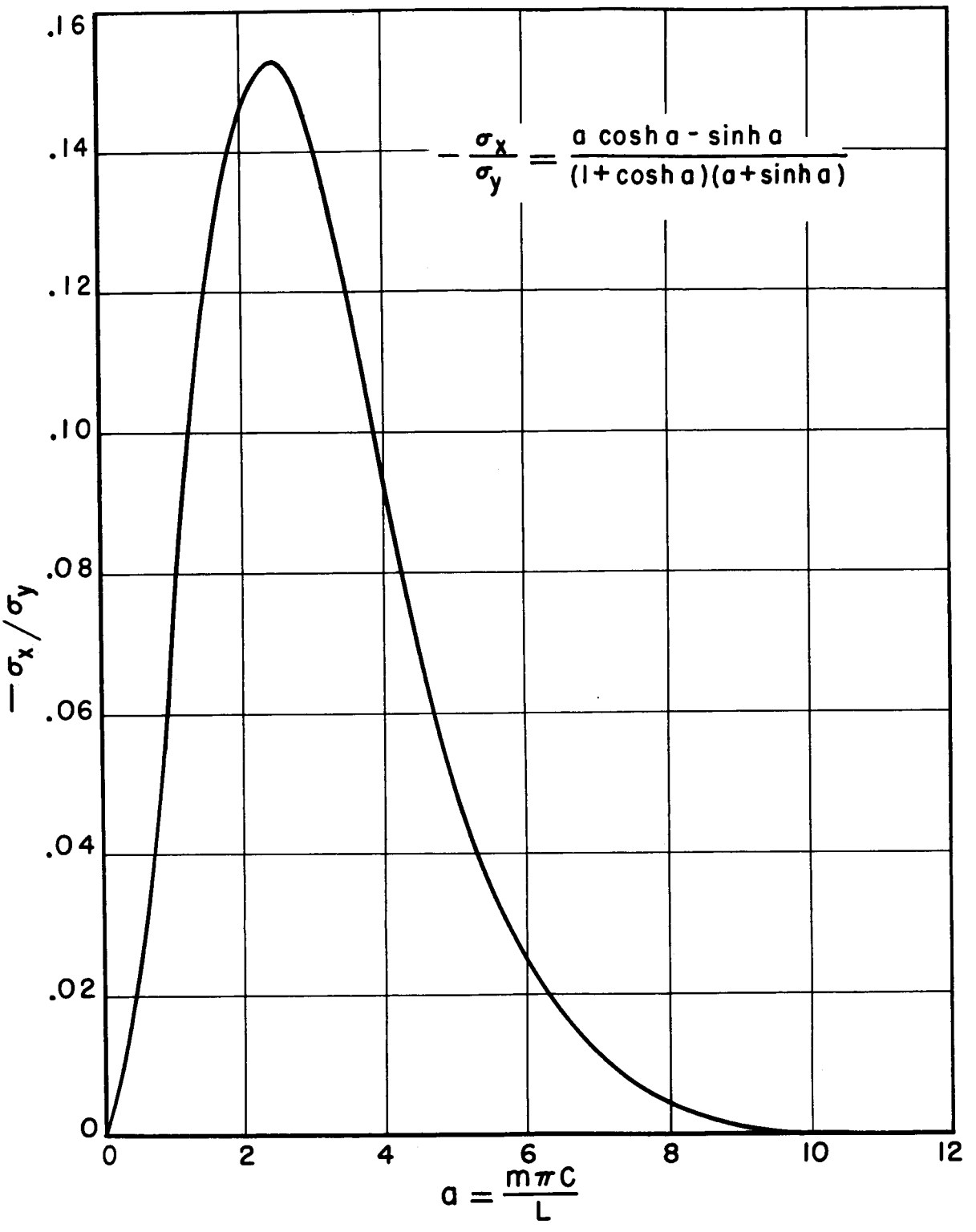

Fig. 11 RATIO OF TRANSVERSE TO AXIAL STRESSES IN A NON-UNIFORMLY LOAD BLOCK

contact, it follows that smaller specimens should be stronger than larger ones. This observation is based on the obvious and simple result from extreme value statistics that the maximum amplitudes are smaller in small specimens.

The ultimate compressive strengths of segmented columns were determined for two glass sizes and two levels of interface roughness for each size. Some of the 2x4x1/2 inch "as received" glass blocks (5-7 lightbands) were lapped to a flatness of 2-3 lightbands. A portion of the segments from each of the resulting groups were then cut to produce 1x2x1/2 inch segments. The columns corresponding to the four types of segments were slowly loaded in compression until catastrophic failure occurred and the maximum nominal stress was recorded. These ultimate compressive strengths are given in Table 1. Each value listed represents the average strength of three five-segment columns. It can be seen that the strength increases as the segments become flatter and as they become smaller.

Although the tests appear to support the roughness hypothesis, it should be pointed out that there are other possible explanations for the observed behavior. First, the small sample sizes used may not lead to a valid statistical inference concerning the average values. Second, if a weakest link mechanism controls the strength of glass in compression, the observed size effect would also appear in monolithic columns. Lastly, the cross-sectional area to circumference ratio of the larger segments is greater than that of the smaller segments; consequently, a "skin strength" theory could produce the observed size effect.

Table 1 ULTIMATE COMPRESSIVE STRENGTHS OF SEGMENTED GLASS COLUMNS

Nominal Size	Ultimate Compressive Stress	
	"As Received" 5-7 Lightbands	"Lapped" 2-3 Lightbands
2 x 4 x 1/2 in.	52, 450 psi	53, 445 psi
1 x 2 x 1/2 in.	56, 966 psi	66, 533 psi

3. Tri-Axial Compression Tests

If, as we contend, premature failure of a segmented column is caused by the presence of transverse tensile stresses, dramatic increases in axial compressive strength can be anticipated through the application of a lateral compressive prestress. In the tests described in this section, it was pragmatic to apply the lateral prestress by means of a hydrostatic pressure. In real members the lateral prestress may be achieved by tension wrapping the member with high strength tendons or perhaps shrink fitting a jacket about them.

The tri-axial compression setup shown in Fig. 12 was used to determine the ultimate compressive strengths of segmented column specimens similar to that illustrated in Fig. 13. The apparatus used subjected the columns to an axial force in addition to a hydrostatic pressure. The test results are summarized in Table 2 where we observe that the increase in axial failure stress is greater than the lateral stress. When interpreting the test results, one must bear in mind that only the axial force can produce transverse tensile stresses since the fluid penetrates between the segments.

Table 2

COMPRESSION EXPERIMENTS ON FOUR INCH SEGMENTED GLASS PLATE COLUMNS IN A HYDROSTATIC PRESSURE ENVIRONMENT

Test No.	Segment Size	Mean Hydrostatic Pressure (psi)	Environment	Axial Stress at Failure (psi)
1	2"x2"	0	Air	29, 600
2	1"x1"	0	Air	30, 400
3	1"x1"	10, 000	Mil-H-5606A Hydraulic Oil (Red)	58, 400
4	1"x1"	20, 000		72, 200

D. Design Implications of the Interface Problem

Using the setup shown in Fig. 7, the compression stress-strain curves were determined for a number of segmented columns under several different circumstances. Three such curves are shown in Fig. 14 where

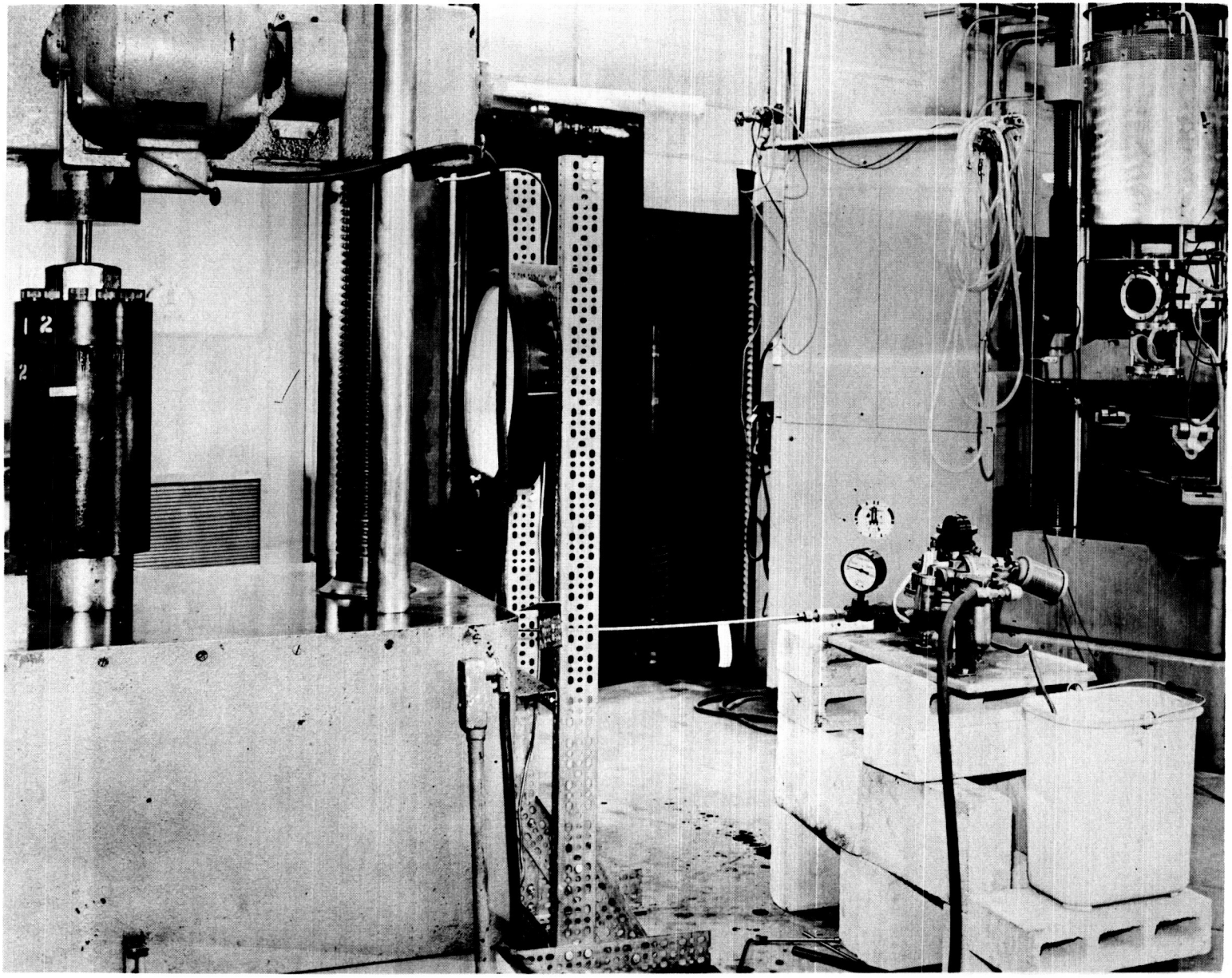

Fig.12 TRI-AXIAL COMPRESSION TEST SET-UP

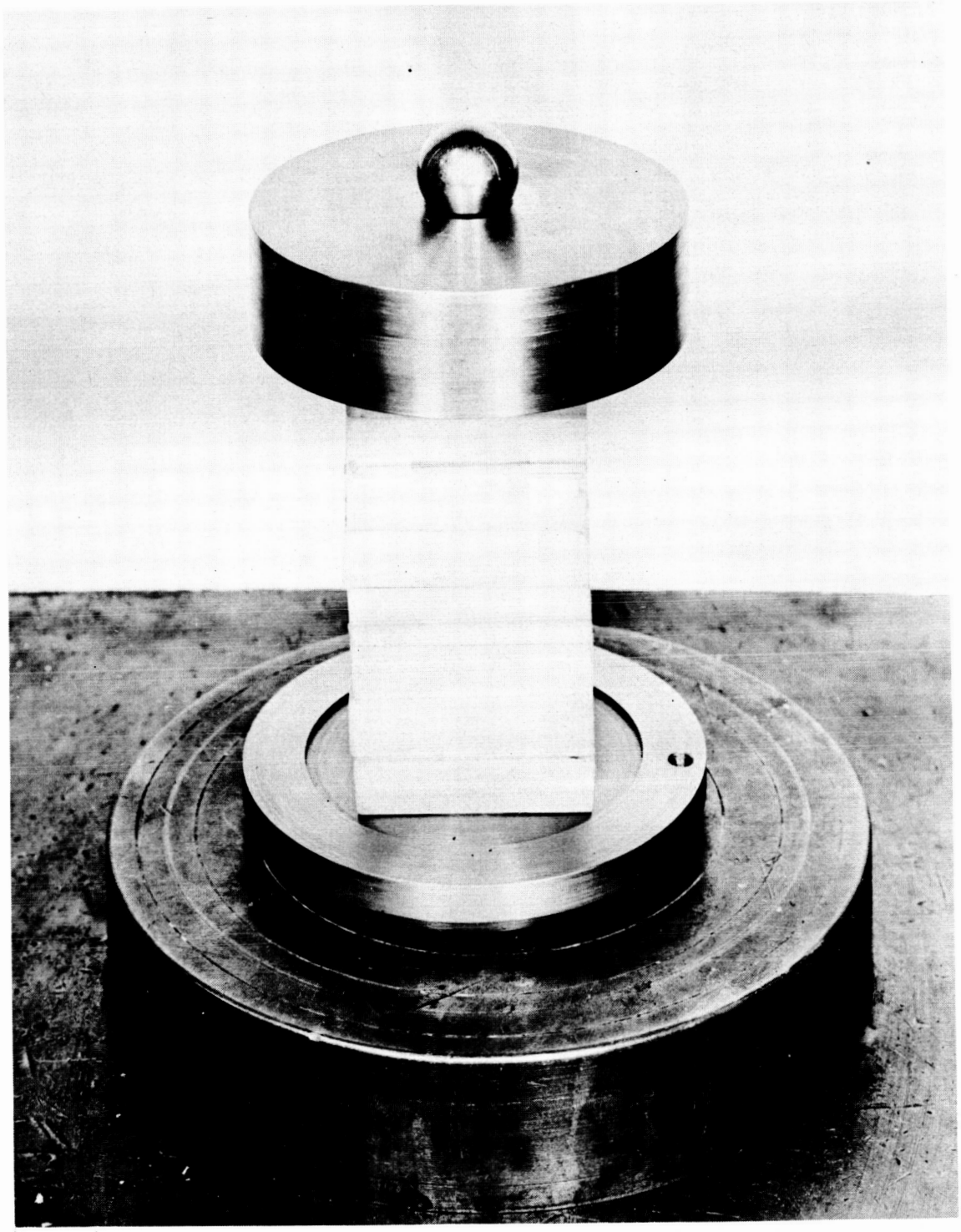

Fig.13 TYPICAL TRI-AXIAL SPECIMEN

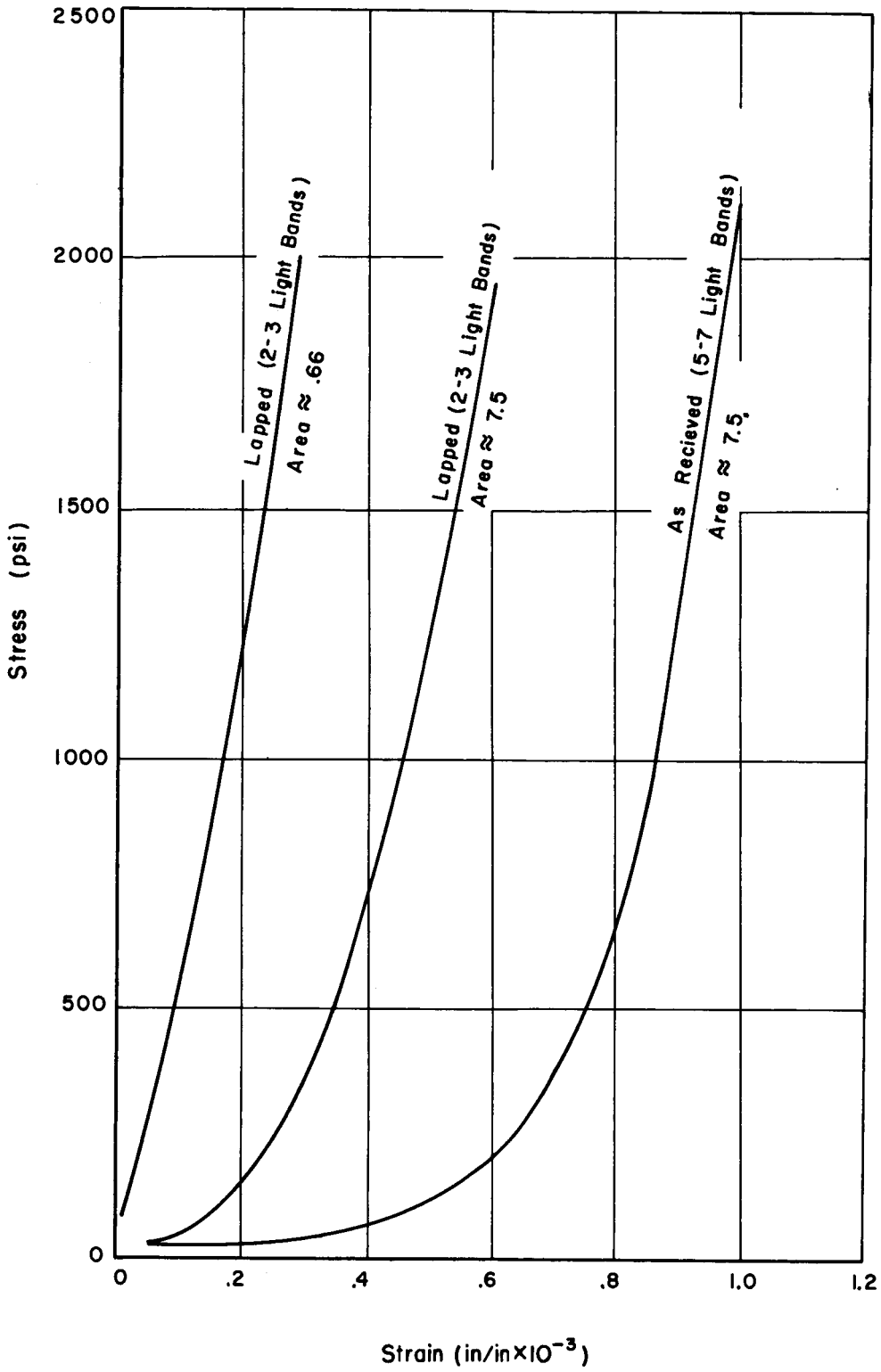

Fig.14 EFFECT OF SIZE ON THE COMPRESSIVE STRESS-STRAIN DIAGRAM OF SEGMENTED GLASS COLUMNS

we observe the general characteristic of a monotonically increasing slope or stiffness. The slope of each of the curves approaches the modulus of elasticity of monolithic glass; however, the lapped specimen has the greatest stiffness at the low stress levels. This size effect precludes the possibility of describing a segmented linear material by an equivalent non-linear material. Because of the monotonically increasing stiffness, the possibility exists that a segmented column can be stable at high loads and unstable at a lower one. This problem can be circumvented by prestressing the column, but not without a weight penalty.

One further complication is found when the reproducibility of a stress-strain curve is examined. As long as a column is never completely unloaded, the stress-strain curve is almost perfectly reproducible in the sense that continuous loading and unloading produces stress-strain coordinates which fall on the same curve. However, if the relative positions of the segments are disturbed after loading and unloading, the subsequent stress-strain curve will be different and sometimes quite different.

IV. LOAD-DEFLECTION CHARACTERISTICS OF PRESTRESSED SEGMENTED BEAMS

This chapter considers the problem of predicting the load-deflection relationship of a prestressed segmented bending member from a knowledge of the properties of its component materials. Specifically, an attempt is made to relate bending behavior to simple column behavior. The approach used to accomplish this objective consists of establishing a first order analytical model of bending behavior and studying how closely the proposed assumptions describe the actual conditions found in real segmented beams.

A. Mathematical Models

Two distinct mathematical models have been developed to account for the segment separation which occurs during the bending of a segmented beam. The first of these, the incremental model shown in Fig. 15a, considers the beam at some instant during the loading process. At this instant the beam is in equilibrium with the applied moment M(x), and in general, cracks will have penetrated into the beam section for some distance along the segment interfaces. The relationship between crack penetration and the bending moment at a station along the beam is established in a straightforward manner from moment equilibrium. If an additional infinitesimal moment $\delta M(x)$ is added to this beam, the resulting infinitesimal response can be calculated as the linear response of the uncracked beam section. The total live load deflection is then found by summing all such infinitesimal responses which occur between $M(x) = 0$ and $M(x) = M(x)\Big|_{final}$.

In the second model, the equilibrium model shown in Fig. 15b, the beam is considered in its final loading state. The portion of the beam which is uncracked is considered to be an elastic beam under the external loading M(x) and the internal loading caused by the prestressing. Since the deflection of an elastic beam can be uniquely determined for every loading, the deflection of the entire beam can be viewed as the deflection of the uncracked portion.

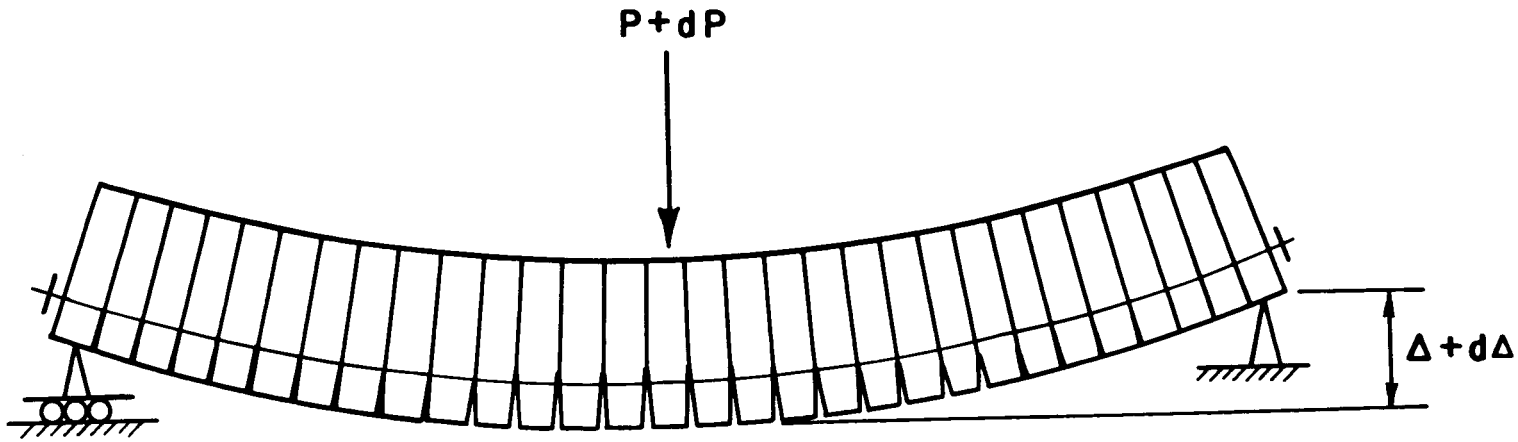

(a) Incremental Model

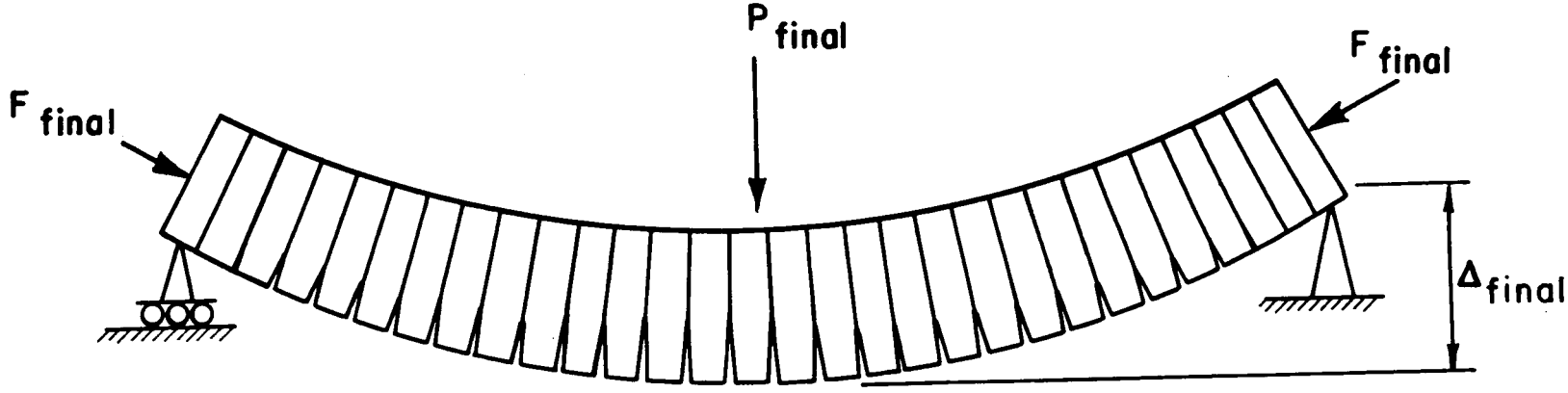

(b) Equilibrium Model

Fig.15 MATHEMATICAL MODELS FOR BENDING RESPONSE

1. General Formulation of the Bending Models (Zero Stiffness Tendons)

Formulation of the incremental and equilibrium models will proceed under the following assumptions: (1) the segment material is linearly elastic up to its ultimate compressive strength, (2) the interfaces are absolutely flat, (3) the tendon stiffness is zero (negligible compared to the segments), (4) the tendons are constrained to deflect with the segments (this eliminates any beam-column action), (5) the number of segments is infinite, and (6) the resultant prestressing force is located within the section kern (this precludes the existence of tensile bending stresses and hence cracking under zero external load).

a) Crack Penetration-Moment Relationship

If the bending moment at a section of a prestressed segmented beam is continuously increased from zero, we experience conventional elastic behavior until a net tensile stress becomes incipient in say the bottom fibers. As the moment is increased further, cracks are formed between the segments (segment separation) at the bottom of the section. That part of the cross-section which is not penetrated by cracks remains linearly elastic. The stresses in this portion of the section must be linearly distributed with a zero tensile stress in the bottom fibers and compressive stresses in the top fibers. These conditions yield the stress block shown in Fig. 16a.

Specializing to the rectangular beam (Fig. 16b), the various properties of a cracked section may be written as functions of the crack penetration f.

$$A_c = b\,(d - f) \tag{5}$$

$$I_c = \frac{b(d - f)^3}{12} \tag{6}$$

$$n_c = (d - f)/2 \tag{7}$$

where A_c, I_c, and n_c are respectively the area, moment of inertia, and distance from the centroid to the outer fiber of the unseparated portion of a crack beam section. The width and depth of the beam are b and d. The

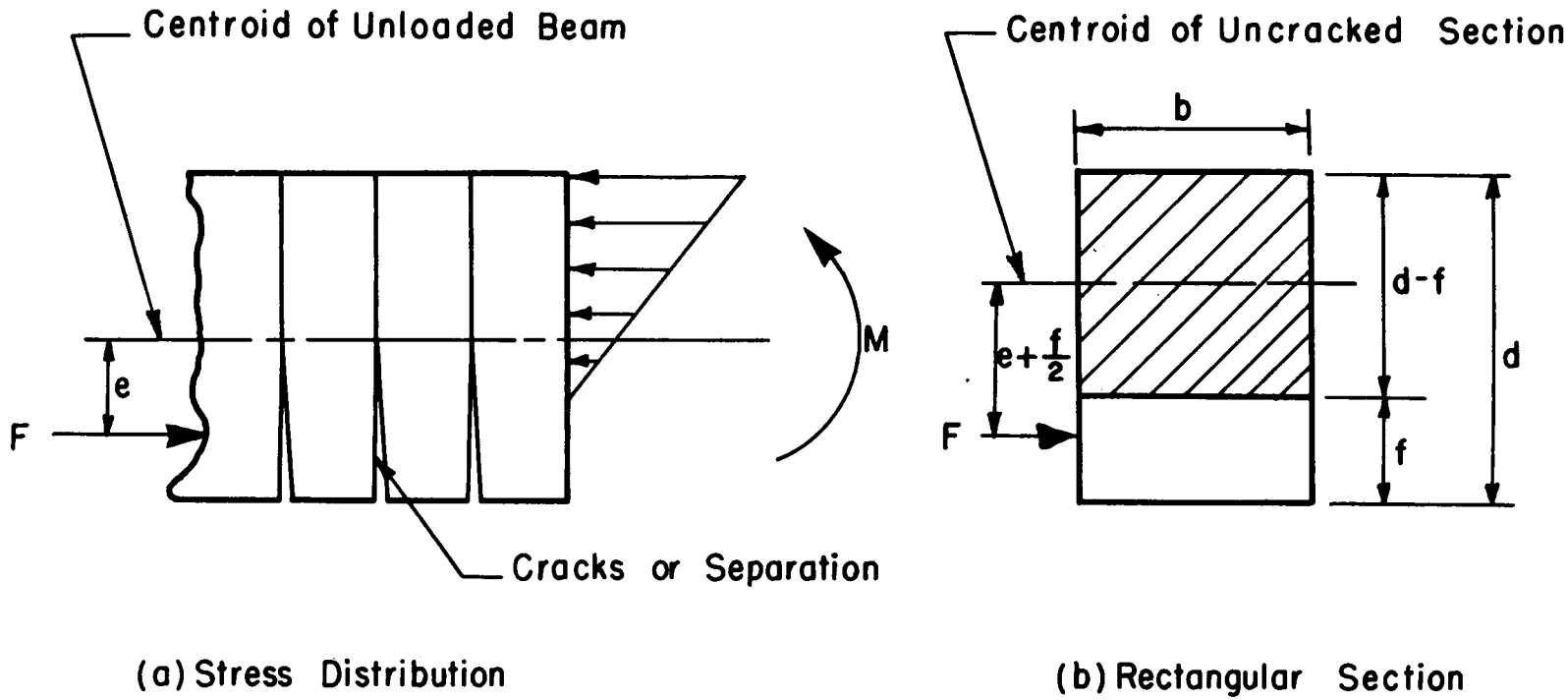

Fig.16 STRESS DISTRIBUTION IN PARTIALLY SEPERATED SEGMENTS

condition of zero stress in the bottom fiber gives us a relation between the bending moment M and the penetration. Hence,

$$\sigma_{bot} = 0 = \frac{-F}{b(d-f)} + \frac{\left[M - F(e + f/2)\right] \frac{(d-f)}{2}}{\frac{b(d-f)^3}{12}} \tag{8}$$

or

$$f = \frac{3M}{F} - \frac{d}{2} - 3e \tag{9}$$

where F is the resultant prestressing force or tendon force and e is its eccentricity. In rectangular beams where negative moments do not occur, one criterion defining the uncracked regions of the span is simply $f \leq 0$. Using Eq. 6, and 9, the moment of inertia of an uncracked cross-section becomes

$$I_c = \alpha(1 - \beta M)^3 \tag{10}$$

$$\alpha \equiv \frac{9b}{4}(e + \frac{d}{2})^3 \; ; \; \beta \equiv \frac{1}{F(e + \frac{d}{2})} \tag{11}$$

We observe that I approaches zero as M approaches $1/\beta = F(e + \frac{d}{2})$. Consequently, for the case of zero stiffness tendons both the deflections and the stresses become unbounded for a finite value of the loading.

b) Incremental Model

Consider a prestressed segmented beam subjected to a distribution of non-negative bending moments of the form

$$M = Pg(x) \tag{12}$$

where P is a load intensity parameter and x is a coordinate along the span. The moment required to crack this beam, M_c, can be found by setting f = 0 in Eq. 9 , thus,

$$M_c = F(e + \frac{d}{6}) \tag{13}$$

The load parameter associated with the appearance of the first crack in the beam is given by

$$P_c = M_c / g_{max}(x) \tag{14}$$

The corresponding deflections Δ_c can be found by conventional methods; for example,

$$\Delta_c = \int_S \frac{\left[P_c g(x) - F e\right] m}{EI} \, dx \tag{15}$$

where E is the modulus of elasticity of the segments, I is the principal moment of inertia of the uncracked beam section, m is the virtual moment resulting from a unit load placed at the point and in the direction of the desired deflection and S represents the portions of the span which are uncracked (here, the entire span). When the beam is in equilibrium under loading P which is greater than P_c, the beam span is divided into the cracked portions S_c defined by $M(x) \geqslant M_c$ and uncracked portions S defined by $M(x) < M_c$. If the loading on this beam is increased by the infinitesimal load dP, the resulting infinitesimal response $d\Delta_k$ is given by

$$d\Delta_k = \int_S \frac{m\, g(x)\, dx}{EI} \, dP + \int_{S_c} \frac{m\, g(x)\, dx}{EI_c(P)} \, dP \tag{16}$$

The total deflection Δ for loads greater than P_c can be found by summing the infinitesimal responses and adding the cracking deflection Δ_c. Hence,

$$\Delta = \Delta_c + \int_{P_c}^{P} \int_{S(P)} \frac{m\, g(x)\, dx}{EI} \, dP + \int_{P_c}^{P} \int_{S_c(P)} \frac{m\, g(x)\, dx}{EI_c(P)} \, dP, \quad P_c \leqslant P < \frac{F\left(e + \frac{d}{2}\right)}{g_{max}(x)} \tag{17}$$

also,

$$\Delta = \int_S \frac{m\left[P\,g(x) - F\,e\right]}{EI}\,dx \qquad P \leqslant P_c \tag{18}$$

c) Example: Terminal Couples by Incremental Method

Specializing Eq. 15, 17 and 18 to the case of a rectangular beam under terminal couples C we obtain for the central deflection

$$\Delta = 2\int_0^{L/2} \frac{(C_c - F\,e)\,(x/2)}{EI}\,dx + 0 + \int_{C_c}^{C} 2\left[\int_0^{L/2} \frac{(x/2)\cdot 1}{E\,\alpha\,(1-\beta\,C)^3}\,dx\right] dP$$

$$= \frac{L^2}{16\,E\alpha\beta\,(1-\beta\,C)^2} \qquad F\left(e + \frac{d}{6}\right) \leqslant C < F\left(e + \frac{d}{2}\right) \tag{17a}$$

$$\Delta = 2\int_0^{L/2} \frac{(x/2)\,(C - F\,e)}{EI}\,dx$$

$$= \frac{3(C - F\,e)\,L^2}{2\,E\,b\,d^3} = \frac{(C - Fe)\,L^2}{8\,E\alpha\,(1-\beta C_c)^3} \qquad C < F\left(e + \frac{d}{6}\right) = C_c \tag{18a}$$

where $m = x/2$, P was replaced by C, and $g(x) \equiv 1$. The value of C is limited by the compressive strength of the material σ_o. The maximum compressive stress in the cracked section is given by

$$\sigma_{top} = -\frac{2F^2\beta}{3b\,(1-\beta C)} \tag{19}$$

From this we find the limiting moment to be

$$C \leqslant F\left[e + \frac{d}{2} + \frac{2F}{3b\,\sigma_o}\right] \tag{20}$$

We note that when $C \to \frac{1}{\beta} = F\left(\frac{d}{2} + e\right)$ both the deflection Δ and the maximum stress σ_{top} become infinite.

The load deflection diagram and the crack penetration diagram are shown in Fig. 17 for a rectangular titanium-carbide beam with the following characteristics:

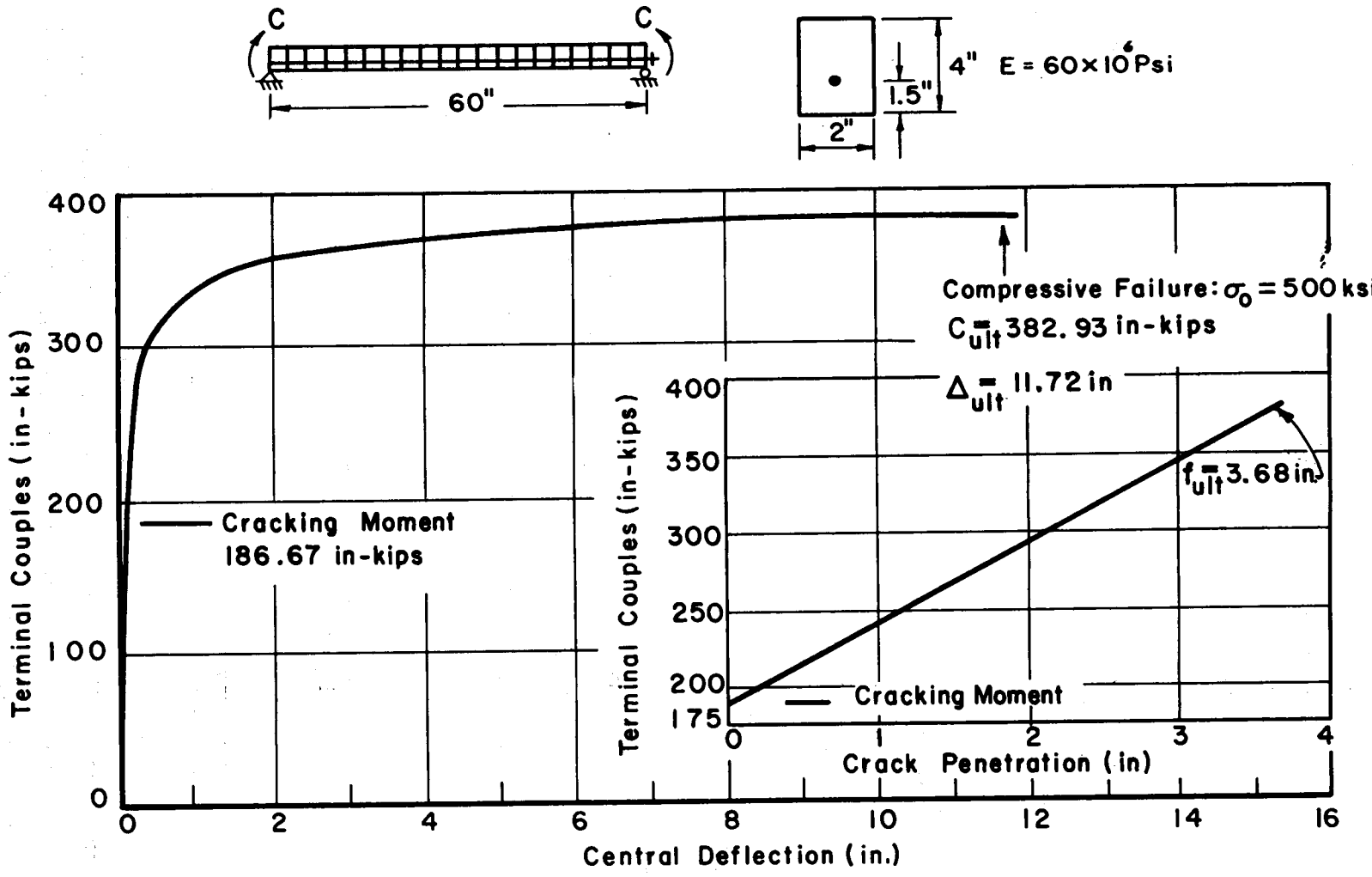

Fig.17 LOAD DEFLECTION AND CRACK PENETRATION DIAGRAMS
PRESTRESSING FORCE: 160 kips

$b = 2$ in.

$d = 4$ in.

$e = 0.5$ in.

$E = 60 \times 10^6$ psi

$P = 160$ kips

$\sigma_o = -500,000$ psi

d. Equilibrium Model

Returning to the beam treated in Section (b), we shall formulate the deflection problem by considering the beam in equilibrium under its final state of loading. If no cracks have formed in the beam, that is if $M(x) \leq M_c$, the deflection is identical to Eq. 18, i.e.,

$$\Delta = \int_S \frac{(M - Fe)\, m}{EI}\, dx \qquad M(x) \leq M_c \tag{21}$$

On the other hand, when part of the span has been penetrated by cracks the deflection becomes

$$\Delta = \int_S \frac{(M - Fe)m}{EI}\, dx + \int_{S_c} \frac{\left[M - F(e + \frac{f}{2})\right] m}{E\alpha(1 - \beta M)^3}\, dx \;, \quad M_c \leq M < F(e + \frac{d}{2}) \tag{22}$$

e. Example: Terminal Couples by Equilibrium Method

For the central deflection, Eq. 22 specializes as follows:

$$\Delta = 0 + 2\int_0^{L/2} \frac{\left[C - F(e + \frac{f}{2})\right] (x/2)}{E\alpha(1-\beta C)^3}\, dx \tag{22a}$$

$$= \frac{\left[C - F(e + \frac{f}{2})\right] L^2}{8\, E\alpha(1 - \beta C)^3} = \frac{L^2}{16\, E\alpha\beta(1-\beta C)^2}$$

We observe that the two models produce identical results for terminal bending, but that the equilibrium model is analytically much simplier. In all of the cases studied, with zero stiffness or elastic tendons, both models always produced identical load-deflection relationships.

f. Example: Concentrated Load on a Simple or Cantilever Beam

The constant bending moment associated with terminal loading suppresses several of the complications which arise in the general loading case. For example, a number of spanwise discontinuities appear in the integrands of our two formulations. These occur at discontinuities in the form or slope of the external bending moment diagram, at the point of application of the virtual unit load, and at the stations separating the cracked and uncracked portions of the span. To illustrate how these discontinuities are handled, the general deflection analysis of an end loaded cantilever is formulated in Fig. 18 and 19 using the two models. Both formulations lead to impressive algebraic problems which produce, nevertheless, identical closed form solutions. Instead of presenting these results, we shall describe the general solution for the deflection curve of a simply supported beam subjected to a concentrated load placed anywhere in the span. The solution for the cantilever is, of course, embedded in this solution which is given in Fig. 20.

2. Simply Supported Beams with Elastic Tendons (Equilibrium Method)

In general the tendon force will not remain constant as the magnitude of the loading on the beam increases. This fact introduces another complication into the mathematical description of the bending behavior of prestressed segmented beams. In fact only the simplest of loadings - terminal couples - is tractable without recourse to a computer. The equilibrium method was chosen in this section because of its analytic simplicity. Although it was also programmed for the computer, there is a possibility that the incremental model is better suited for this purpose.

a. General Relationships

If the applied bending moment distribution, M(x), is represented in the form of Eq. 12

$$M(x) = P\,g(x) \tag{12}$$

where P is a load intensity parameter and x is a coordinate along the

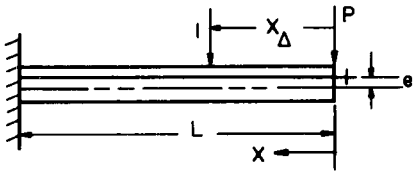

$$P \le P_c = \frac{F}{L}\left(e + \frac{d}{6}\right)$$

$$\Delta_1(P) = \int_0^{X_\Delta} \frac{(Px - Fe)(0)}{EI}\,dx + \int_{X_\Delta}^{L} \frac{(Px - Fe)(X - X_\Delta)}{EI}\,dx$$

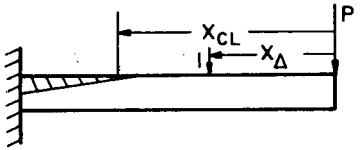

$$P_c \le P \le P_\Delta = \frac{F}{X_\Delta}\left(e + \frac{d}{6}\right)$$

$$\Delta_2(P) = \Delta_1(P_c) + \int_{P_c}^{P}\int_0^{X_\Delta} \frac{X(0)}{EI}\,dx\,dP + \int_{P_c}^{P}\int_{X_\Delta}^{X_{CL}(P)} \frac{X(X - X_\Delta)}{EI}\,dx\,dP + \int_{P_c}^{P}\int_{X_{CL}(P)}^{L} \frac{X(X - X_\Delta)}{E\alpha(1 - \beta Px)^3}\,dx\,dP$$

Where $X_{CL} = \frac{F}{P}\left(e + \frac{d}{6}\right)$

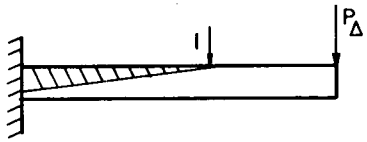

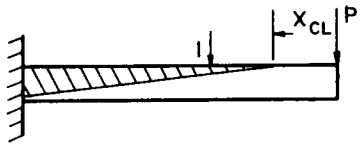

$$P_\Delta \le P \le P_\infty = \frac{F}{L}\left(e + \frac{d}{2}\right)$$

$$\Delta_3(P) = \Delta_2(P_\Delta) + \int_{P_\Delta}^{P}\int_0^{X_{CL}(P)} \frac{X(0)}{EI}\,dx\,dP + \int_{P_\Delta}^{P}\int_{X_{CL}(P)}^{X_\Delta} \frac{X(0)}{E\alpha(1 - \beta Px)^3}\,dx\,dP + \int_{P_\Delta}^{P}\int_{X_\Delta}^{L} \frac{X(X - X_\Delta)}{E\alpha(1 - \beta Px)^3}\,dx\,dP$$

Fig. 18 INCREMENTAL FORMULATION FOR A RECTANGULAR CANTILEVER BEAM

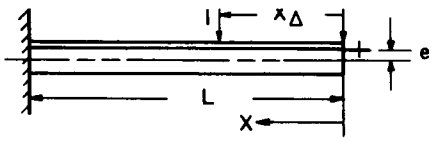

$$P \le P_c = \frac{F}{L}\left(e + \frac{d}{6}\right)$$

$$\Delta_1(P) = \int_0^{X_\Delta} \frac{(Px - Fe)(0)}{EI}\,dx + \int_{X_\Delta}^{L} \frac{(Px - Fe)(X - X_\Delta)}{EI}\,dx$$

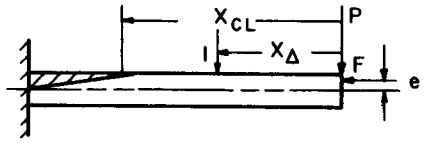

$$P_c \le P \le P_\Delta = \frac{F}{X_\Delta}\left(e + \frac{d}{6}\right)$$

$$\Delta_2(P) = \int_0^{X_\Delta} \frac{(Px - Fe)(0)}{EI}\,dx + \int_{X_\Delta}^{X_{CL}} \frac{(Px - Fe)(X - X_\Delta)}{EI}\,dx + \int_{X_{CL}}^{L} \frac{\left[Px - F\left(e + \frac{f}{2}\right)\right](X - X_\Delta)}{E\alpha(1 - \beta Px)^3}\,dx$$

Where $X_{CL} = \frac{F}{P}\left(e + \frac{d}{6}\right)$, $f = \frac{3M}{P} - \frac{d}{2} - 3e$

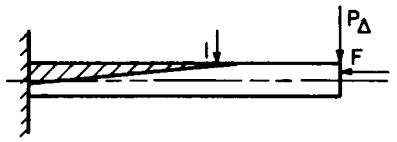

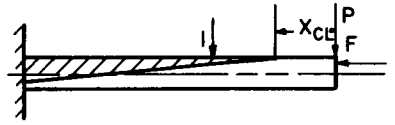

$$P_\Delta \le P \le P_\infty = \frac{F}{L}\left(e + \frac{d}{2}\right)$$

$$\Delta_3(P) = \int_0^{X_{CL}} \frac{(Px - Fe)(0)}{EI}\,dx + \int_{X_{CL}}^{X_\Delta} \frac{\left[Px + F\left(e + \frac{f}{2}\right)\right](0)}{E\alpha(1 - \beta Px)^3}\,dx + \int_{X_\Delta}^{L} \frac{\left[Px + F\left(e + \frac{f}{2}\right)\right](X - X_\Delta)}{E\alpha(1 - \beta Px)^3}\,dx$$

Fig. 19 EQUILIBRIUM FORMULATION FOR A RECTANGULAR CANTILEVER BEAM

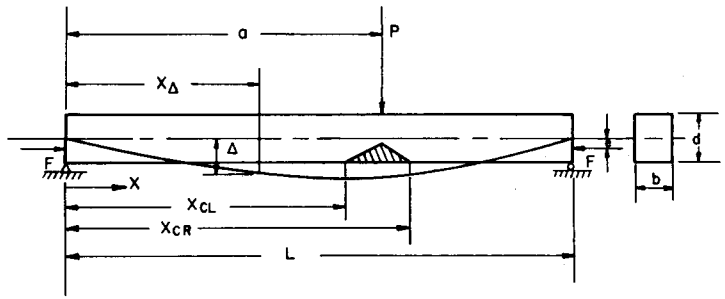

For $0 \le P \le \frac{F\left(e+\frac{d}{6}\right)}{a\left(1-\frac{a}{L}\right)}$ and $0 \le X_\Delta \le a$ $\quad \Delta = \frac{12}{bd^3E}\left(\frac{X_\Delta}{L}\right)\left\{\frac{PL^3}{6}\left(1-\frac{a}{L}\right)\left[\left(\frac{a}{L}\right)\left(2-\frac{a}{L}\right)-\left(\frac{X_\Delta}{L}\right)^2\right]-\frac{FeL^2}{2}\left(1-\frac{X_\Delta}{L}\right)\right\}$

For $\frac{F\left(e+\frac{d}{6}\right)}{a\left(1-\frac{a}{L}\right)} \le P \le \frac{F\left(e+\frac{d}{2}\right)}{a\left(1-\frac{a}{L}\right)}$, and

Case (1) $0 \le X_\Delta \le \frac{F\left(e+\frac{d}{6}\right)}{P\left(1-\frac{a}{L}\right)}$

$$\Delta = \frac{12}{bd^3E}\left(\frac{X_\Delta}{L}\right)\left[-\frac{PL^3}{6}\left(1-\frac{a}{L}\right)\left(\frac{X_\Delta}{L}\right)^2+\frac{FeL^2}{2}\left(\frac{X_\Delta}{L}\right)+\frac{F^2L\left(e+\frac{d}{6}\right)\left(\frac{d}{6}-e\right)}{2P\left(1-\frac{a}{L}\right)}-\frac{F^3d^3}{54P^2}\left\{\frac{2\left(\frac{a}{L}\right)-1}{\left\{\frac{a}{L}\left(1-\frac{a}{L}\right)\right\}^2}\left\{\ln\left[\frac{3}{d}\left(e+\frac{d}{2}\right)-\frac{3PL}{Fd}\left(\frac{a}{L}\right)\left(1-\frac{a}{L}\right)\right]-\frac{3}{d}\left(e+\frac{d}{2}\right)\right.\right.$$

$$\left.\left.+\frac{F\left(e+\frac{d}{2}\right)}{F\left(e+\frac{d}{2}\right)-PL\left(\frac{a}{L}\right)\left(1-\frac{a}{L}\right)}+\frac{9\left(e+\frac{d}{6}\right)^2\left(\frac{d}{3}-e\right)}{d^3}\right\}-\frac{1}{1-\frac{a}{L}}\left[\frac{PL}{F\left(e+\frac{d}{2}\right)-PL\left(\frac{a}{L}\right)\left(1-\frac{a}{L}\right)}-\frac{3PL}{Fd}\right]\right\}\right]$$

Case (2) $\frac{F\left(e+\frac{d}{6}\right)}{P\left(1-\frac{a}{L}\right)} \le X_\Delta \le a$

$$\Delta = \frac{2F^3}{9P^2bE}\left\{\frac{9\left(e+\frac{d}{6}\right)^2\left(\frac{d}{3}-e\right)}{d^3\left(1-\frac{a}{L}\right)^2}\left\{1-\left(\frac{X_\Delta}{L}\right)\left(\frac{L}{a}\right)^2\left[2\left(\frac{a}{L}\right)-1\right]\right\}+\frac{1}{\left(1-\frac{a}{L}\right)^2}\left\{\ln\left[\frac{3}{d}\left(e+\frac{d}{2}\right)-\frac{3PL}{Fd}\left(1-\frac{a}{L}\right)\left(\frac{X_\Delta}{L}\right)\right]+\frac{F\left(e+\frac{d}{2}\right)}{F\left(e+\frac{d}{2}\right)-PL\left(1-\frac{a}{L}\right)\left(\frac{X_\Delta}{L}\right)}-\frac{3}{d}\left(e+\frac{d}{2}\right)\right\}\right.$$

$$\left.+\frac{1}{1-\frac{a}{L}}\left(\frac{X_\Delta}{L}\right)\left\{\frac{PL}{F\left(e+\frac{d}{2}\right)-PL\left(\frac{a}{L}\right)\left(1-\frac{a}{L}\right)}-\frac{PL}{F\left(e+\frac{d}{2}\right)-PL\left(1-\frac{a}{L}\right)\left(\frac{X_\Delta}{L}\right)}\right\}-\frac{2\left(\frac{a}{L}\right)-1}{\left\{\frac{a}{L}\left(1-\frac{a}{L}\right)\right\}^2}\left(\frac{X_\Delta}{L}\right)\left\{\ln\left[\frac{3}{d}\left(e+\frac{d}{2}\right)-\frac{3PL}{Fd}\left(\frac{a}{L}\right)\left(1-\frac{a}{L}\right)\right]+\frac{F\left(e+\frac{d}{2}\right)}{F\left(e+\frac{d}{2}\right)-PL\left(\frac{a}{L}\right)\left(1-\frac{a}{L}\right)}-\frac{3}{d}\left(e+\frac{d}{2}\right)\right\}\right]$$

Fig. 20 PRESTRESSED SEGMENTED SIMPLY SUPPORTED BEAM-ZERO STIFFNESS TENDON

pan, then the tendon force F may be expressed as a function of P, i.e.

$$F = F(P) \tag{23}$$

'he initial tendon force or prestress, F_o, is defined when P = o, i.e.,

$$F_o = F(o) \tag{24}$$

'efine T to be the resultant moment acting about the "neutral axis" of ıe uncracked portion of the cross section. Referring to Fig. 16, for ectangular cross section,

$$T = M - F(e + \frac{f}{2}) \tag{25}$$

he crack penetration f becomes

$$\begin{aligned} f &= o \ , \quad \text{for } \frac{M}{F} \leq e + \frac{d}{6} \\ f &= d - \frac{6T}{F} \ , \quad \text{for } \frac{M}{F} \geq e + \frac{d}{6} \end{aligned} \tag{26}$$

hus the resultant moment may be further expressed as

$$\begin{aligned} T &= M - Fe \ , \quad \text{for } \frac{M}{F} \leq e + \frac{d}{6} \\ T &= \frac{1}{2}\left[F(e + \frac{d}{2}) - M\right], \quad \text{for } \frac{M}{F} \geq e + \frac{d}{6} \end{aligned} \tag{27}$$

'he section properties may be expressed as

$$\begin{aligned} A &= A(M) \\ A_o &= A(o) = bd \\ A_c &= b(d-f) = 6b\frac{T}{F} \end{aligned} \tag{28}$$

$$\begin{aligned} I &= I(M) \\ I_o &= I(o) \\ I_c &= \frac{b(d-f)^3}{12} = 18b\left(\frac{T}{F}\right)^3 \end{aligned} \tag{29}$$

or a simply supported beam, the deflection at $x = x_\Delta$ may be expressed as

$$\Delta = \int_0^L \frac{T\, m_\Delta}{EI}\, dx \tag{30}$$

where

$$m_\Delta = (1 - \frac{x_\Delta}{L})\, x \quad , \text{ for } \; o \leqslant x \leqslant x_\Delta$$

$$m_\Delta = \frac{x_\Delta}{L}\,(L-x) \quad , \text{ for } \; x_\Delta \leqslant x \leqslant L \tag{31}$$

The slope at the left end is given by

$$\theta_L = \int_0^L \frac{T m_L}{EI}\, dx \tag{32}$$

where

$$m_L = (1 - \frac{x}{L}) \tag{33}$$

and the slope at the right end is given by

$$\theta_R = \int_0^L \frac{T m_R}{EI}\, dx \tag{34}$$

where

$$m_R = \frac{x}{L} \tag{35}$$

Dividing the beam into its uncracked portions S, $M/F \leqslant e + d/6$, and its cracked portion S_c, $M/F \geqslant e + d/6$, and utilizing Eq. 27 and 29, Eq. 30 may be expressed as

$$\Delta = \frac{1}{EI_o} \int_S T m_\Delta dx + \frac{F^3}{18bE} \int_{S_c} \frac{m_\Delta dx}{T^2} \tag{36}$$

$$= \frac{1}{EI_o} \int_S \left[M(x) - Fe\right] m_\Delta(x)\, dx + \frac{2F^3}{9bE} \int_{S_c} \frac{m_\Delta(x)\, dx}{\left[F(e+\frac{d}{2}) - M(x)\right]^2}$$

Similarly, Eq. 32 and 34 become

$$\theta_L = \frac{1}{EI_o} \int_S \left[M(x) - Fe\right] m_L(x)\, dx + \frac{2F^3}{9bE} \int_{S_c} \frac{m_L(x)\, dx}{\left[F(e + \frac{d}{2}) - M(x)\right]^2} \tag{37}$$

$$\theta_R = \frac{1}{EI_o} \int_S \left[M(x) - Fe\right] m_R(x)\, dx + \frac{2F^3}{9bE} \int_{S_c} \frac{m_R(x)\, dx}{\left[F(e + \frac{d}{2}) - M(x)\right]^2} \tag{38}$$

If M(x) is represented in the form of Eq.12, then

$$\begin{aligned} \Delta &= \Delta(P) \\ \Delta_o &= \Delta(o) \end{aligned} \tag{39}$$

$$\begin{aligned} \theta_L &= \theta_L(P) \\ \theta_{Lo} &= \theta_L(o) = -\frac{F_o eL}{2EI_o} \end{aligned} \tag{40}$$

$$\begin{aligned} \theta_R &= \theta_R(P) \\ \theta_{Ro} &= \theta_R(o) = -\frac{F_o eL}{2EI_o} \end{aligned} \tag{41}$$

If A_t and E_t are respectively the cross sectional area and the modulus of elasticity of the tendon, and if f_L and f_R represent respectively the crack penetrations at the left and right ends of the beam, then the change in the length of the tendon may be expressed as

$$\frac{(F-F_o)L}{A_t E_t} = (e + \frac{f_L}{2})(\theta_L - \theta_{Lo}) + (e + \frac{f_R}{2})(\theta_R - \theta_{Ro}) - \frac{F-F_o}{E} \int_0^L \frac{dx}{A} \tag{42}$$

Regrouping this equation into a more convenient form, we obtain,

$$F = F_o + \frac{(e + \frac{f_L}{2})(\theta_L - \theta_{Lo}) + (e + \frac{f_R}{2})(\theta_R - \theta_{Ro})}{\frac{L}{A_t E_t} + \frac{1}{E} \int_0^L \frac{dx}{A}} \tag{43}$$

Now, given the loading M(x), the value of the tendon force F may be determined from Eq. 43; however, even in the simplest case, M(x) = constant, F cannot be determined explicitly.

b. Example: Terminal Couples - Central Deflection

Returning to the example of a rectangular beam under terminal couples, $M(x) = C$, we may now determine the effect of tendon stiffness. For this very special case the spanwise integrations are very simple and Eq. 36 and 38 may be expressed as

$$\Delta = \frac{T L^2}{8 E I} \tag{44}$$

$$\theta_L = \theta_R \equiv \theta = \frac{T L}{2 E I} \tag{45}$$

The resultant moment from Eq. 27 becomes

$$\begin{aligned} T &= C - Fe \quad , \quad \text{for } \frac{C}{F} \leqslant e + \frac{d}{6} \\ T &= \frac{1}{2} \left[F(e + \frac{d}{2}) - C \right], \quad \text{for } \frac{C}{F} \geqslant e + \frac{d}{6} \end{aligned} \tag{46}$$

Case 1. Before Cracking: $\frac{C}{F} \leqslant e + \frac{d}{6}$

Thus

$$\theta = \frac{(C - Fe) L}{2 E I_o} \tag{47}$$

$$f_L = f_R = 0 \tag{48}$$

$$\int_o^L \frac{dx}{A} = \frac{L}{A_o} \tag{49}$$

Insertion of Eq. 47, 48 and 49 into Eq. 42 yields

$$F = F_o + \frac{Ce}{K_1} \tag{50}$$

where

$$K_1 \equiv e^2 + \frac{d^2}{12} \left[1 + \frac{A_o E}{A_t E_t} \right] \tag{51}$$

From Eq. 46

$$T = C\left(1 - \frac{e^2}{K_1}\right) - F_o e \tag{52}$$

From Eq. 44, the center deflection is

$$\Delta = \frac{\left[C\left(1 - \frac{e^2}{K_1}\right) - F_o e\right] L^2}{8 E I_o} \tag{53}$$

The value of the cracking load, C_c, may be found from

$$C_c = F_c\left(e + \frac{d}{6}\right) = \left(F_o + \frac{C_c e}{K_1}\right)\left(e + \frac{d}{6}\right)$$

Thus

$$C_c = \frac{F_o\left(e + \frac{d}{6}\right)}{1 - \frac{e}{K_1}\left(e + \frac{d}{6}\right)} \tag{54}$$

Case 2. After Cracking: $\frac{C}{F} \geqslant e + \frac{d}{6}$

$$\theta = \frac{TL}{2E} \cdot \frac{F^3}{18 b T^3} = \frac{F^3 L}{36 b E T^2} = \frac{FL}{9 b E\left[e + \frac{d}{2} - \frac{C}{F}\right]^2} \tag{55}$$

$$f_L = f_R = d - 3\left(e + \frac{d}{2} - \frac{C}{F}\right) = -3\left(e + \frac{d}{6}\right) + 3\frac{C}{F} \tag{56}$$

$$\int_0^L \frac{dx}{A} = \frac{L}{3 b\left[e + \frac{d}{2} - \frac{C}{F}\right]} \tag{57}$$

Define

$$K_2 \equiv e + \frac{d}{2} \tag{58}$$

$$v \equiv \frac{C}{F} \tag{59}$$

Insertion of Eq. 55, 56 and 57 into Eq. 42 and utilizing Eq. 58 and 59 yields

$$\frac{F}{F_o} = 1 + \frac{1 + \frac{54\,e}{d^3}(K_2 - v)^2}{\frac{3(K_2-v)}{(3v - K_2)}\left[1 + \frac{3\,b(K_2-v)\,E}{A_t E_t}\right] - 1} \tag{60}$$

This is the best that can be done algebraically. In order to determine $F = F(C)$, a plot of F vs. v is made which is subsequently modified to a plot of F vs. C.

From Eq. 44, the center deflection is

$$\Delta = \frac{T L^2}{8 E} \cdot \frac{F^3}{18\,b T^3} = \frac{F^3 L^2}{144\,b E T^2} = \frac{F^3 L^2}{36\,b E \left[F(e + \frac{d}{2}) - C\right]^2} \tag{61}$$

where the corresponding values of F and C must be substituted simultaneously.

Inspection of Eq. 60 reveals some interesting characteristics of elastic tendons. When v attains a certain value, v_u, the denominator is zero and F has a discontinuity.

$$1 + \frac{3\,b\,(K_2 - v_u)\,E}{A_t E_t} = \frac{3\,v_u - K_2}{3(K_2 - v_u)} \tag{62}$$

Solving Eq. 62 for v_u yields

$$v_u = K_2 - \frac{A_t E_t}{3\,b E}\left[\sqrt{1 + \frac{2\,b E K_2}{A_t E_t}} - 1\right] \tag{63}$$

Now $v = v_u$ with $F = \infty$ implies that $C = \infty$ and thus v_u is the maximum value that v attains. The crack penetration is given by

$$f = 3v - 3K_2 \tag{64}$$

and since v attains a maximum, so does f.

$$f_{max} = d - \frac{A_t E_t}{b E}\left[\sqrt{1 + \frac{2\,b E K_2}{A_t E_t}} - 1\right] \tag{65}$$

The implication of Eq. 65 is as follows: When it is assumed that the tendons have zero stiffness, the cracks will open all the way (f = d) at some finite load and this permits an infinite deflection at that load. With elastic tendons, the cracks will never open completely and an infinite deflection can only be attained with an infinite load.

A numerical example is illustrated in Fig. 21 and 22. Figure 21 illustrates the determination of F vs. C while Fig. 22 compares the resulting load deflection curve to the corresponding zero stiffness tendon ($F=F_o$) curve. In this example, it is observed that beyond the cracking load, the elastic tendon makes a significant contribution to the load deflection curve.

c. Numerical Computation Scheme

In order to facilitate the analysis of prestressed segmented beams with elastic tendons under more complex loadings, a numerical scheme has been developed for use on a digital computer. Essentially, the numerical scheme involves nothing more than the evaluation of integrals using Simpson's 1/3 rule and routines for the determination of the tendon force and the cracking load.

In this section, the applied bending moment distribution, M(x), will again be expressed by Eq. 12

$$M(x) = P\,g(x) \tag{12}$$

However, now the load intensity parameter, P , will be chosen such that $g(x)_{max} = 1$.

i. Determination of Cracking Load

The cracking load, P_c , may be expressed as

$$P_c = F_c\,(e + \frac{d}{6}) \tag{66}$$

where F_c is the tendon force corresponding to $P = P_c$. For $0 < P < P_c$, everything behaves linearly, see Fig. 23, and F is expressible as a linear function of P, i.e.,

$$F = F_o + \gamma P \tag{67}$$

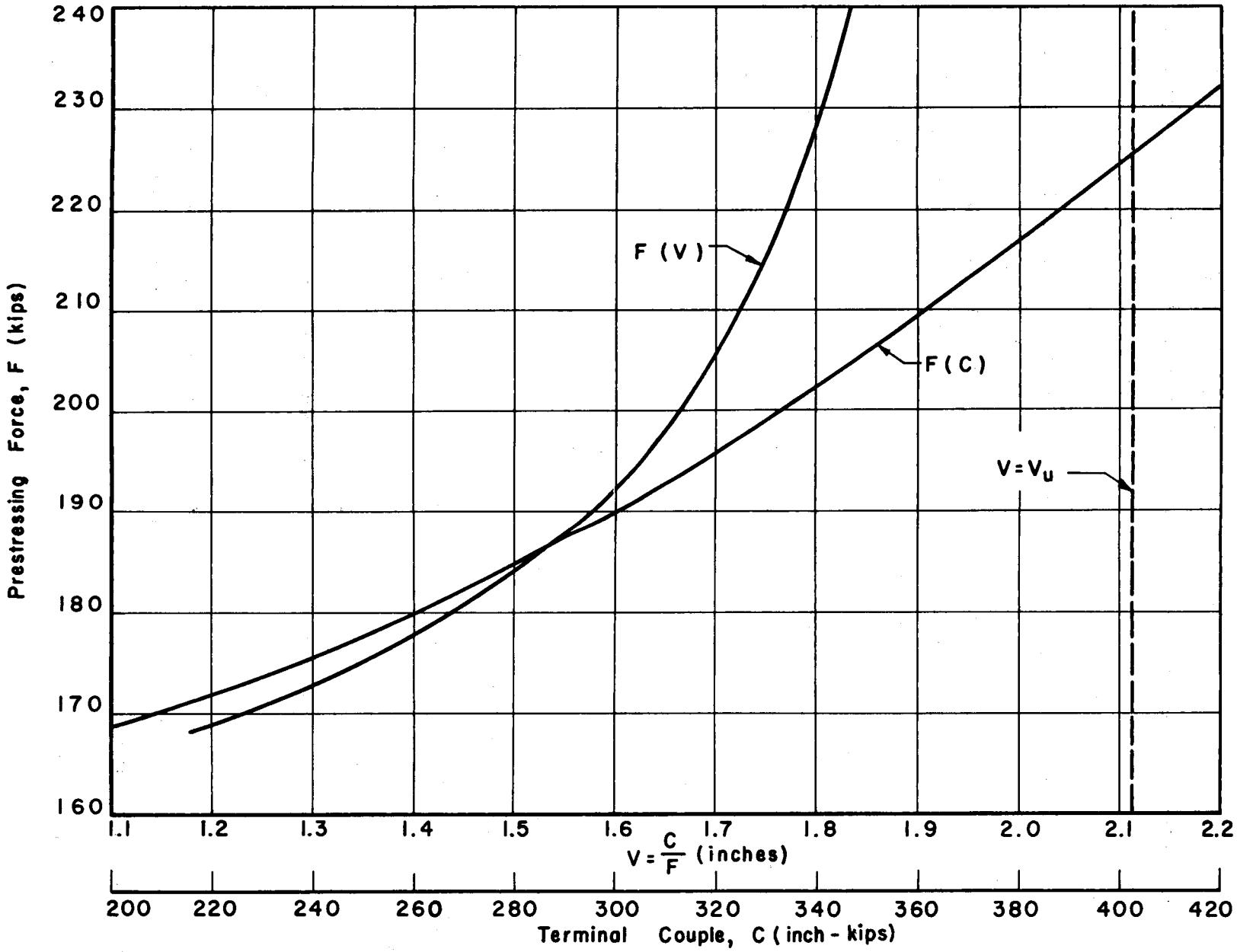

Fig. 21 DETERMINATION OF F vs. C FOR FIGURE 22

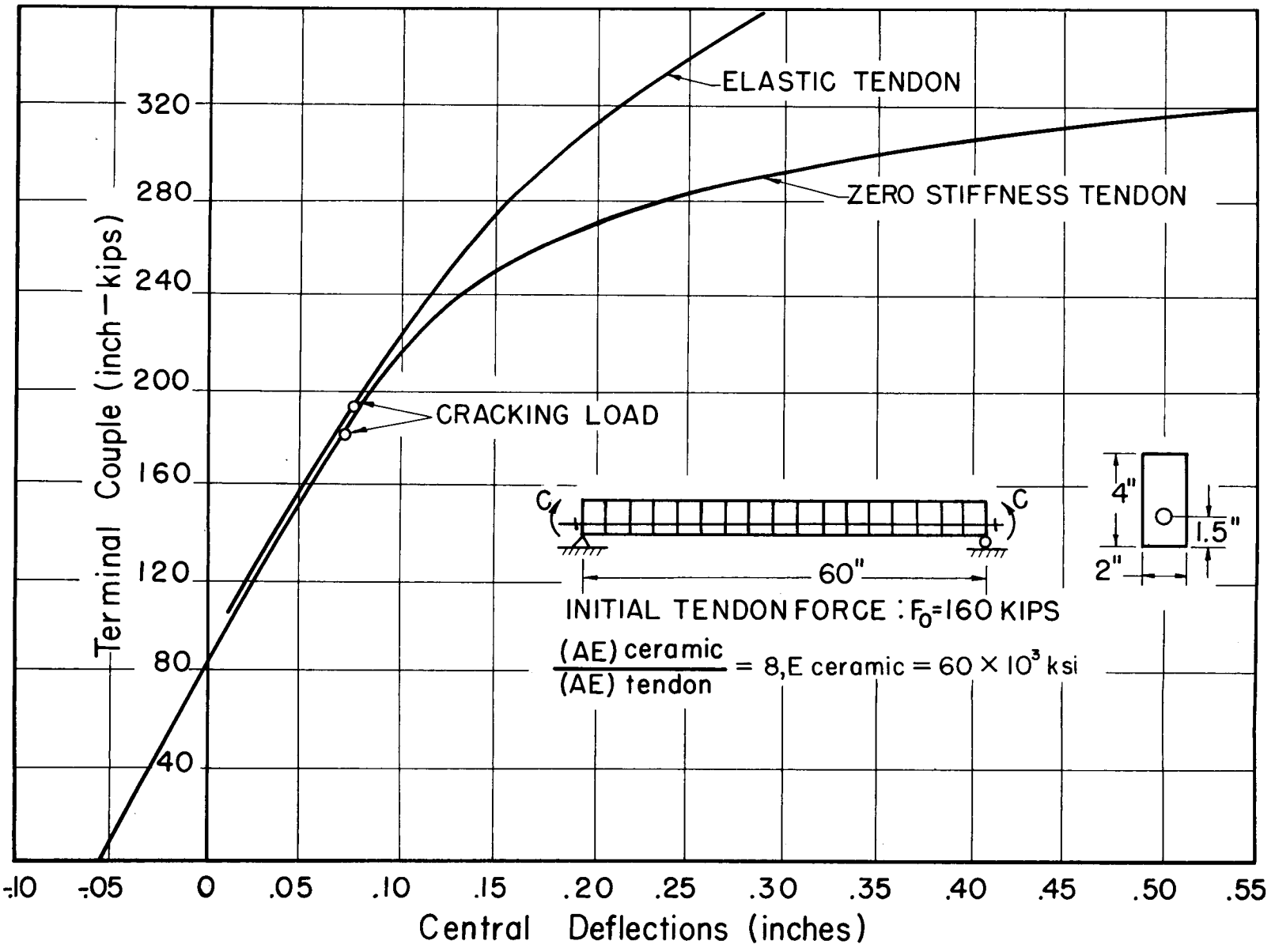

Fig. 22 LOAD-DEFLECTION DIAGRAM FOR A PRESTRESSED SEGMENTED BEAM

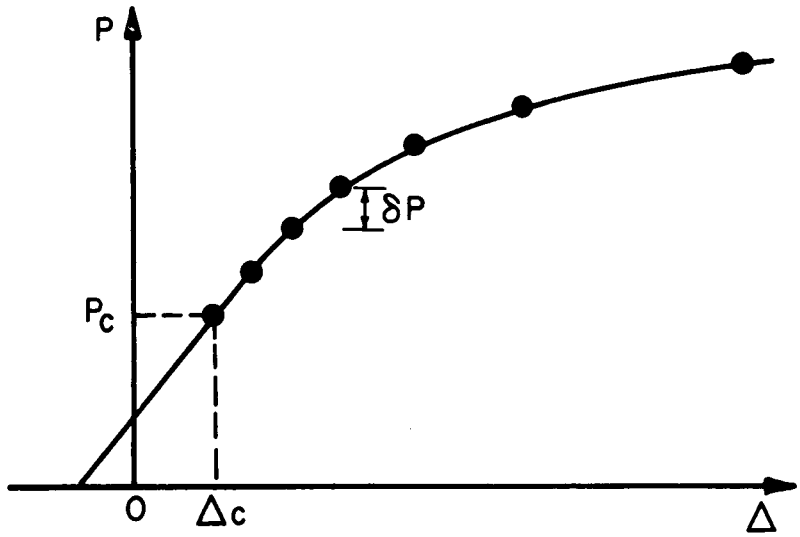

Fig.23 GENERAL LOAD DEFLECTION DIAGRAM

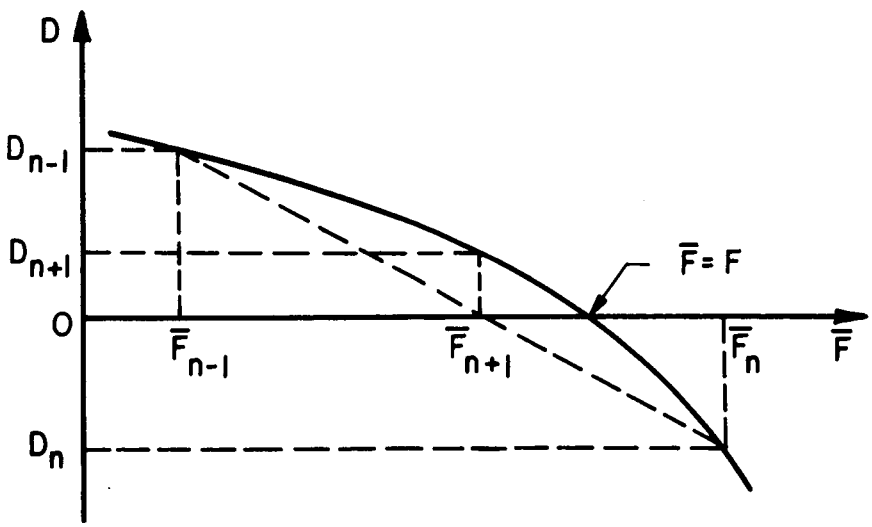

Fig.24 SECANT METHOD FOR DETERMINING THE TENDON FORCE

Let us arbitrarily choose $P = P' = F_o\,(e + \frac{d}{6})$ and solve Eq. 43 for F'. Having P' and F', γ in Eq. 67 may be determined as

$$\gamma = \frac{F' - F_o}{F_o(e + \frac{d}{6})} \tag{68}$$

Eq. 67 now becomes

$$F = F_o + \left(\frac{F' - F_o}{F_o}\right) \frac{P}{(e + \frac{d}{6})} \tag{69}$$

Insertion of $P = P_c$ and $F = F_c$ into Eq. 69, using Eq. 66, yields the cracking load

$$P_c = \frac{F_o^2\,(e + \frac{d}{6})}{2F_o - F'} \tag{70}$$

where F' is determined from Eq. 43 with $P = P' = F_o(e + \frac{d}{6})$.

ii. Determination of Tendon Force

In general, Eq. 43 represents an implicit relationship between the tendon force F and the load intensity P. Thus an iterative scheme is necessary to determine F. One such scheme is the secant method.

Referring to Eq. 43, define

$$D = F_o + \frac{(e + \frac{f_L}{2})(\theta_L - \theta_{Lo}) + (e + \frac{f_R}{2})(\theta_R - \theta_{Ro})}{\frac{L}{A_t E_t} + \frac{1}{E}\int_o^L \frac{dx}{A}} - F \tag{71}$$

Thus, given the value of P, the value of F is sought which makes $D = 0$.

Define $\bar{F}_n$ to be the n^{th} estimate of the tendon force F and D_n to be the corresponding value of D. Thus Eq. 71 may be expressed as

$$D_n = D_n(P, \bar{F}_n) \tag{72}$$

Given $\bar{F}_{n-1}$, D_{n-1} and $\bar{F}_n$, D_n, Fig. 24 illustrates how the secant method is used to determine the following expression for the n+1 estimate.

$$\bar{F}_{n+1} = \frac{\bar{F}_{n-1} D_n - \bar{F}_n D_{n-1}}{D_n - D_{n-1}} \tag{73}$$

In order to use Eq. 72 and 73, all that is needed is two initial guesses: $\bar{F}_1$ and $\bar{F}_2$. Once started, the procedure is to merely cycle back and forth between Eq. 72 and 73 until D_n becomes satisfactorily small enough.

Figure 23 illustrates that the numerical scheme was programmed to increment P by δP for $P > P_c$. Thus when computing the "new" value of the tendon force, F_{new}, corresponding to the "new" load, P_{new}, the old value of the tendon force, F_{old}, is available as a first estimate of F_{new}.

Thus, it seems logical to specify $\bar{F}_1$ and $\bar{F}_2$ as follows:

$$\bar{F}_1 = F_{old} \tag{74}$$

$$\bar{F}_2 = \bar{F}_1 + D_1 \tag{75}$$

These estimates were used in the program and for the lower values of load the routine worked perfectly. However, for higher values of the load it became apparent that these estimates were causing Eq. 72 to yield discontinuous results.

Reflecting back to the previous section where the example of terminal couples was investigated, the tendon force was expressed as a function of the ratio of the terminal couple and itself and that for a certain value of the ratio, the function was discontinuous. It now seems that this characteristic is preserved with more complex loadings and thus in general F is a function of V where $V = P/F$ and F is discontinuous at $V = V_u$. See Fig. 25a.

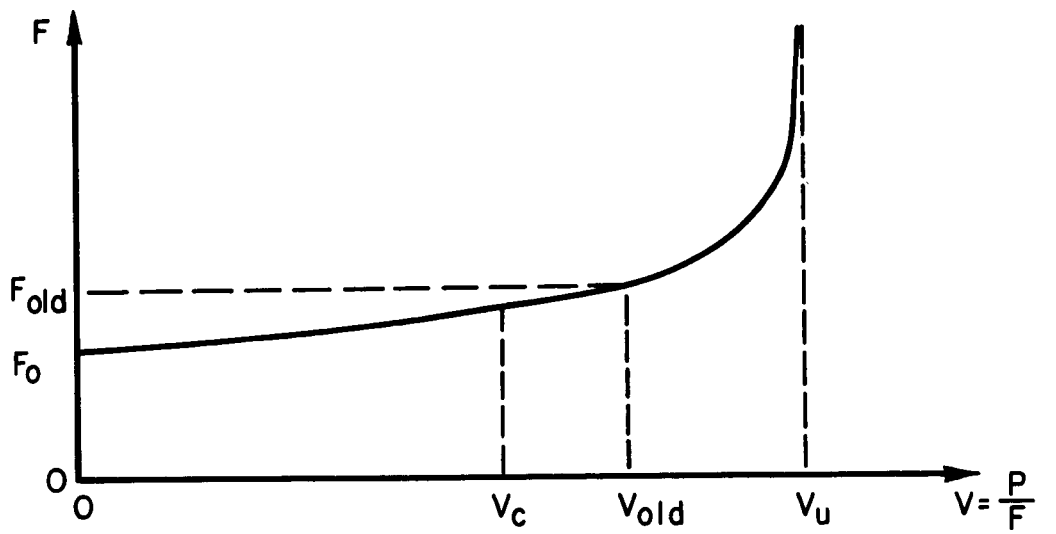

(A) F vs.V ILLUSTRATING DISCONTINUITY AT $V=V_u$

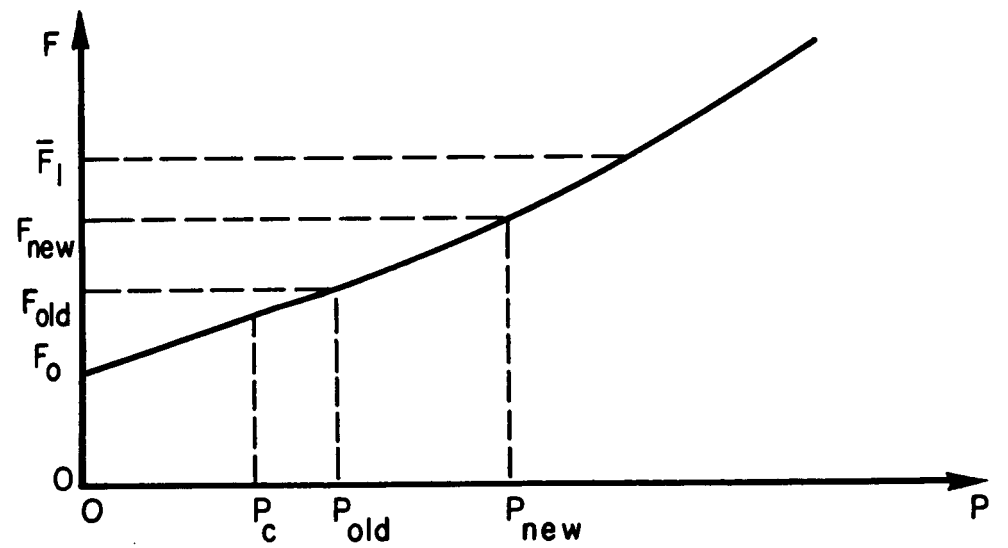

(B) TENDON FORCE vs. LOAD INTENSITY

Fig.25 GENERAL CHARACTERISTICS OF THE TENDON FORCE

Thus as the load increases, V approaches V_u and the ratio P_{new}/F_{old} may exceed V_u, generating erroneous values of D. In order to prevent the ratio $P_{new}/\bar{F}_1$ from exceeding V_u and to otherwise improve the initial estimate of F_{new}, $\bar{F}_1$ and $\bar{F}_2$ are chosen as:

$$\bar{F}_1 = \frac{P_{new}}{V_{old}} = F_{old}\left(\frac{P_{new}}{P_{old}}\right) \tag{76}$$

$$\bar{F}_2 = \bar{F}_1 + D_1 \tag{77}$$

The estimate $\bar{F}_1$ improves with increasing load since V approaches a constant with increasing load. Figure 25b illustrates the relative placement of F_{old}, F_{new} and $\bar{F}_1$.

iii. Computer Program

A computer program was written which reflects the numerical scheme developed in this section. Its gross features are illustrated in the flow diagram shown in Fig. 26. It was convenient to write this program in such a way that the loading function g(x) could be isolated. This makes it possible to effect loading modifications without changing the body of the program.

The various assumptions made in the general formulation of the bending problem apply to the computer program. In addition, the program is further restricted to:

1. Rectangular cross sections
2. Simply supported beams
3. Load systems which produce non-negative bending moments
4. Tendons which lie in a single horizontal plane.

d. Properties of Prestressed Segmented Beams

Using the computer program described in the previous section, it has been possible to quickly investigate some of the important properties of segmented beams. Certainly, one of their most provocative characteristics

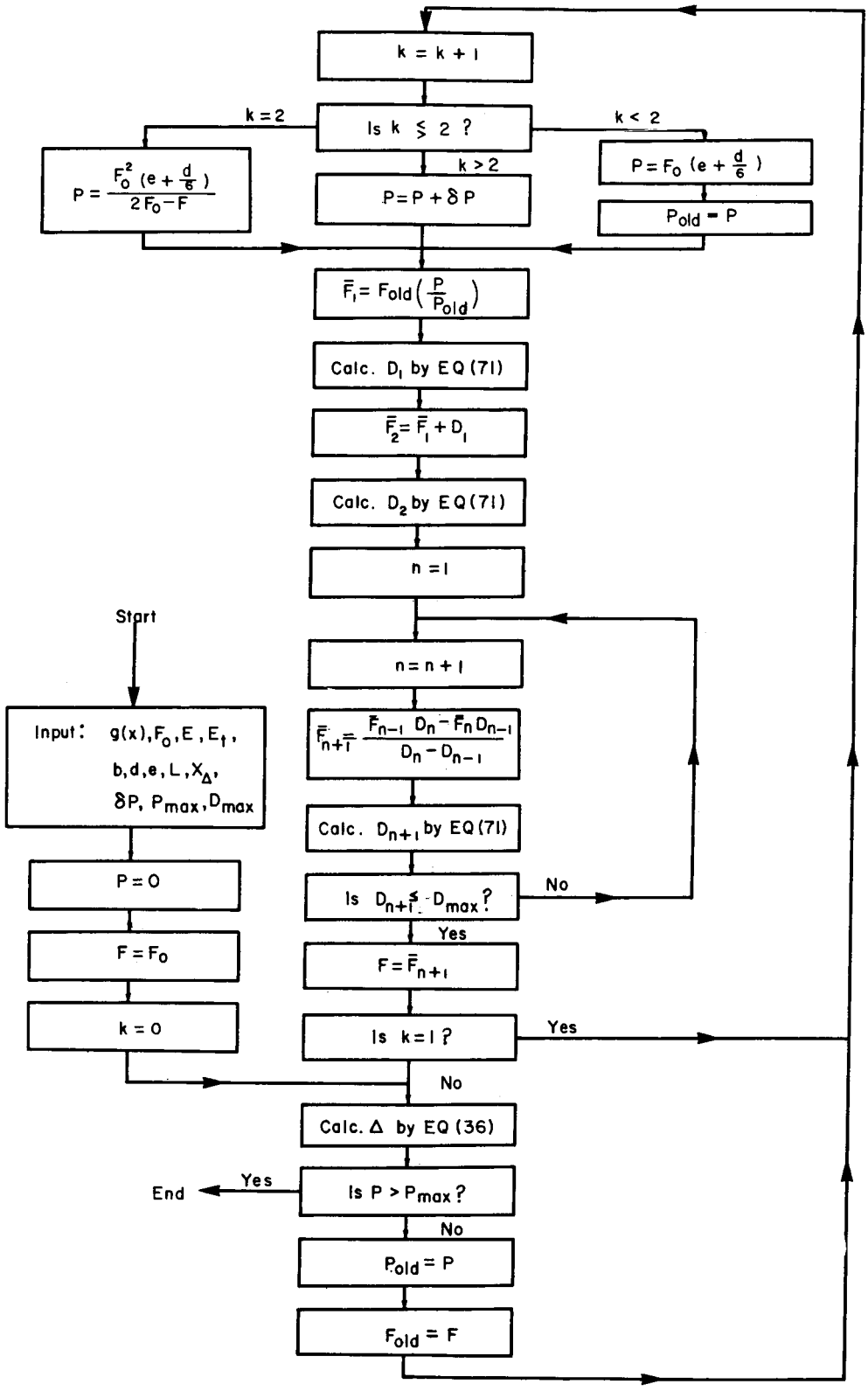

Fig. 26 OVERALL FLOW DIAGRAM FOR COMPUTER PROGRAM

stems from the possibility of approximating their load-deflection diagram by one which is elastic-perfectly plastic. This suggests the possibility of using the methods of limit analysis for segmented structures. We hasten to point out that the prestressed segmented beam is completely elastic, and consequently, the unloading curve will differ from that of an elastic-perfectly plastic beam. Fortunately, however, the upper and lower limit analysis theorems do not depend on the unloading characteristics of the material.

When a simply supported elastic-perfectly plastic beam is subjected to a sufficiently large central load, a plastic hinge forms in the center. Those portions of the beam away from the center remain practically undistorted. The similarity between this type of deflection pattern and that of the corresponding prestressed segmented beam can be inferred from the deflection curves shown in Fig. 27 for a segmented member.

The influence of tendon eccentricity can be ascertained from the load-deflection diagrams shown in Fig. 28 for values of e which vary within the limits of the kern. The stiffness and strength at large deflections are found to fall off rapidly with decreasing eccentricity. In all of the cases of zero eccentricity investigated, the influence of tendon stiffness was found to be extremely slight suggesting that the simpler deflection analysis using zero stiffness tendons might be appropriate.

Selecting $e \doteq 0.66$ where the tendon stiffness is the most predominant, a series of load-deflection curves were plotted for various ratios of beam stiffness to tendon stiffness. It appears from Fig. 29 that the zero stiffness approximation is not appropriate for the extreme values of eccentricity.

To complete the study of beam parameters, load-deflection diagrams are shown in Fig. 30 for different values of prestress. The strength is found to vary linearly with the prestress level.

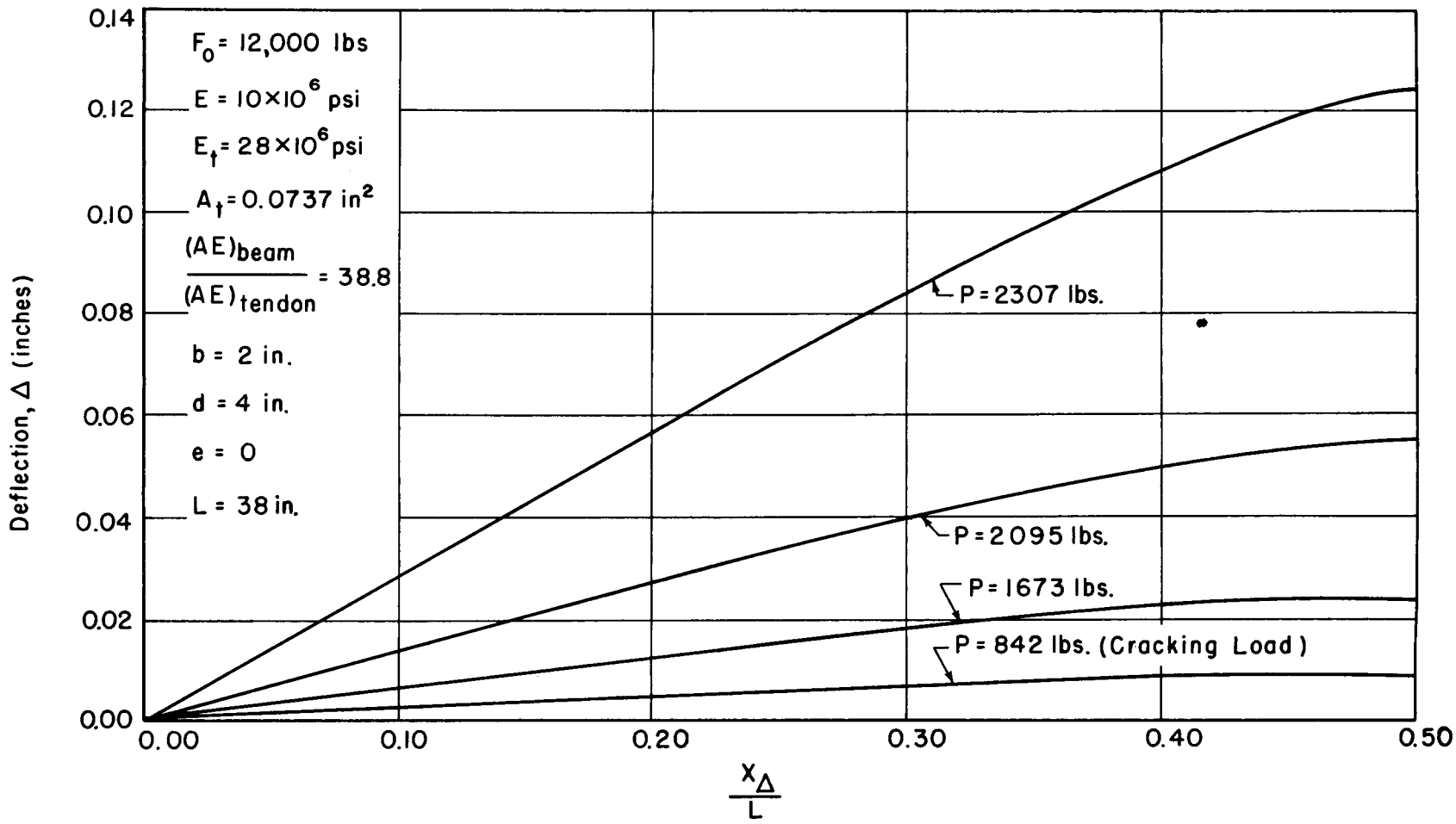

Fig.27 DEFLECTION CURVES FOR A SIMPLY SUPPORTED CENTRALLY LOADED PRESTRESSED SEGMENTED BEAM

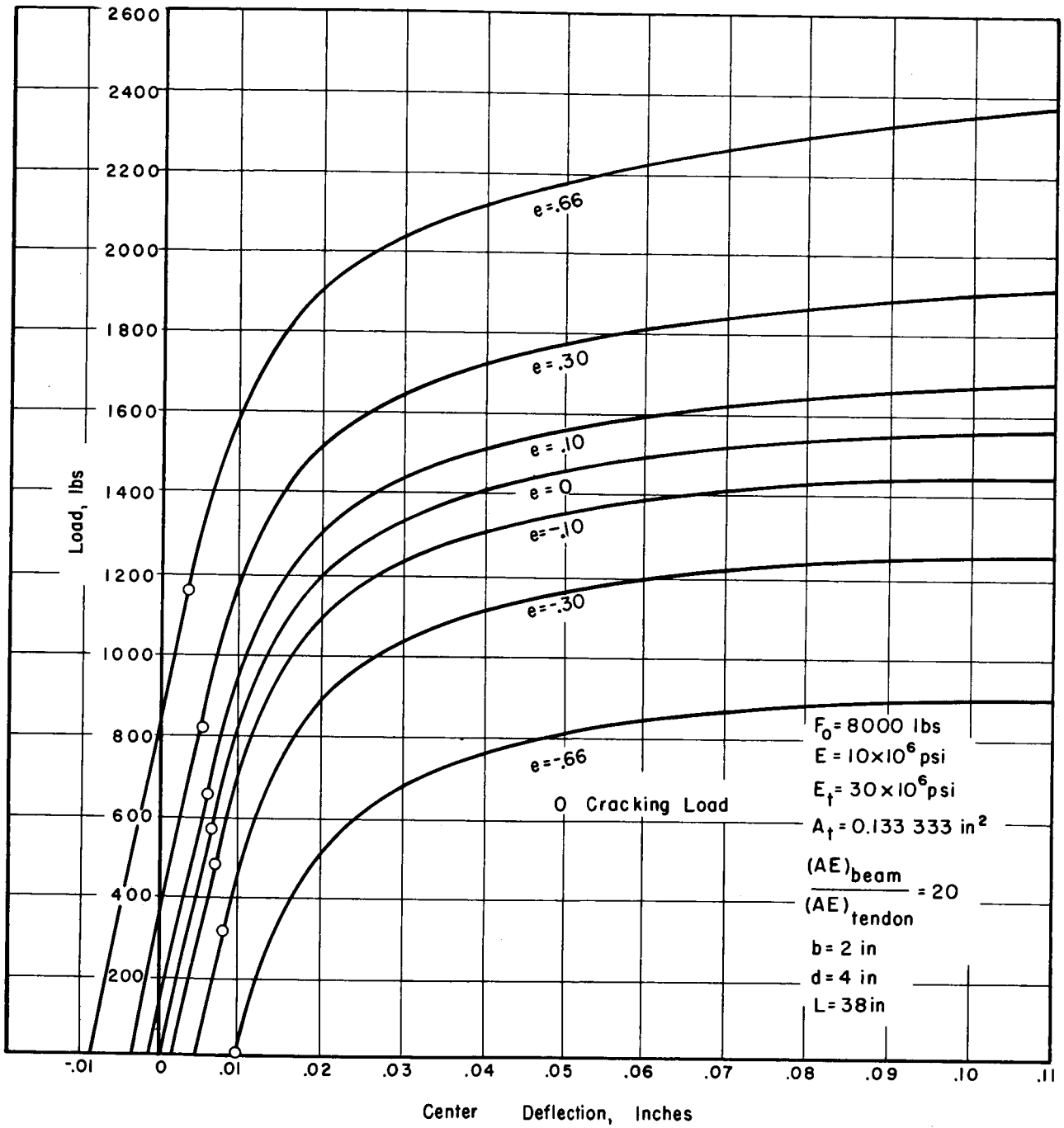

Fig. 28 EFFECT OF TENDON ECCENTRICITY ON THE LOAD-DEFLECTION CURVES FOR A SIMPLY SUPPORTED CENTRALLY LOADED PRESTRESSED SEGMENTED BEAM

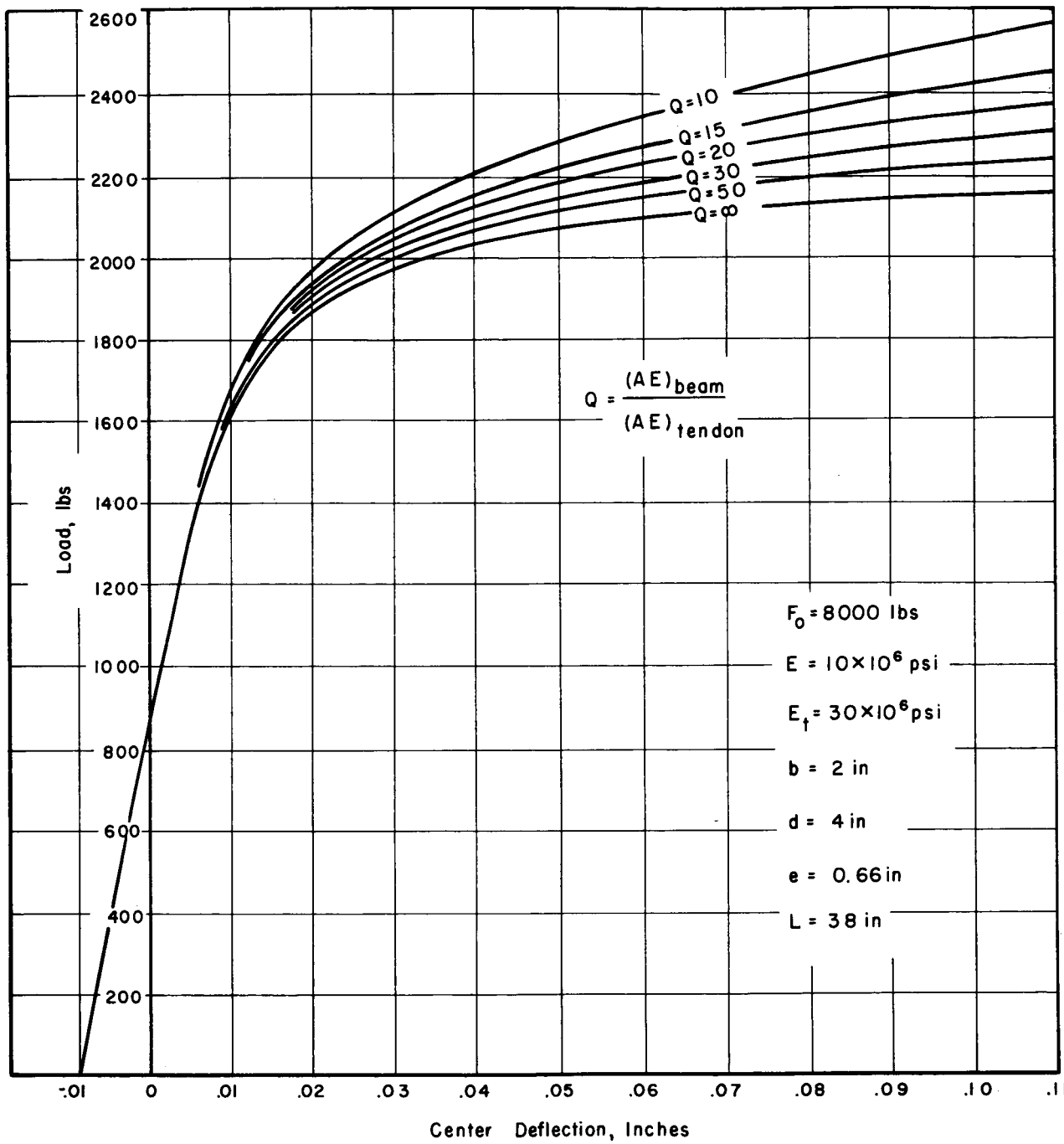

Fig.29 EFFECT OF TENDON STIFFNESS ON THE LOAD DEFLECTION CURVES FOR A SIMPLY SUPPORTED CENTRALLY LOADED PRESTRESSED SEGEMENTED BEAM

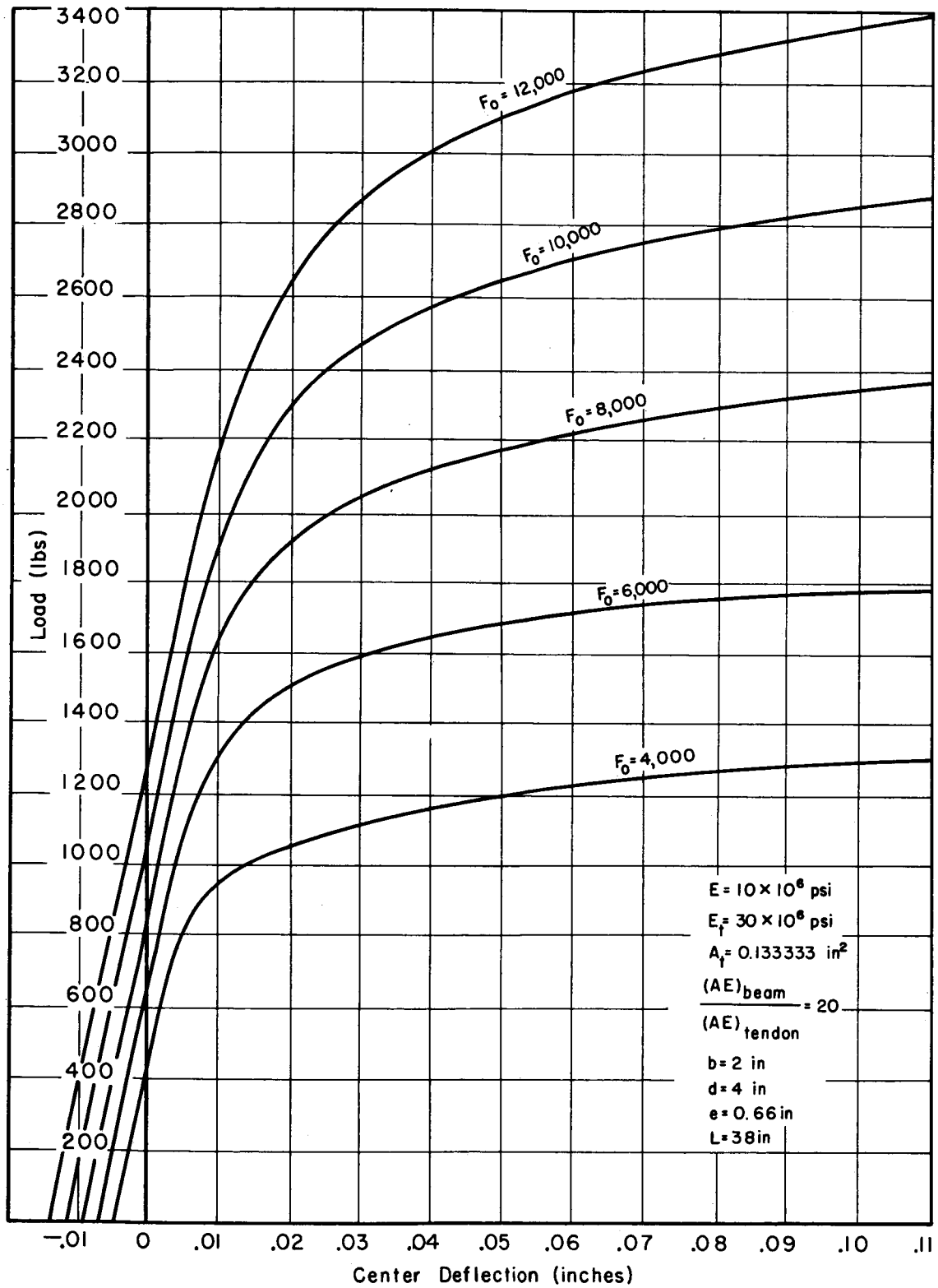

Fig. 30 EFFECT OF INITIAL PRESTRESS ON THE LOAD - DEFLECTION CURVES FOR A SIMPLY SUPPORTED CENTRALLY LOADED PRESTRESSED SEGMENTED BEAM

3. Relationship Between Theory and Experiments

a. Relationship Between Moment of Inertia and Area

It has previously been indicated that the interface contact area of a segmented column increases with increasing compressive force. By comparing the stiffness of a segmented column to that of an equivalent monolithic column, we can obtain the effective area of the segmented column at any load. In the case of a linearly elastic material (Fig. 14), the effective area at load P is given by

$$A_{eff} = \frac{L}{E} \text{(slope of load-deflection curve at P)} \qquad (78)$$

where L is the span length or gage length of the column and E is the modulus of elasticity of the segments. It is important to emphasize that the actual contact area between any two segments may be higher or lower than A_{eff}. That is, A_{eff} averages the effects of all of the contact areas within the gage length. Since the segments are finite in number, the average real contact area is probably less than A_{eff}.

The procedure for determining the effective moment of inertia I_{eff} for a prestressed segmented beam parallels that used to find A_{eff}, that is, we compare the initial stiffness of a segmented beam under a prestress F and terminal couples to an equivalent monolithic beam. For a linearly elastic material we obtain,

$$I_{eff} = \frac{L}{2E} \text{(initial slope of the terminal couple-end rotation curve)} \qquad (79)$$

where L is the span length and where the beam is under a prestressing force F. As in the case of the segmented column, the actual moment of inertia at any station of the beam cannot be inferred from I_{eff} which averages the effects of many segments. This situation has an important consequence. If the deflection of a beam is very sensitive to the characteristics of a certain few segments, the beam will exhibit random behavior. We would, for example, expect to find more variability in the central deflection of a centrally loaded beam than one subjected to terminal couples. Because of the shape of the moment diagrams, the central segments

in the former case have the greater influence on beam deflection.

A necessary condition in the development of a general analysis capability is the prediction of bending behavior from a knowledge of simple tension or compression. The first step in satisfying this requirement for the case of segmented members is to establish the relationship between A_{eff} and I_{eff}. Now, if the contact area is uniformly distributed over the segment interfaces, the moment of inertia of a rectangular cross section with n per cent contact is simply

$$I = \frac{bd^3}{12} n \tag{80}$$

where

$$n = A_{eff}/bd \tag{81}$$

On the other hand, if the total contact area is confined to the region about the neutral axis we obtain the minimum possible moment of inertia, I_{min}

$$I_{min} = \frac{bd^3}{12} n^3 \tag{82}$$

The maximum moment of inertia I_{max} corresponds to the symmetrical placement of the contact area at the top and bottom of the cross section, hence,

$$I_{max} = \frac{bd^3}{12} \left[1 - (1 - n)^3\right] \tag{83}$$

The types of contact corresponding to I_{max} and I_{min} are shown in Fig. 31 for segments which are partially separated.

Although it is clear that on the average I_{eff} lies between I_{max} and I_{min}, it is not evident whether it is equal to the average moment of inertia I given by Eq. 80, or to the average of the extreme values, $(I_{max} + I_{min})/2$, or to some other measure. Experimentally, we can find the average I_{eff} from either the terminal couple-end rotation curve of a long segmented beam (many segments), or from the average of the effective moments of inertia obtained from a number of beams tested under a general loading. Unfortunately, neither of these tests were scheduled for this first program phase and any conclusions regarding the relationship

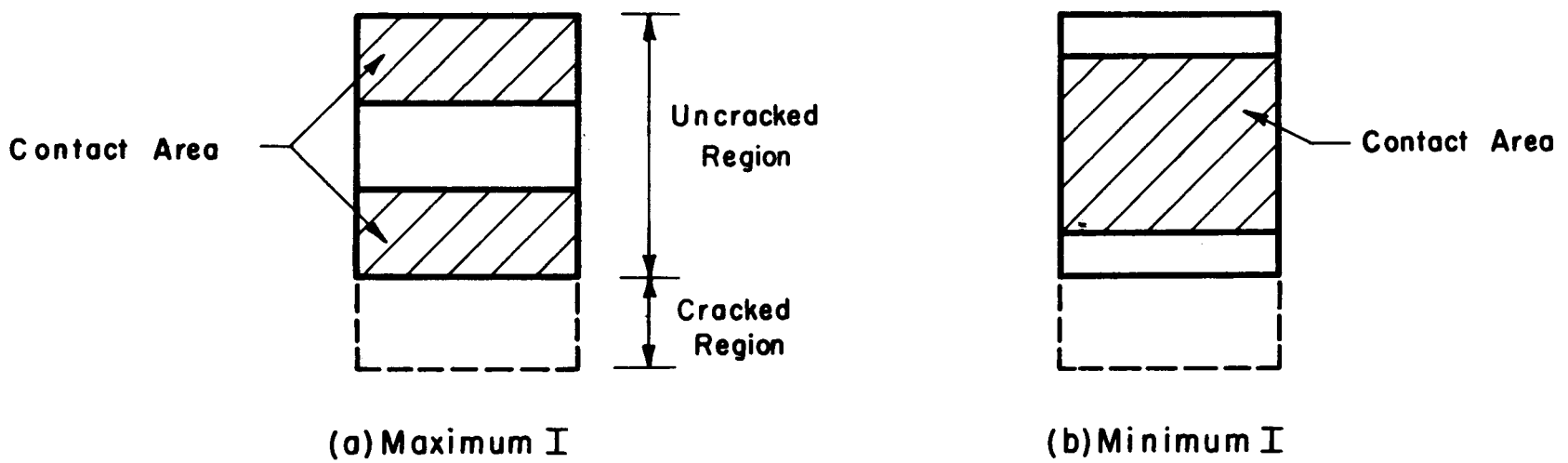

Fig.31 EXTREME DISTRIBUTIONS OF CONTACT AREAS IN SEGMENTED BEAMS

between A_{eff} and I_{eff} must await our future studies.

b. Centrally Loaded Simple Beam Tests

Using the test fixture and the prestressed glass beam shown in Fig. 32, we obtained central load-central deflection diagrams for prestressing forces of 4, 6, 8 and 12 kips. The results are shown in Fig. 33 through 36. For the 6 kip and 8 kip cases, two separate tests were run to indicate the scatter which results from removal and reapplication of the prestressing force. Prior to the performance of these bending tests, the compressive load-deflection characteristics of the segments were measured in situ at the middle and two ends of the member using the technique illustrated in Fig. 37. To prevent relative movement between the segments, the axial load was never completely removed from the member. The resulting three load-deflection diagrams shown in Fig. 38 are almost identical indicating that the 10 in or 20 segment gage length is adequate for estimating the effective area A_{eff}.

The average A_{eff} (and hence n) obtained from the compression tests described in Fig. 38 have been used to compute I_{max} and I_{min} These values have in turn been used to define the bounds on the linear portions of the load-deflection curves in Fig. 33 to 36. Bounds on the load-deflection curves can be found in the "cracked" range if n continues to hold for the unseparated portions of the cross section. The computer program described in Section IV-2-ciii was modified to reflect the two extreme contact area distributions shown in Fig. 31 and the resulting extreme load-deflection curves are plotted with the data in Fig. 33 to 36. It must be pointed out that these curves are not bounds on the performance of an individual beam; but rather, they are bounds on the average load-deflection curve of many beams. As it turns out for the beam considered, all the data falls on or between these bounds.

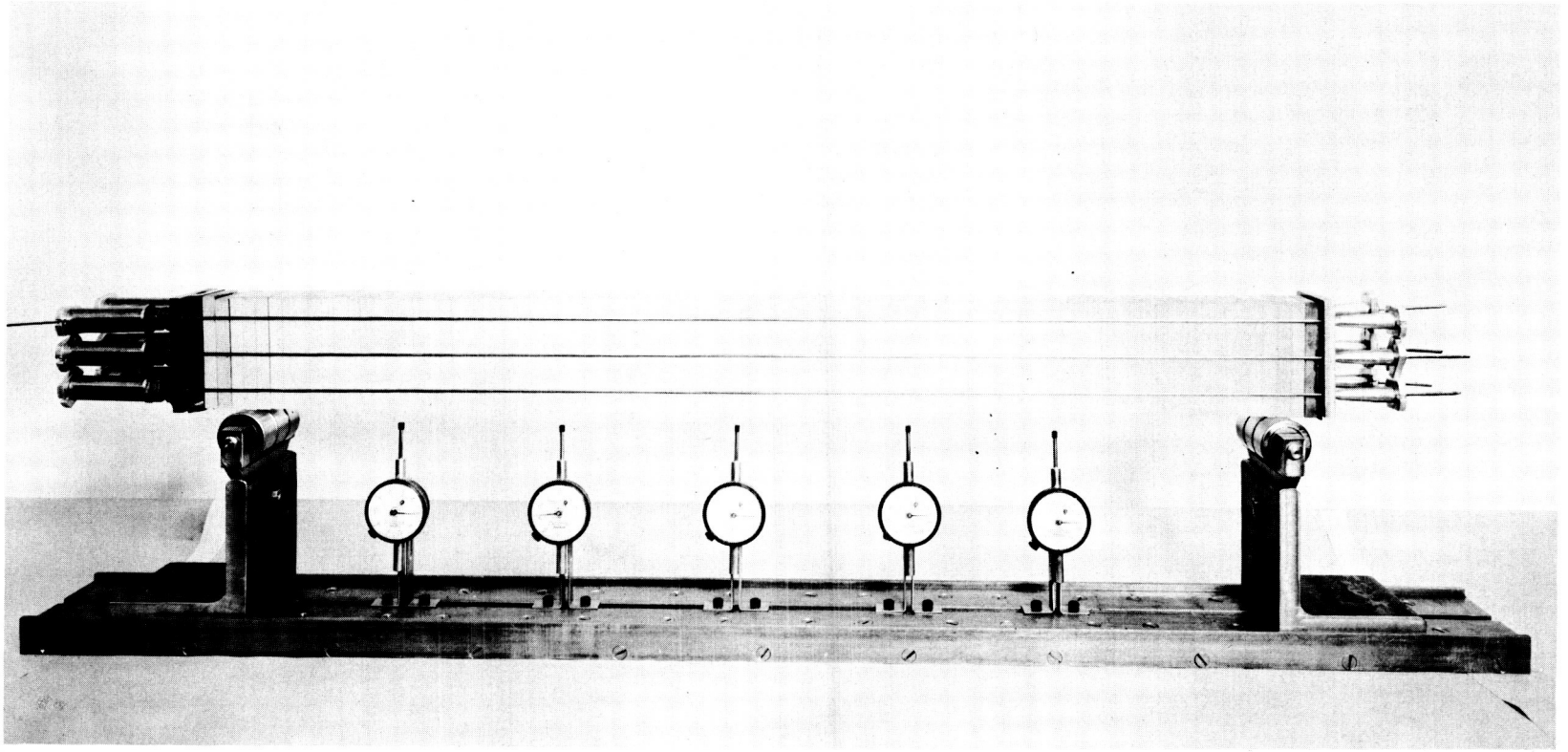

Fig.32 BENDING FIXTURE FOR A SEGMENTED GLASS BEAM (SPAN: 40"; DEPTH: 4"; WIDTH: 2"; SEGMENT THICKNESS: $\frac{1}{2}$")

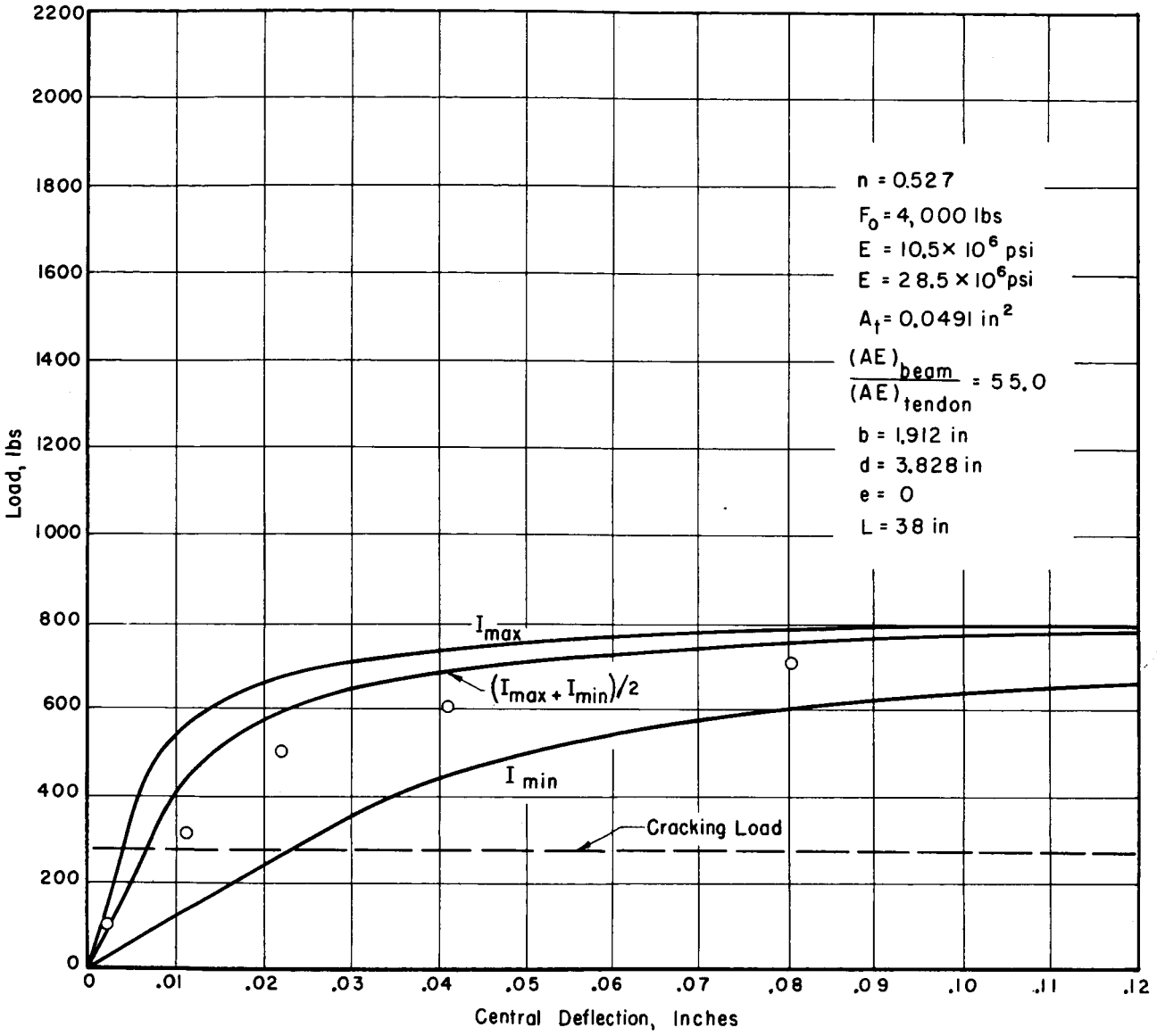

Fig.33 BOUNDED EXPERIMENTAL LOAD-DEFLECTION CURVE FOR A SIMPLY SUPPORTED CENTRALLY LOADED PRESTRESSED SEGMENTED GLASS BEAM, F_0 = 4,000 lbs

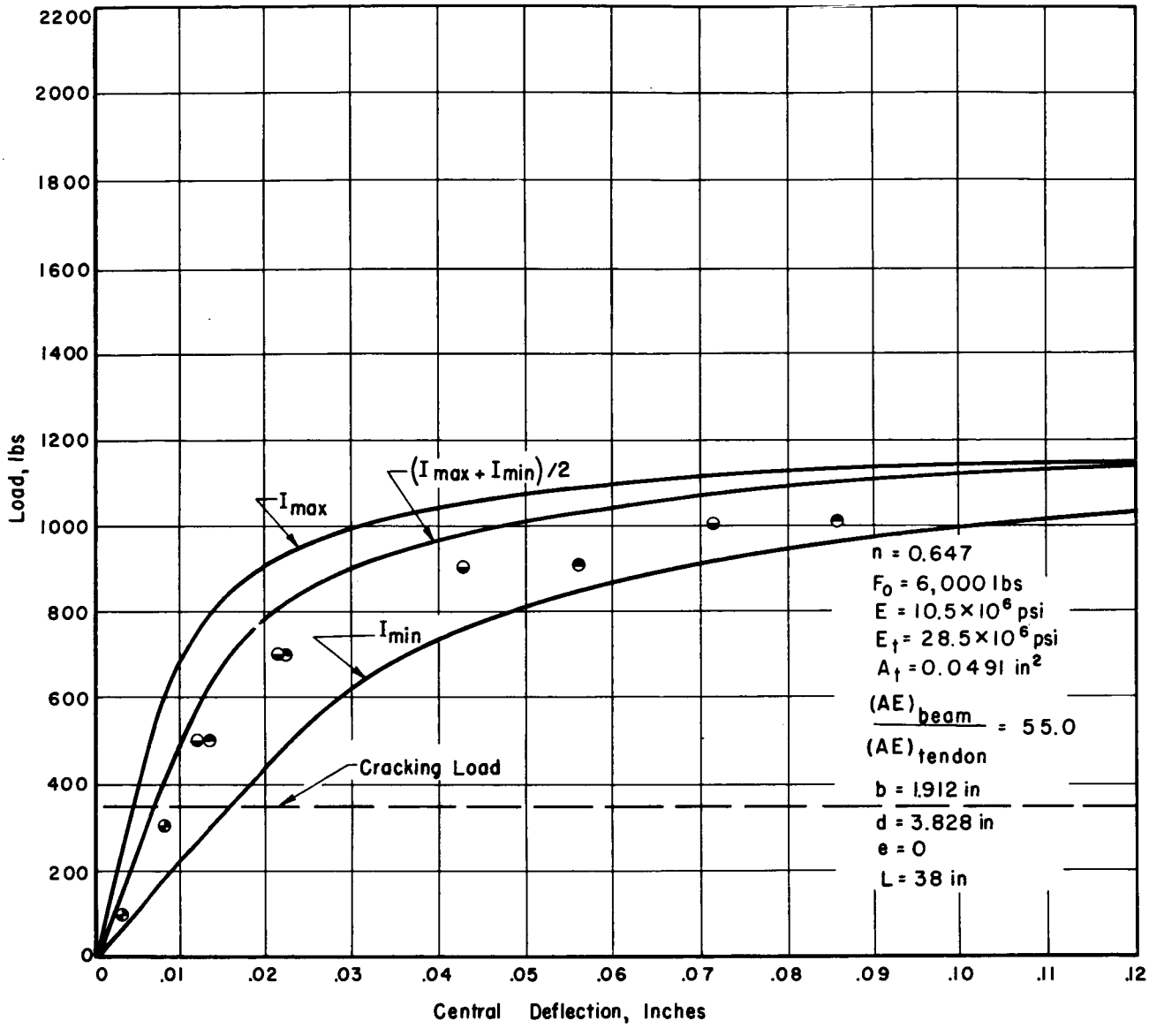

Fig.34 BOUNDED EXPERIMENTAL LOAD-DEFLECTION CURVE FOR A SIMPLY SUPPORTED CENTRALLY LOADED PRESTRESSED SEGMENTED GLASS BEAM, F_0 = 6,000 lbs

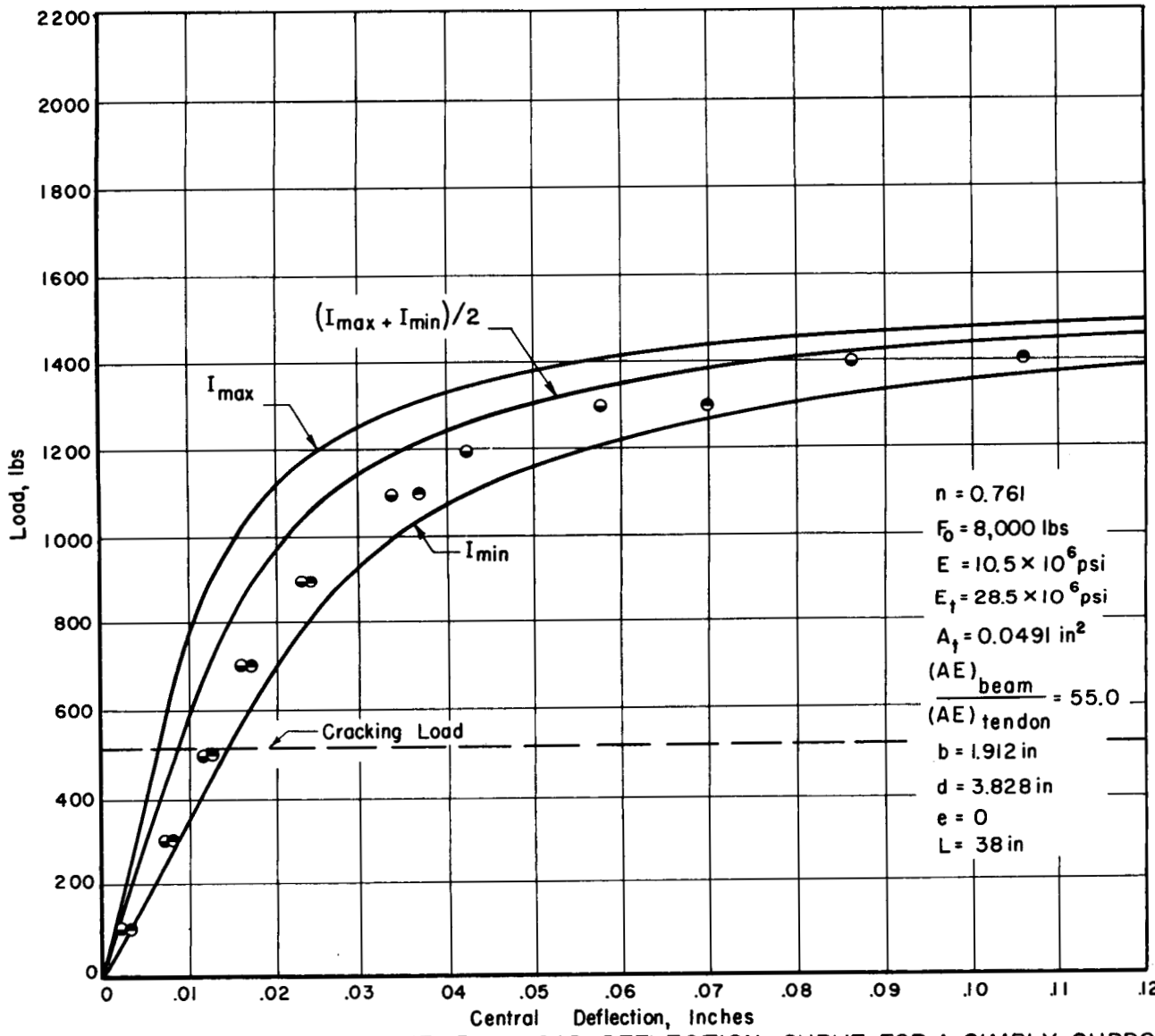

Fig.35 BOUNDED EXPERIMENTAL LOAD-DEFLECTION CURVE FOR A SIMPLY SUPPORTED CENTRALLY LOADED PRESTRESSED SEGMENTED GLASS BEAM, F_0 = 8,000 lbs

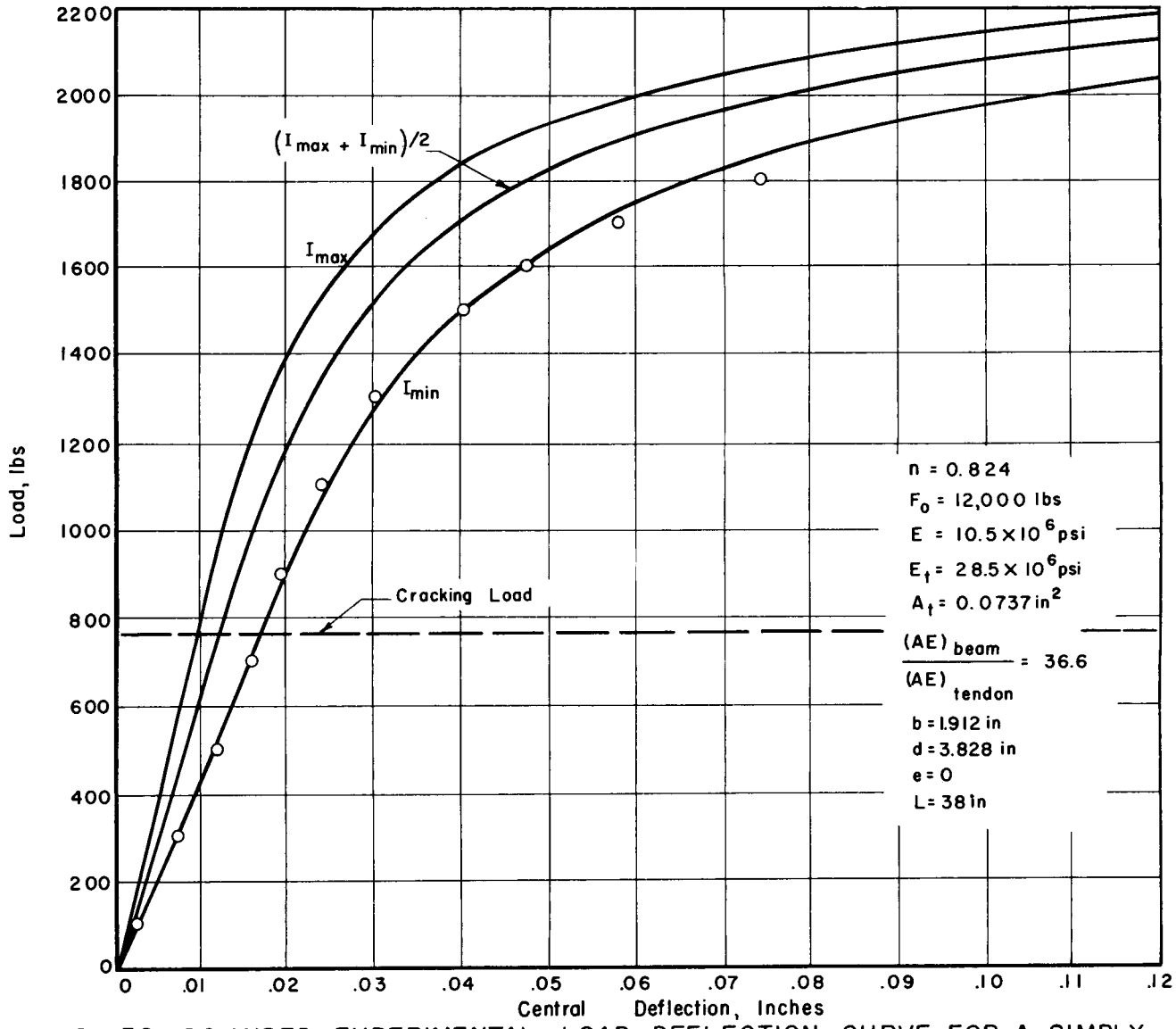

Fig.36 BOUNDED EXPERIMENTAL LOAD-DEFLECTION CURVE FOR A SIMPLY SUPPORTED CENTRALLY LOADED PRESTRESSED GLASS BEAM F_0=12,000 lbs

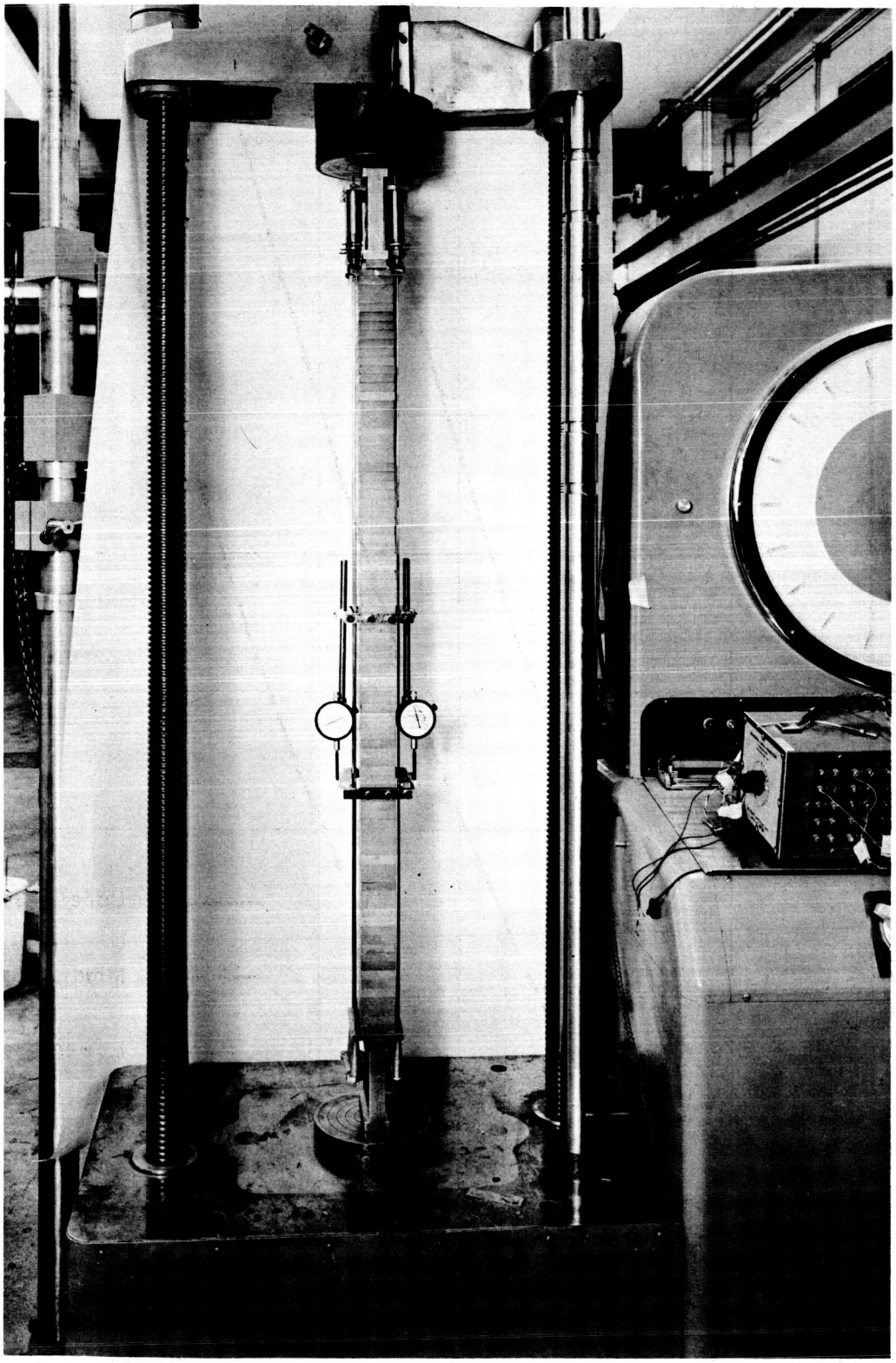

Fig.37 COMPRESSIVE LOAD DEFLECTION DETERMINATION IN SITU

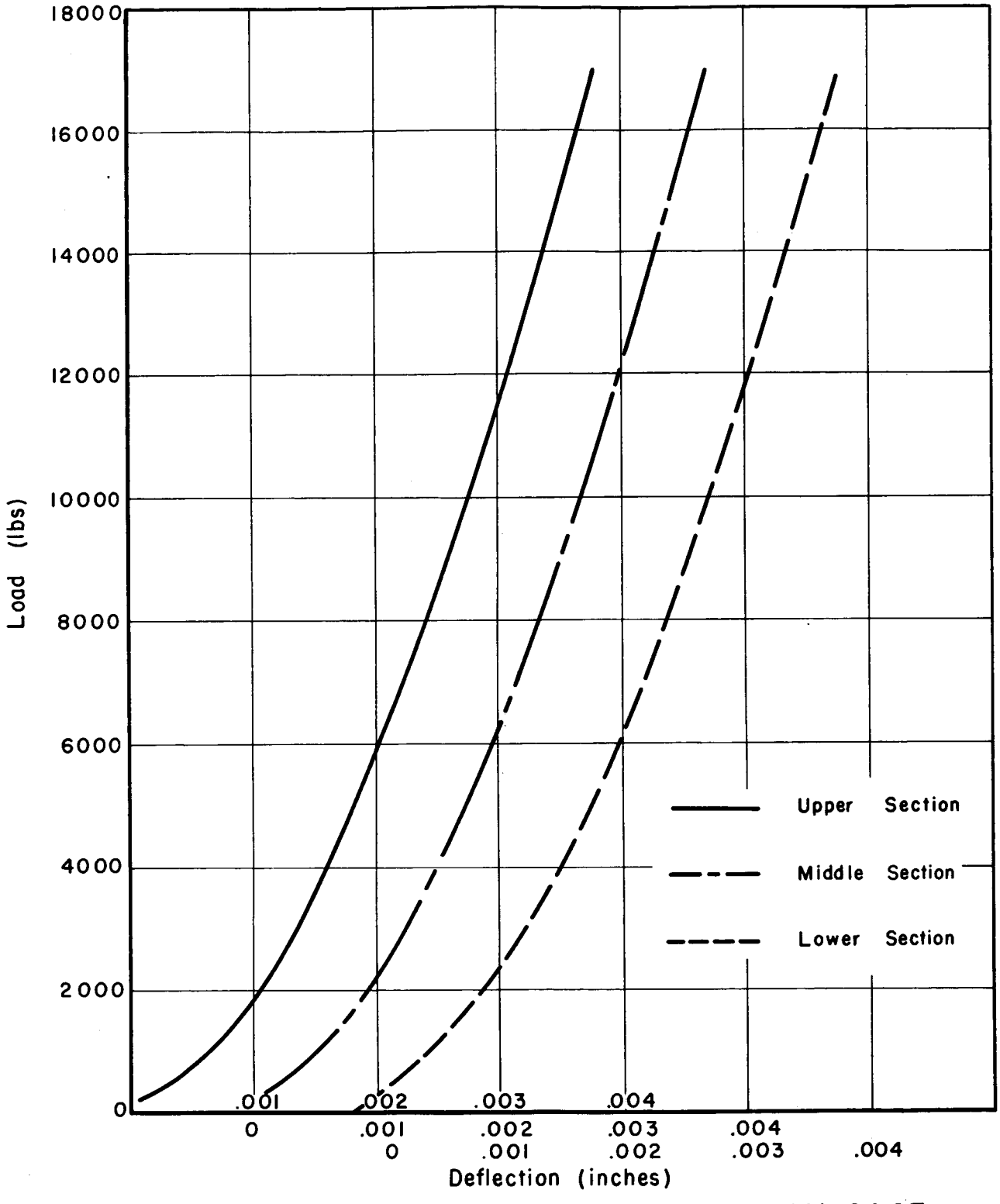

Fig.38 COMPRESSION TEST ON GLASS BEAM GAGE LENGTH = 10"; AVG. AREA = 7.32 IN^2

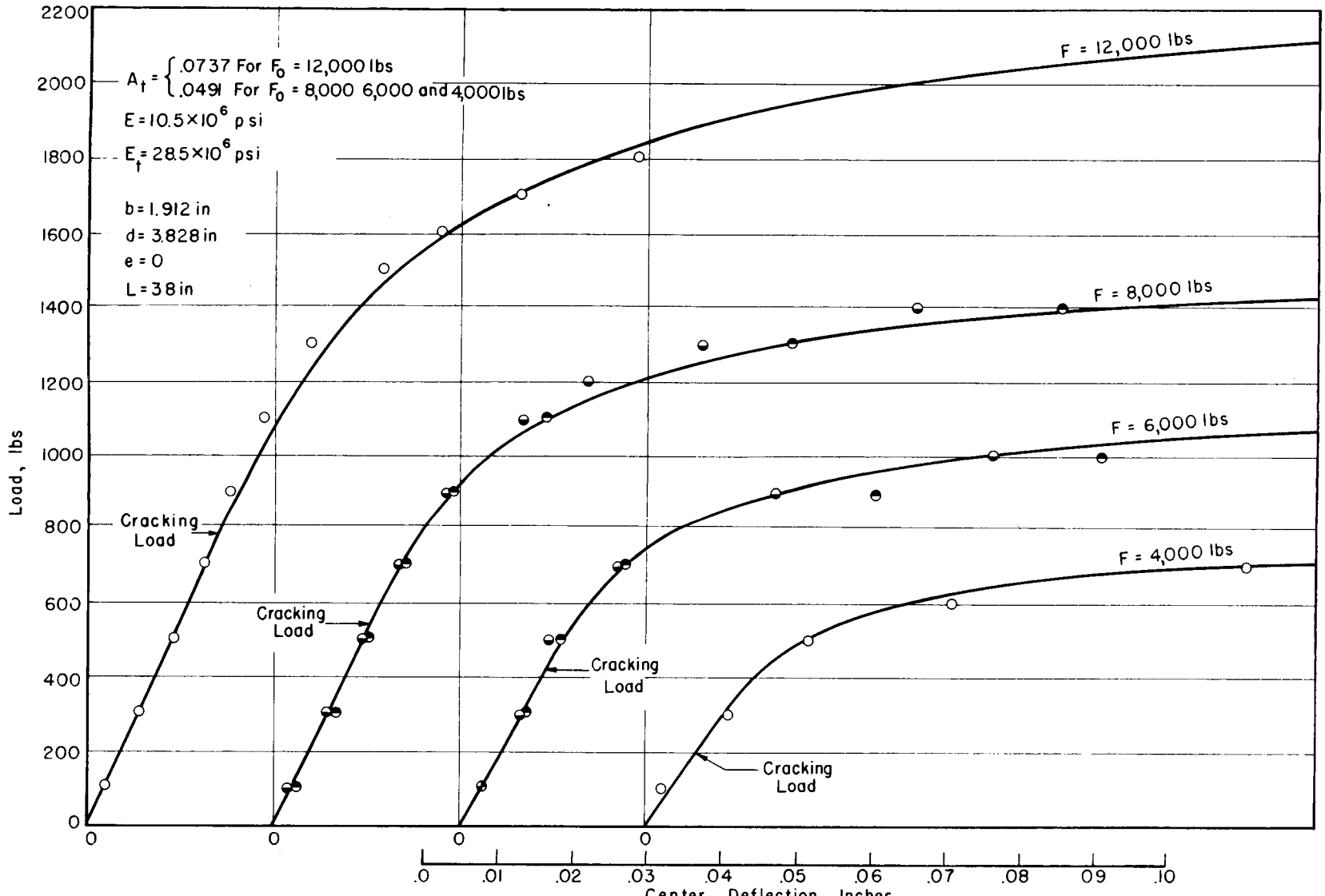

Fig.39 FITTED EXPERIMENTAL LOAD - DEFLECTION CURVES FOR A SIMPLY SUPPORTED CENTRALLY LOADED PRESTRESSED SEGMENTED GLASS BEAM

c. Interpretation of the Experimental Results

Recognizing that the statistical nature of the interface contact problem precludes the prediction of the initial bending stiffness of any particular beam, we proceeded to choose a moment of inertia which matched up the initial slope of the bending data. Assuming that the contact area is uniformly distributed over the cross section, matching the I is tantamount to defining the beam width as nb. On this basis we can apply our previous results in a straightforward manner to obtain theoretical curves for each level of prestress. The results are shown in Fig. 39 where we observe a remarkable agreement between the theory and the experiments in the "cracked" regions. The curves were, of course, choosen to match in the linear regions. Consequently in the range of parameters considered, we have reduced the prediction of the load-deflection diagram of a prestressed segmented beam to the determination of the one parameter n. That is, if I_{eff} can be related to A_{eff} we have solved the bending problem.

In the present series of tests, it was found that the effects of shear deflection and beam-column action were negligible relative to the bending deflection. There are, however, practical situations where these effects can become quite pronounced.

At this time it is thought that the validity of the present analysis will improve as:

1. the number of segments increases
2. the prestressing force increases
3. the interfaces become flatter
4. the bending problem more closely approximates the terminal couple-end rotation case
5. the cross section approaches the ideal I-beam section

d. Calibration and Test Fixtures

Before the bending fixture or the compressometers were used to measure the properties of segmented members, their reliability was investigated through the use of monolithic steel and aluminum beams and rods. The fixtures were only accepted when the values of E obtained in bending and compression were within 2 per cent of each other and were approximately

equal to the published values.

The prestressing tendons used in the bending experiments were prestressed and secured with the strand-vice-grips (Reliable Electric Company) shown in Fig. 40 . The first attempts to measure the tendon forces were made with strain gages attached to the steel wires. This method was abandoned because of excessive strain gage slippage and drift. The eventual use of force washers provided an extremely satisfactory method of monitoring the tendon force. Each force washer was calibrated in a standard jig, and as an additional check, the entire strand was tensioned using the technique illustrated in Fig. 41. In this way the force derived from the force washer could be compared directly to that recorded by the testing machine under the identical conditions which prevailed in the prestressing assembly.

Optical flats were used to measure the flatness of the segment interfaces. A monochromatic helium light source was used with a wavelength of 23.1×10^{-6} in.

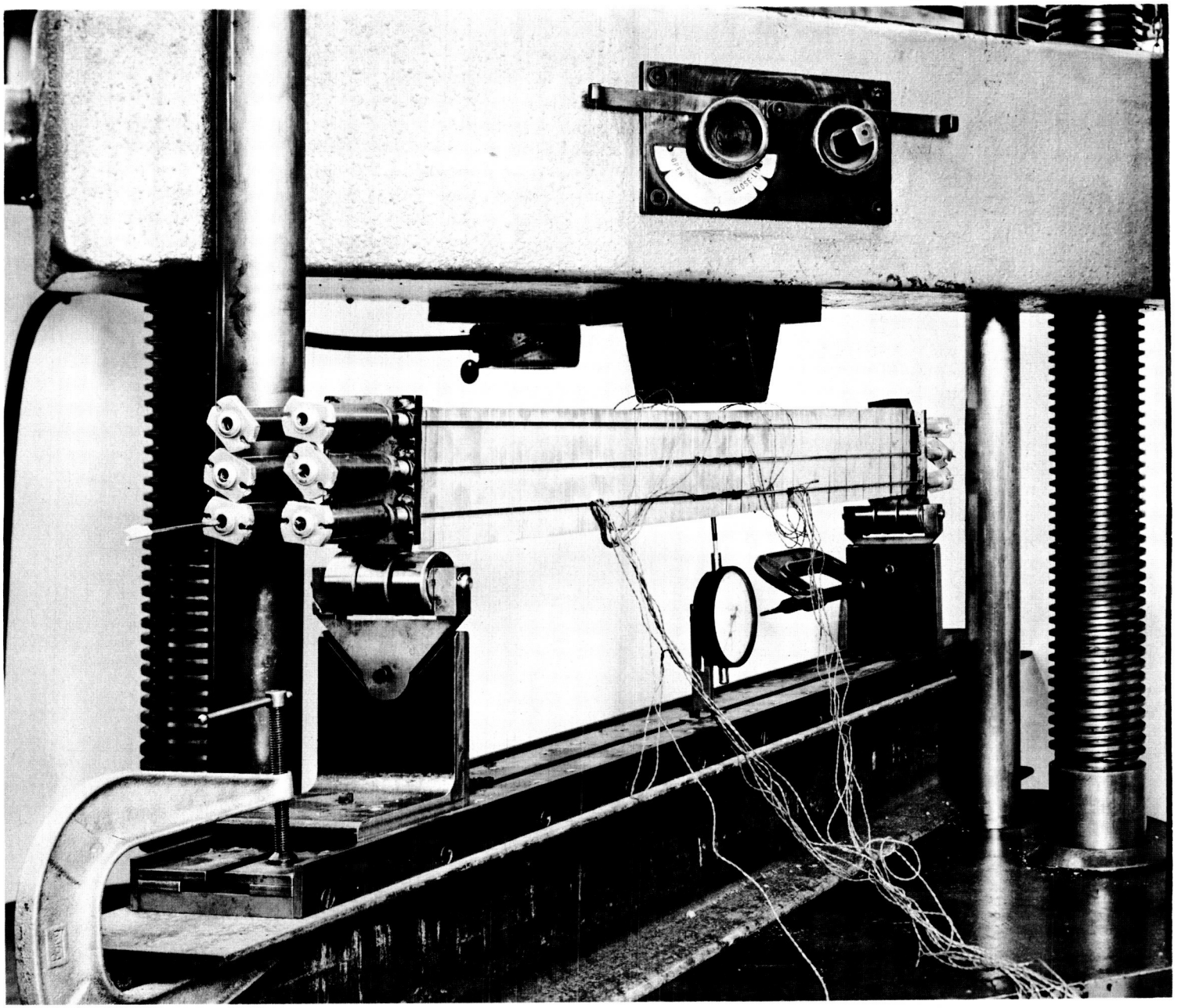

Fig. 40 PRESTRESSED SEGMENTED GLASS BEAM

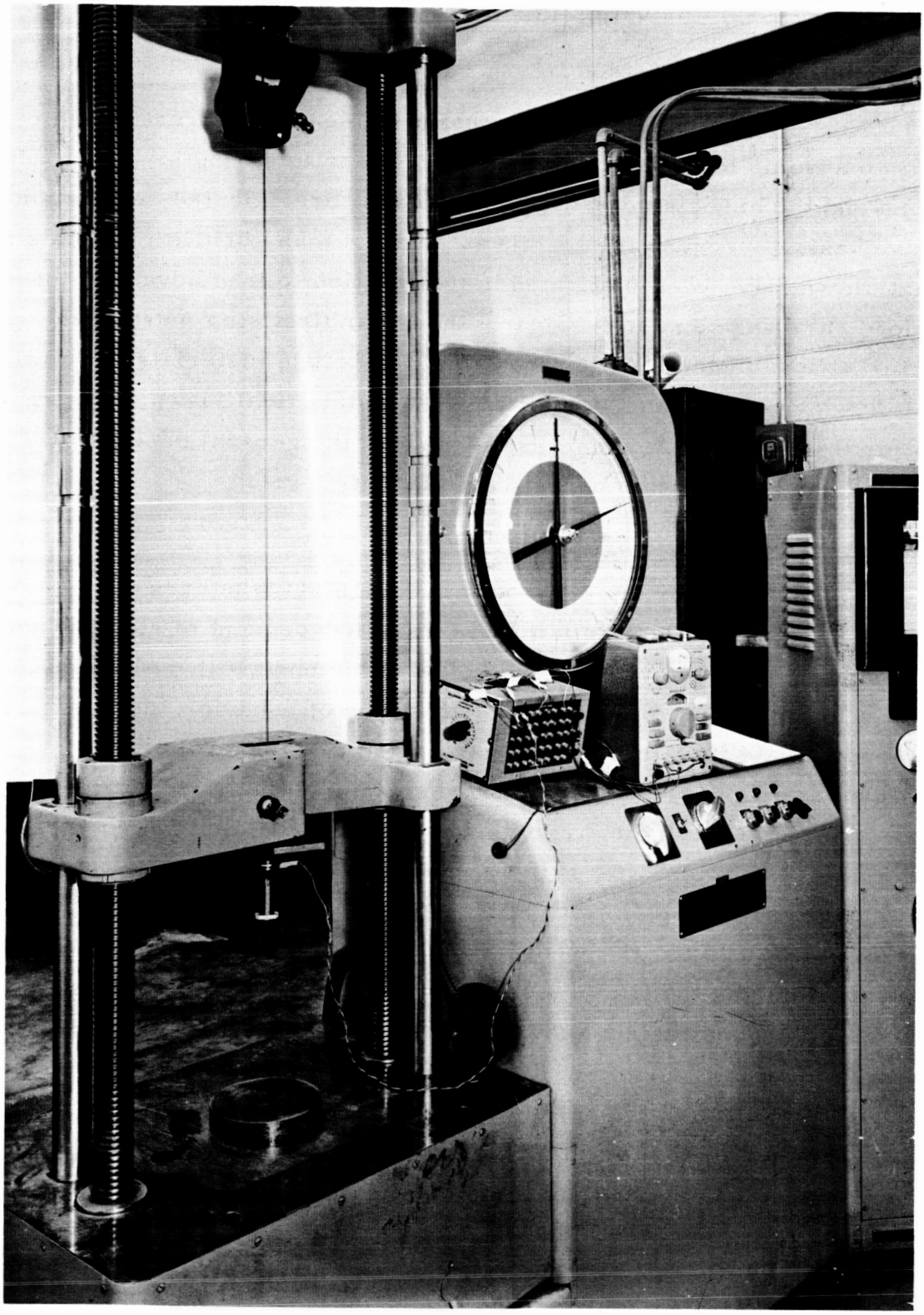

Fig.41 CALIBRATION CHECK ON THE FORCE WASHER

V. PRESTRESSED MONOLITHIC BEAMS

A. Conventional Prestressed Design

The usual practice in the design of monolithic prestressed concrete is to assume that the concrete has zero tensile strength. The tendon positions and the associated prestressing forces are selected on this conservative basis. Because the tensile strength of many brittle materials is substantial, we have been motivated in this section to take advantage of this latent load carrying capacity. Clearly then, our first step must be the characterization of the tensile strength of the brittle materials to be utilized. In the following subsection, we indicate that a statistical viewpoint is required for this purpose, and as a consequence, the general design approach demands the specification of a desired reliability level.

B. The Probabilistic Nature of Structural Design

The basis for the conventional design of structures is the assumption that there exists a certain failure stress, independent of size, at and above which all samples will fail and below which none will. Although it is known that no material exhibits exactly this type of behavior, ductile materials approximate it well enough to have permitted the evolution of a deterministic design procedure. Tests on such materials indicate that yield stresses are distributed very tightly around the mean value-which is taken to be the failure stress. Now it is obvious that about (in the case of a symmetrical distribution, exactly) fifty per cent of the samples will yield below, but very close to, the mean value. There are two approaches taken to assure that during the life of a structure none of its members are likely to be stressed beyond their actual yield points. One is the rather obvious expedient of applying a factor of safety to the observed mean yield stress, and using the resulting estimate of the failure stress, called the working stress. The other method is the limit or ultimate design technique. Here the mean yield stress is used and a factor of safety is applied to the design loads. This latter approach has gained acceptance in recent years, perhaps on the grounds that there is considerably more uncertainty about the loads which will be applied to a structure, particularly, say, a large bridge or building, during its lifetime than there is about the yield stresses of its

individual members. Using either approach, if the maximum loads and the cumulative distribution of yield stresses are known, a reliability can be computed for a structure. However, this is not done in practice, since the safety factors are chosen so conservatively that the resulting reliability is very close to one-hundred per cent.

In the case of brittle materials, the distribution of failure strengths in tension is one of large variability and, to all appearances, heavily dependent on the size of the member. As a result of the second property alone, a simplified design procedure analogous to the one used for ductile materials is impossible. The most promising scheme seems to be one in which the distribution of failure stresses is found experimentally and used to determine the reliability of each member. Thus, the overall reliability of the structure under a specified loading condition may be computed. For example, if a simple frame were composed of three members having reliabilities of .99, .98, and .95, the frame reliability would be (.99) (.98) (.95) = .921.

C. The Statistical Distribution of Fracture Strength

The most popular theory of the fracture of materials leading to a distribution of fracture stress is due to Griffith. [16] Basically it postulates that in a volume of material there are a number of flaws, randomly distributed, which act as stress concentrators. When the magnified stress at one of these points reaches the theoretical molecular strength, a running crack develops and failure occurs. This theory accounts for the fact that specimens are commonly observed to fail in tension at nominal stresses three or more orders of magnitude smaller than the molecular bonding strength. It also implies that the probability of failure at a given stress will increase with the volume of the specimen since the largest flow in a big volume is likely to be greater than the largest flaw in a small volume.

Recognizing that the Griffith theory leads to a weakest link model for the behavior of brittle materials, Weibull [17] expressed a formula for the probability of failure as a function of the stress distribution in a body:

$$F(x) = 1 - \exp\left[-\iiint g \, d\xi_1 \, d\xi_2 \, d\xi_3\right] \tag{84}$$

$$g = \frac{1}{v}\left[\frac{x\phi(\xi_1, \xi_2, \xi_3) - x_u}{x_o}\right]^m \quad ; \quad x\phi \geq x_u \geq 0$$

$$g = 0 \quad ; \quad x\phi < x_u$$

where x is an intensity level; $x\phi$ is the actual stress distribution in the body; ξ_1, ξ_2, ξ_3 are space coordinates; v is a unit volume; $F(x)$ is the probability of fracture; and m, x_u, x_o are statistical distribution parameters. Weibull's theory has been widely studied as a possible design tool for brittle materials. Because it represents the general behavior patterns of such materials, it has been adopted here for purposes of demonstration. For a stress condition of uniform tension, $\phi = 1$ and the distribution of failures is given by

$$F(x) = 1 - \exp\left\{-V\left[\frac{x-x_u}{x_o}\right]^m\right\}; \quad x \geq x_u \tag{85}$$

$$F(x) = 0 \quad ; \quad x \leq x_u$$

where x is the stress level and V is the number of unit volumes in the member. Figure 42a depicts this distribution of failure stress for $2 < m < \infty$ together with its associated probability density function $f(x) = \frac{dF}{dx}$. The volume has been incorporated into the scale parameter x_o. The location parameter x_u may be interpreted as the stress below which no sample will fail while m may be taken as a measure of the variability of the material. As shown in Fig. 42b, as $m \to \infty$ the behavior approaches that of the classical material model - all samples fail at exactly the same stress.

For convenience in notation, the integral over the volume, indicated in Eq. (84), is designated as B and called the risk of rupture. Since $F(x) = 1-\exp(-B)$, the reliability $R = \exp(-B)$. Thus determining the reliability of the structure can be reduced to two steps. First, finding the parameters x_o, x_u, and m for the material to be used and, then, evaluating the definite integral B which is obviously dependent on the type of loading and the geometry of the member. A considerable amount of work has been done in both of these areas with mixed success and this work is thoroughly reviewed in Ref. 18.

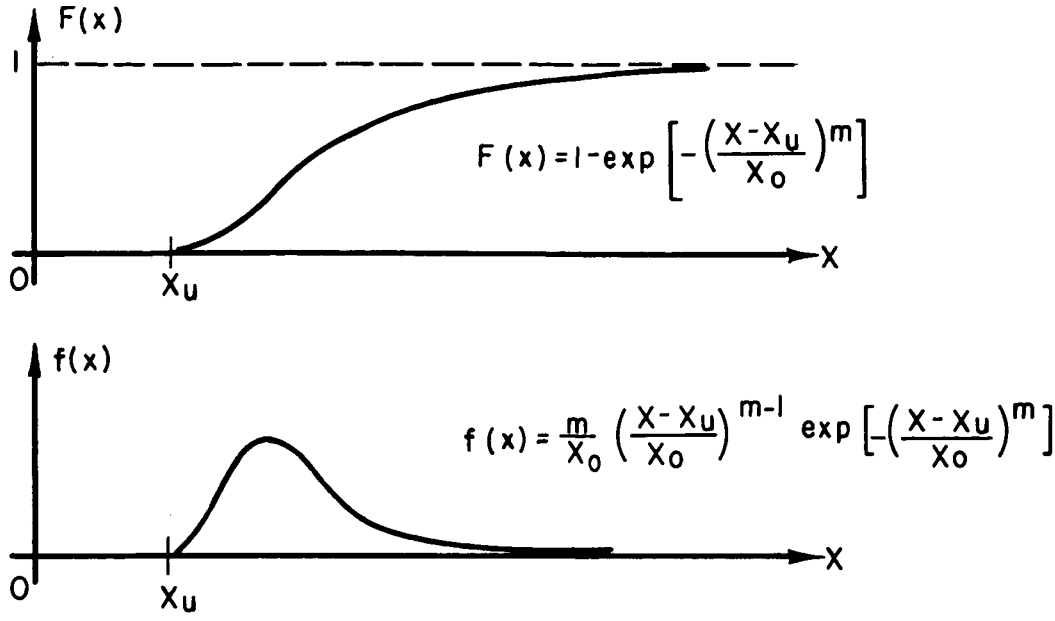

Fig. 42 a. WEIBULL DISTRIBUTION, $2 < m < \infty$

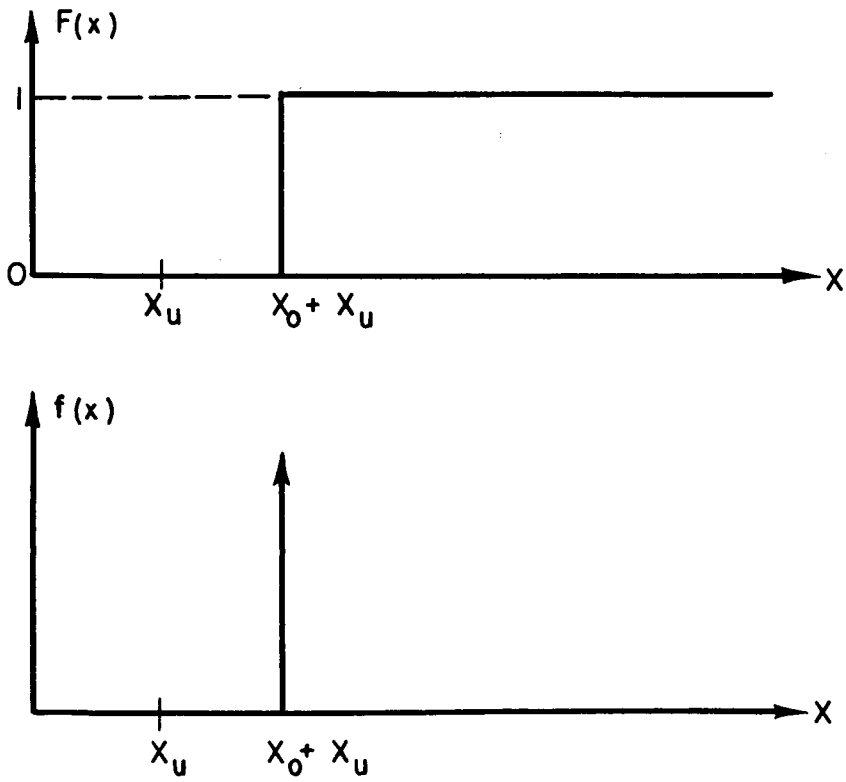

Fig. 42 b. WEIBULL DISTRIBUTION, $m = \infty$

With regard to the definite integral, B , the sole distinction concerning its application hinges on the existence of a solution in closed form for the loading and geometry to be investigated. As shown previously, the solution for the case of uniform tension is the trival

$$B = V \left[\frac{x - x_u}{x_o} \right]^m \tag{86}$$

For other load conditions, such as torsion or flexure, a resort generally must be made to numerical procedures, thus requiring a computation for each set of values of x_o, x_u and m. It has been shown however [19] that for the special case $x_u = 0$ a great number of closed form solutions do exist for such regular cross-sections as the rectangular and circular. The difficulty encountered here is, of course, not a theoretical one but simply an inconvenience in practice. In the interest of brevity and clarity the subsequent illustrations of probabilistic design will be restricted to a pure couple M acting on a rectangular cross-section. Here it is possible to express the risk of rupture as

$$B = \int_{\frac{x_u d}{2x_b}}^{\frac{d}{2}} \left(\frac{\frac{2x_b}{d} y - x_u}{x_o} \right)^m L\, b\, dy = \frac{V}{2(m+1)} \frac{(x_b - x_u)^{m+1}}{x_b x_o^m} \tag{87}$$

where V is the volume of a beam of length L, width b , and depth d ; the maximum fiber stress $x_b = \frac{6M}{bd^2}$ is taken as the intensity level x ; ϕ is taken as $\frac{2y}{d}$ in Eq. (84); and y is the coordinate through the beam depth measured from the neutral axis. It is easy to check this formula by integrating the stress gradient, which is constant in the direction of length and width and varies from zero at the neutral axis to x_b at the outer fiber, over the half of the beam in tension. It is clear that if a reliability is specified for a beam of given dimensions and material, Eq. (87) yields a value of x_b and, hence, the moment which can be supported. To demonstrate, we cite the following example.

Find the pure couple M which can be supported with reliability of

95 per cent by a rectangular beam with L = 100", b = 2", d = 4". The material used is a ceramic with m = 5, x_u = .5 ksi, and x_o = 2 ksi.

Since R = exp (-B) = .95 (B = .05), we may substitute into formula (87) and find

$$(.05) = \frac{(x_b - .5)^6}{x_b (2)^5} \cdot \frac{(100 \times 4 \times 2)}{2(6)}$$

Solving for x_b, we find x_b = 1.04 ksi.

Thus, $M = \frac{x_b b d^2}{6} = \frac{(1.04)(2)(16)}{6} = 5.54$ in-k.

D. The Prestressing of Brittle Materials

It is well known that the load carrying capacity of beams constructed with material which is much stronger in compression than in tension can be increased by introducing a compressive prestress. This is no less true when the tensile failure stresses are considered to have a probability distribution. Considering an axial prestress x_p it is clear that

$g = \frac{1}{v}\left[\frac{x\phi - x_u - x_p}{x_o}\right]^m$ and that for the linear stress gradient we have considered previously $B = \frac{V}{2(m+1)} \frac{(x_b - x_p - x_u)^{m+1}}{x_b x_o^m}$. Thus in bending it is possible to treat an axial prestress as an increase in the paramter x_u Comparing the moment-carrying capacities of two beams of the same material, one axially prestressed and the other not (and denoted by primes) we find that

$$\frac{B}{B'} = \frac{x'_b}{x_b} \frac{V}{V'} \left[\frac{x_b - x_u - x_p}{x'_b - x_u}\right]^{m+1} \qquad (88)$$

We may note that this is by no means the most efficient method of prestressing but it will serve for purposes of illustration. As a matter of fact, it is easily seen that the most rewarding technique would be to use an eccentricity such that the outer fiber would have a tensile stress of x_u under the prestressing load.

It is possible by means of Eq. (88) to make a comparison showing

quantitatively the advantage of prestressing. One can hold the reliabilities, span lengths, and total weight constant and compute the increased moment carrying capacity as a function of the prestress. The condition of equal weight implies that $\rho_b V_b' = \rho_b V_b + \rho_t V_t$ where the subscript. t indicates the prestressing tendon. Since we are comparing beams of equal span length, $\rho_b A_b' = \rho_b A_b + \rho_t A_t$. The axial prestressing force must be equilibrated by the uniform prestress, x_p. Using a tendon stress x_t,

$$P = x_p A_b = x_t A_t. \quad \text{Thus } A_t = \frac{A_b x_p}{x_t}, \text{ and, } \frac{A_b}{A_b'} = \frac{V_b}{V_b'} = \frac{1}{1 + \frac{\rho_t x_p}{\rho_b x_t}}.$$

From Eq. (88), the condition of equal reliabilities leads to

$$x_b = x_b' \left[\frac{1}{1 + \frac{\rho_t x_p}{\rho_b x_t}} \right] \frac{(x_b - x_u - x_p)^{m+1}}{(x_b' - x_u)^{m+1}} \tag{89}$$

Although an algebraic solution for x_b is not generally feasible, for any given comparison all other terms are known and x_b can be found numerically. But

$$\frac{x_b}{x_b'} = \frac{6M/A_b d}{6M'/A_b' d'} = \frac{M}{M'} \frac{A_b' d'}{A_b d}. \quad \text{So} \quad \frac{M}{M'} = \frac{x_b}{x_b'} \frac{A_b d}{A_b' d'} \tag{90}$$

The ratio A_b/A_b' is specified by equilibrium; but d/d' is as yet indeterminate. For our purposes we will make the most conservative choice in reducing the cross section of the prestressed beam - keeping the width constant. Then since

$b = b'$, $\frac{A_b}{A_b'} = \frac{d}{d'} = \left[\frac{1}{1 + \frac{\rho_t x_p}{\rho_b x_t}} \right]$. And finally $M/M' = \frac{x_b}{x_b'} \left[\frac{1}{1 + \frac{\rho_t x_p}{\rho_b x_t}} \right]^2$ (91)

It is apparent that, generally, $M/M' = \frac{x_b}{x_b'} \left[\frac{1}{1 + \frac{\rho_t x_p}{\rho_b x_t}} \right]^c$, $1 \leq c \leq 2$, (92)

where c depends on the way in which the cross section is reduced. The most efficient method, at least on its face, is to keep the depth constant and reduce the width. In order to beg the question of lateral stability which may limit width reductions, we will use a constant width scheme in the following example:

Find the improved moment carrying capacity attainable in the beam of the previous example by applying a uniform prestress, x_p. Let $\rho_b = 240\#/ft^3$, $\rho_t = 480\#/ft^3$, $x_t = 200$ ksi. Assume that the width of the beam will be held constant and that the limiting condition will be compressive failure at $x_p + x_b = x_{ult} = 200$ ksi, which is a reasonable value for the crushing strength of a ceramic material.

From the previous example we see that $x_b' = 1.04$ ksi. Substitution into Eq. (88) yields

$$x_b = (1.04)\left[\frac{1}{1+\frac{x_p}{100}}\right]\frac{(x_b-.5-x_p)^6}{(1.04-.50)^6}, \text{ or } x_b = 41.6\left[\frac{1}{1+\frac{x_p}{100}}\right](x_b-.5-x_p)^6$$

where x_p and x_b are in ksi. This equation can be solved for x_b given any particular value of x_p. Then, corresponding to that value of x_p, we can complete M/M' and $x_p + x_b$. The most expedient procedure is to plot both of these as functions of x_p. Then it is possible to determine, by inspection, the maximum moment increase permissible by the compressive strength of the material. Such a plot has been made for this example and is shown in Fig. 43. On examination of this graph we see that by introducing a prestress the allowable moment can be increased by a factor of almost 25.

Now, from the design standpoint, we will address the problem of choosing a cross-section and prestress so as to minimize the total weight required to support a given moment. We shall consider a beam of rectangular section, with depth, d, and width, b, subjected to a pure moment, M, and with a prestressing force, P. Let the cross sectional area of the beam be denoted by A_b, its density by ρ_b and those of the tendon by A_t and ρ_t. The design stress in the tendon will be designated as x_t. We wish to minimize the total weight W, or since the beam is of constant section throughout its span, L, the function,

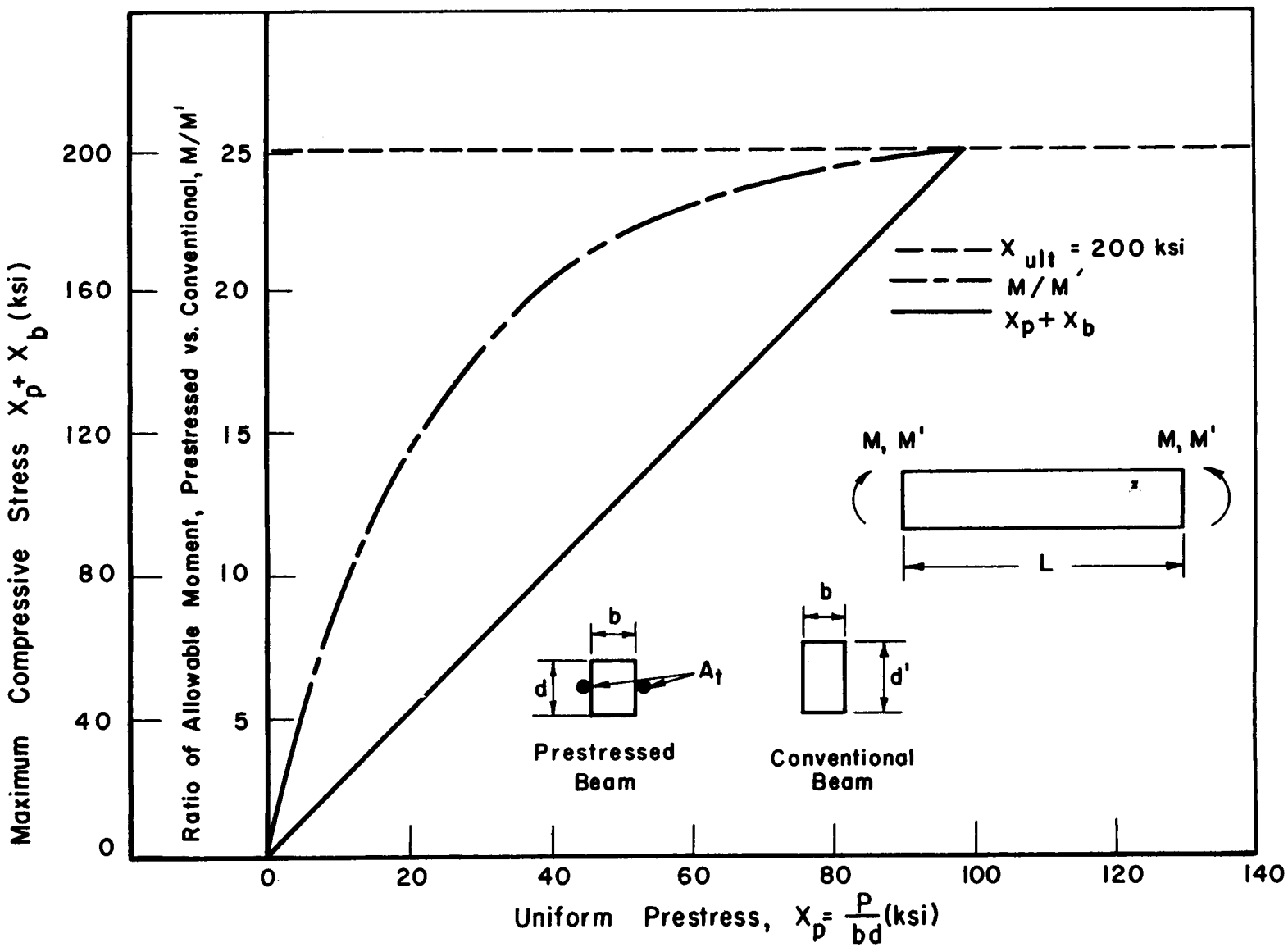

Fig.43 COMPARISON OF PRESTRESSED AND CONVENTIONAL BEAMS OF EQUAL RELIABILITY AND TOTAL WEIGHT

$$w = W/L = \rho_t A_t + \rho_b A_b.$$

But since $P = x_t A_t = x_p A_b$,

$$w = bd\left[\rho_b + \frac{\rho_t}{x_t} x_p\right].$$

If we rewrite Eq. (87), we see that $B = \frac{V_b}{2(m+1)} \frac{(x_b - x_u - x_p)^{m+1}}{x_b x_o^m}$ and,

so, for a given reliability x_p can be expressed as a function of x_b. But $x_b = \frac{6M}{bd^2}$. Hence w is a function only of the depth d. Denoting differentiation with respect to d by a prime, a turning point can be found by solving $w'(d) = 0$.

$$w'(d) = b\left[\rho_b + \frac{\rho_t}{x_t}(x_p + d\, x_p')\right] = 0. \tag{93}$$

Solving Eq. (93) for x_p we find

$$x_p = x_b - x_u - \left[\frac{2B(m+1)x_o^m x_b}{L\, bd}\right]^{\frac{1}{m+1}} \tag{94}$$

Substituting and recognizing that b cannot be zero, we see that the critical value of d is given by the solution of the equation

$$x_t \frac{\rho_b}{\rho_t} = \frac{6M}{bd^2} + x_u + \left(\frac{m-2}{m-1}\right)\left[\frac{12\,MB\,(M+1)\,x_o^m}{L\,b^2}\right]^{\frac{1}{m+1}} d^{-3/(m+1)} \tag{95}$$

If this is to be a minimum, $w''(d)$ must be positive.

$w''(d) = \frac{b\rho_t}{x_t}\left[2\,x_p' + d\,x_p''\right]$ and substituting again, we find

$$w''(d) = \frac{b\rho_t}{x_t}\left[\frac{12M}{bd^3} + \frac{3(m-2)}{(m+1)^2}\left(\frac{12MB\,(m-1)x_o^m}{L\,b^2}\right)^{\frac{1}{m+1}} d^{-\frac{m-4}{m+1}}\right]$$

Thus when m is greater than or equal to two, the value of d assuredly corresponds to a minimum. For m less than two a substitution is the

simplest manner of checking the minimization.

By way of illustration we will now find the minimum weight design to support the moment which could be carried by the unprestressed beam of the previous example and compare the weights.

Find the minimum weight design to support, with a reliability of 95 per cent, a moment of 5.54 in-k on a rectangular beam with L = 100", b = 2". The material to be used is a ceramic with m = 5, x_u = .5 ksi, x_o = 2 ksi. Let $\rho_b = 240\#/ft^3$, $\rho_t = 480\#/ft^3$ and x_t = 200 ksi.

Substituting in Eq. (95), we find, using r = 1/d,

$$16.65\, r^2 + .548\, r^{1/2} = 99.5.$$

Hence, $r = 2.437 \Rightarrow d = .411$ in.

So, $A_b = bd = .822\ in^2 \Rightarrow V_b = 82.2\ in.^3$

$$x_b = \frac{6M}{bd^2} = \frac{6(5.54)}{2(.411)^2} = 98.3 \text{ ksi}$$

Substituting in Eq. (94) we find x_p = 96.6 ksi.

We note as a design check that, since ceramics have compressive strengths in excess of 200 ksi, we are in no danger of compressive failure. The maximum compressive stress is $x_b + x_p = 98.3 + 96.6 = 194.9$ ksi.

$$A_t = \frac{x_p}{x_t} A_b = \frac{96.6}{200} (.822) = .398\ in.^2$$

Thus,

$$W = \frac{480}{1728} (39.8) + \frac{240}{1728} (82.2) = 22.4\#$$

We may compare this with the weight of the 2 x 4 x 100 section of the previous example which could withstand the same load and which is

$$\left(\frac{240}{1728}\right) 800 = 111.1\#.$$

BIBLIOGRAPHY

1. Roark, R. J. , "Formulas for Stress and Strain," McGraw - Hill Book Co., New York, 3rd. Ed., pp 42 - 44, 1954.

2. Bruner, G., "Wings in Prestressed Concrete," The Aeroplane, Vol. LXXXVI, No. 2217, pp 72-77, January 15, 1954.

3. Philips Technical Review, Vol. 20, No. 1, pp. 1-36, and No. 2/3, pp. 37-49, 1958/1959.

4. Shanley, F. R., Knapp, W. J., and Needham, R. A., "Prestressed Ceramic Structures," WADC Tech. Report 54-75, Part II, pp 43, January 1955.

5. Gerwick, B. C. Jr.,'Precast Segmental Construction for Long-Span Bridges," Civil Engineering, pp 43-47 , Janaury 1964.

6. Magnel, Gustave, "Structures In Precompressed Steel," Ossature Metalligue (Brussels, Belgium), Vol. 15, No. 6, pp. 300-313, 1950.

7. Barnett, R., "Prestressed Truss-Beams," Transactions, ASCE, Vol. 124, pp 472, 1959.

8. A. F. Technical Report 5744, "The Design of Aircraft Structures for Aerodynamic Heating Effect," Ohio State University Research Foundation, Columbus, Ohio.

9. Shanley, F. R., "Preliminary Investigation of a Prestressed Ceramic Wing," Rand Research Memo: RM-598, January 24, 1951.

10. Johnston, Chipman, Knapp, "Prestressed Ceramics as a Structural Material," American Ceramics Society, Vol. 36, No. 4, pp. 121-126, April, 1953.

11. Nadai, A., "Theory of Flow and Fracture of Solids," McGraw-Hill Book Co., pp. 343, 1950.

12. Barnett, R. L. , "Lightweight Structures and Prestressed Launcher Components," Rock Island Arsenal, Cont. No. DA-11-070-508-ORD-588 Ord. Proj. No. TU2-70, Vol. I and II, January and October ,1958.

BIBLIOGRAPHY Cont'd

13. Harris, A. J., "High Structural Performance-Advanced Applications of Prestressing," Engineer, pp. 244-246, August 23, 1957.

14. Berenbaum, R. and Brodie, I., "Measurement of the Strength of Brittle Materials," British Journal of Applied Physics, Vol. 10, pp. 281-287, June 1959.

15. Timoshenko, S., and Goodier, J. N., Theory of Elasticity, McGraw-Hill Book Company, New York, 2nd. Ed., pp. 47-49, 1951.

16. Griffith, A. A., "The Phenomena of Rupture and Flow in Solids," Phil. Trans. Roy. Soc., 221A, p. 163, 1920.

17. Weibull, W., "A Statistical Theory of the Strength of Materials," Ing. Vetenskaps Akad., 151, pp. 1-45, 1939.

18. Barnett, R. L., "Review of Structural Design Techniques for Brittle Components under Static Loads," Contract AF 33(657)-8339, ARF Report No. 8259, Phase I - Task 2, pp. 50-74, May 1963.

19. Ibid, pp. 29-32.